INL/EXT-05-00453

Thermal-Hydraulic Analyses of Heat Transfer Fluid Requirements and Characteristics for Coupling a Hydrogen Product Plant to a High-Temperature Nuclear Reactor

C. B. Davis, INL
R. B. Barner, INL
S. R. Sherman, INL
D. F. Wilson, ORNL

June 2005

Idaho National Laboratory

The INL is a U.S. Department of Energy National Laboratory operated by Battelle Energy Alliance

Thermal-Hydraulic Analyses of Heat Transfer Fluid Requirements and Characteristics for Coupling a Hydrogen Production Plant to a High-Temperature Nuclear Reactor

C. B. Davis, C. H. Oh, R. B. Barner, S. R. Sherman (INL)
and D. F. Wilson (ORNL)

June 2005

Idaho National Laboratory

Idaho Falls, Idaho 83415

ABSTRACT

The Department of Energy is investigating the use of high-temperature nuclear reactors to produce hydrogen using either thermochemical cycles or high-temperature electrolysis. Although the hydrogen production processes are in an early stage of development, coupling either of these processes to the high-temperature reactor requires both efficient heat transfer and adequate separation of the facilities to assure that off-normal events in the production facility do not impact the nuclear power plant. An intermediate heat transport loop will be required to separate the operations and safety functions of the nuclear and hydrogen plants. A next generation high-temperature reactor could be envisioned as a single-purpose facility that produces hydrogen or a dual-purpose facility that produces hydrogen and electricity. Early plants, such as the proposed Next Generation Nuclear Plant, may be dual-purpose facilities that demonstrate both hydrogen and efficient electrical generation. Later plants could be single-purpose facilities. At this stage of development, both single- and dual-purpose facilities need to be understood.

Seven possible configurations for a system that transfers heat between the nuclear reactor and the hydrogen and/or electrical generation plants were identified. These configurations included both direct and indirect cycles for the production of electricity. Both helium and liquid salts were considered as the working fluid in the intermediate heat transport loop. Methods were developed to perform thermal-hydraulic and cycle-efficiency evaluations of the different configurations and coolants. The thermal-hydraulic evaluations estimated the sizes of various components in the intermediate heat transport loop for the different configurations. The relative sizes of components provide a relative indication of the capital cost associated with the various configurations. Estimates of the overall cycle efficiency of the various configurations were also determined. The evaluations determined which configurations and coolants are the most promising from thermal-hydraulic and efficiency points of view. These evaluations also determined which configurations and options do not appear to be feasible at the current time.

CONTENTS

FIGURES

1. INTRODUCTION

The Department of Energy is investigating the use of high-temperature nuclear reactors to produce hydrogen using either thermochemical cycles or high-temperature electrolysis. Although the hydrogen production processes are in an early stage of development, coupling either of these processes to the high-temperature reactor requires both efficient heat transfer and adequate separation of the facilities to assure that off-normal events in the production facility do not impact the nuclear power plant. An intermediate heat transport loop will be required to separate the operations and safety functions of the nuclear and hydrogen plants. Although an indirect electrical cycle would also require an intermediate loop similar to the loop required for hydrogen production, an electrical cycle would not be anticipated to have the same requirements for significant separation distances that hydrogen plant safety issues would require.

A next generation high-temperature reactor could be envisioned as a single-purpose facility that produces hydrogen or a dual-purpose facility that produces hydrogen and electricity. At the current time, it is anticipated that early plants may be dual-purpose facilities that demonstrate both hydrogen and efficient electrical generation, and that later plants could be single-purpose facilities. At this stage of development, both single- and dual-purpose facilities need to be understood.

Both helium and liquid salts are being considered as the working fluid in the intermediate heat transport loop. The liquid salts considered in this analysis included LiF-NaF-KF (Flinak) in molar concentrations of 46.5%, 11.5%, and 42%, respectively, and $NaBF_4$-NaF in molar concentrations of 92% and 8%. The use of a liquid salt provides the potential for improved heat transfer and reduced pumping powers, but also introduces materials compatibility issues. These issues are summarized in Appendix A. The thermodynamic states of the working fluid have not been selected.

This report describes various intermediate heat transport loop configurations and summarizes the thermal-hydraulic, structural, and efficiency calculations that have been performed to characterize the advantages and issues associated with each configuration. The key issues that are addressed in this report include:

- Configuration options
- System parameters, such as temperature and pressure
- Structural issues
- Working fluid options and materials issues.

Seven possible configurations for the high-temperature reactor primary coolant system and the intermediate heat transport loop have been identified. The ultimate objective of the program is to evaluate the advantages and disadvantages of each of the configurations and working fluids so that a specific design option can be recommended. However, the recommendation of a specific design requires input from a variety of disciplines related to materials, thermal-hydraulics, economics, safety, and plant operability. The purpose of this work is to evaluate the advantages and disadvantages of the configurations and working fluids to provide input to the decision making process. The work will also identify key research and development issues for the intermediate heat transport loop.

This document describes the methods used to perform the evaluations of the different configurations and coolants as well as the results from the evaluations. The desired outcome of the analysis is to determine which of the configurations are currently feasible and to eliminate any that are not from further consideration. The relative advantages and disadvantages of the remaining configurations were evaluated to determine which of the options appears to have the best chance for resulting in a successful design.

This analysis: (1) identifies key requirements of the high-temperature reactor and the hydrogen production plant that affect the intermediate heat transport loop; (2) describes and justifies key assumptions used in the evaluation; (3) identifies possible configurations of the intermediate heat transport loop; (4) performs preliminary stress evaluations to determine allowable pressures and required component thicknesses based on the creep rupture strengths of currently available materials; (5) estimates the size and thermal-hydraulic performance of various components in the intermediate heat transport loop including the heat exchangers and loop piping; (6) estimates the overall cycle efficiency of each configuration; (7) determines the sensitivity of the cycle efficiency to various parameters, and (8) compares and contrasts the different options to aid in the selection of the configuration and working fluid.

The evaluations of the different configurations and coolants for the intermediate heat transport loop were funded by the National Hydrogen Initiative and the Gen IV Energy Conversion Program. The thermal-hydraulic analyses were funded by the National Hydrogen Initiative. The evaluations of cycle efficiency were funded by the Gen IV Energy Conversion Program. Since the two programs are closely related, results from these analyses were shared between programs. This document describes the methods, results, and conclusions from both evaluations. This document satisfies the NHI Systems Interface milestone to characterize intermediate loop implications for hydrogen production.

The remainder of this report describes key requirements and assumptions used in the analyses, the seven configurations that were evaluated, the methods used to perform the analyses, and results of the analyses. A summary of the work is presented in Section 6.

2. KEY REQUIREMENTS AND ASSUMPTIONS

Two top-level temperature requirements have been identified for the interface between the nuclear and hydrogen plants. These requirements are defined by the outlet temperature of the high-temperature reactor and the maximum temperature delivered to the hydrogen plant. At this stage of development, these maximum system temperatures are active areas of investigation, and parametric studies are more appropriate than point design studies. However, for this initial analysis, the outlet temperature of the high-temperature reactor was set at 900 °C, consistent with current capabilities, and parametric calculations were performed with higher outlet temperatures to determine their effects on component performance.

The efficiency of the hydrogen-production process increases with temperature but is also uncertain at this point. The sulfur-based cycles, which are currently the baseline thermochemical cycles, are considered to require at least 850 °C. High-temperature electrolysis current requires temperatures in the range of 750 to 900 °C. For this analysis, the maximum temperature supplied to the hydrogen plant was assumed to be 850 °C.

In order to provide estimates of component performance, assumptions are required about the basic configuration and operating conditions of the high-temperature reactor, the intermediate heat transport loop, and the hydrogen production plant. For this report, the preliminary designs for the Next Generation Nuclear Plant (NGNP) were used as the basis for analysis. The primary assumptions are described below and summarized in Table 1. Parametric calculations were performed to determine the effects of changes from the basic parameters.

The NGNP was assumed to produce 600 MW of thermal power and use helium coolant. The nominal rise in fluid temperature across the core was assumed to be 400 °C, based on the point design (MacDonald et al. 2003). The nominal reactor pressure was assumed to be 7 MPa (INEEL 2005). The pressure drop across the hot stream of the intermediate heat exchanger (IHX) was assumed to be 0.05 MPa. This value

is the same as the pressure drop across the core in the Gas Turbine-Modular Helium Reactor (GT-MHR) (General Atomics 1996). Since the pumping power associated with this pressure drop across the core was considered acceptable in the GT-MHR, the pumping power associated with this pressure drop across the IHX should also be acceptable. The same pressure drop was generally applied to other components because of pumping power considerations.

The intermediate heat transport loop was assumed to receive 50 MW of thermal power (ANLW 2004). Parametric calculations were performed in which the total output of the reactor (600 MW) was assumed to be used for hydrogen production.

Estimates for the required separation distance between the nuclear and hydrogen plants depend on the design and safety criteria applied and vary considerably. For example, Verfondern and Nishihara (2004) calculated 300 m for the High-Temperature Engineering Test Reactor in Japan whereas Sochet et al. (2004) recommended 500 m for the High-Temperature Reactor. Smith et al. (2005) recommended a separation distance of from 60 to 120 m for the NGNP and the hydrogen production plant. For this analysis, a nominal value of 90 m was used, with parametric variations between 60 and 500 m. The separation distance primarily affects the diameters and insulation requirements of the hot and cold legs in the heat transport loop.

The nominal temperature drop between the outlet of the NGNP and the maximum temperature delivered to the hydrogen production plant is 50 °C. This temperature drop imposes requirements on the effectiveness of the heat exchangers that connect the NGNP and production plant and the amount of heat loss than can be tolerated in the intermediate loop. In order to perform preliminary calculations, heat loss was assumed to cause the fluid temperature to drop 10 °C in the hot leg of the intermediate loop at nominal conditions. Assuming the same geometry in the hot and cold legs of the intermediate loop, more heat is lost from the hot leg than from the cold leg. Based on nominal temperatures, the heat loss from the hot legs is expected to be about 70% of the total. The total temperature drop in the loop piping was assumed to be 10/0.7 = 14.3 °C, with 10 °C occurring in the hot leg and the remaining 4.3 °C occurring in the cold leg. Using a nominal flow rate, the resulting heat losses in the hot and cold legs were 1.25 and 0.54 MW, respectively. This heat loss corresponds to 3.6% of the loop power and 0.3% of the nuclear reactor power. The same heat loss was assumed for all configurations to allow consistent comparisons.

Table 1. Analysis assumptions.

Parameter	Nominal Value
NGNP:	
Power, MW	600
Outlet temperature, °C	900
Core temperature rise, °C	400
Pressure, MPa	7
IHX pressure drop, MPa	0.05
Intermediate heat transport loop:	
Power, MW	50
Separation distance, m	90
Heat loss, MW	1.79
Hydrogen plant:	
Maximum delivered temperature, °C	850
Inlet fluid temperature, °C	341

The IHX is assumed to be a compact heat exchanger of the type designed by Heatric (Dewson and Thonon 2003). The heat exchanger that connects the heat transport loop to the hydrogen production plant is referred to as the process heat exchanger (PHX) and is assumed to be a tube-in-shell heat exchanger with the heat transport fluid flowing on the shell side. This configuration allows the tubes to contain the catalysts necessary for hydrogen production, which is judged to be the most convenient configuration. The tube side was assumed to be at low pressure (< 1 MPa). The hot and cold legs of the intermediate loop are assumed to be separate pipes, as opposed to an annular configuration. The purpose of these calculations is to compare the relative size of components between configurations. These calculations are not intended to achieve a final design for any configuration or to recommend one type of heat exchanger over another.

The required size of the heat exchangers depends on the overall temperature difference between the outlet of the reactor core and the inlet on the cold side of the PHX. For this analysis, the inlet temperature on the cold side of the PHX was assumed to be 341 °C to allow consistent comparisons between the various configurations. This value is reasonable for both thermochemical and high-temperature electrolysis production methods.

3. DESIGN CONFIGURATIONS

Seven plant configurations were evaluated as part of this task. For convenience, the following nomenclature is used relative to the heat exchangers:

- IHX - The first heat exchanger downstream of the NGNP outlet
- PHX - The heat exchanger that connects the intermediate heat transport loop to the hydrogen production plant
- SHX - The heat exchanger that, if present, is located between the IHX and the PHX, and is referred to as the secondary heat exchanger (SHX).

The seven plant configurations evaluated are illustrated in Figures 1 through 7. The configurations include direct and indirect electrical cycles as shown in Figures 1 – 4 and 5 – 7, respectively. The configurations include both serial and parallel heat exchanger options. In the serial option, which is illustrated in Figures 1, 3, and 5, the IHX or SHX is located upstream of the power conversion unit (PCU). In the serial option, the heat exchanger removes less than 10% of the reactor power and directs it towards the hydrogen production plant. With this configuration, the hydrogen production plant receives the highest possible temperature fluid while the PCU receives a lower temperature fluid. This configuration is relatively simple and is especially suitable for the demonstration of hydrogen production. However, the overall efficiency of the electrical production process will be reduced. In the parallel heat exchanger option, which is illustrated in Figures 2, 4, 6, and 7, the hottest fluid is divided, with most going towards the PCU and the remainder going towards the hydrogen production plant. This configuration is more complicated, but results in a higher overall efficiency because both the electrical and hydrogen production plants see the maximum possible temperature. With these options, a small compressor or blower is required to compensate for the pressure loss across the IHX or SHX and allow the fluid streams to mix downstream of the recuperator. The final option uses a SHX as shown in Figures 3, 4, 5, and 6. This option utilizes a third or tertiary coolant loop that provides additional separation between the nuclear and hydrogen plants, which should increase the safety of both plants and may make the nuclear plant easier to license. However, this option requires more capital investment and lowers the overall efficiency of the plant.

4
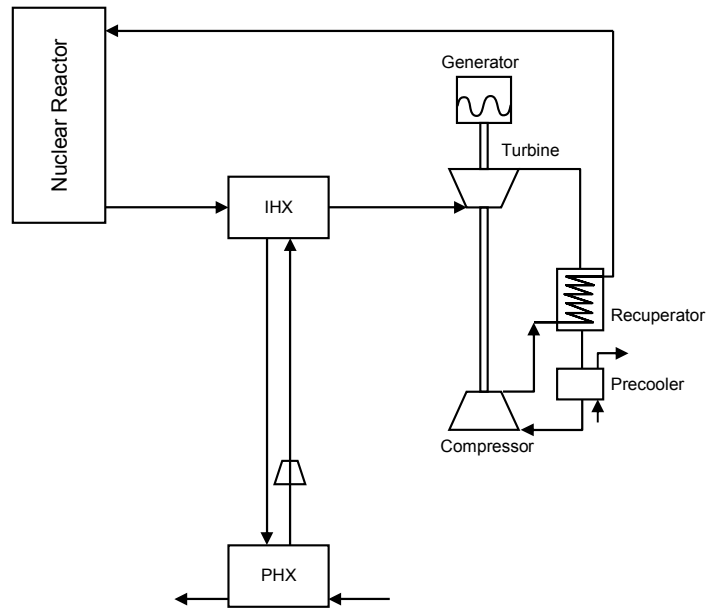
Figure 1. Configuration 1 (direct electrical cycle and a serial IHX).
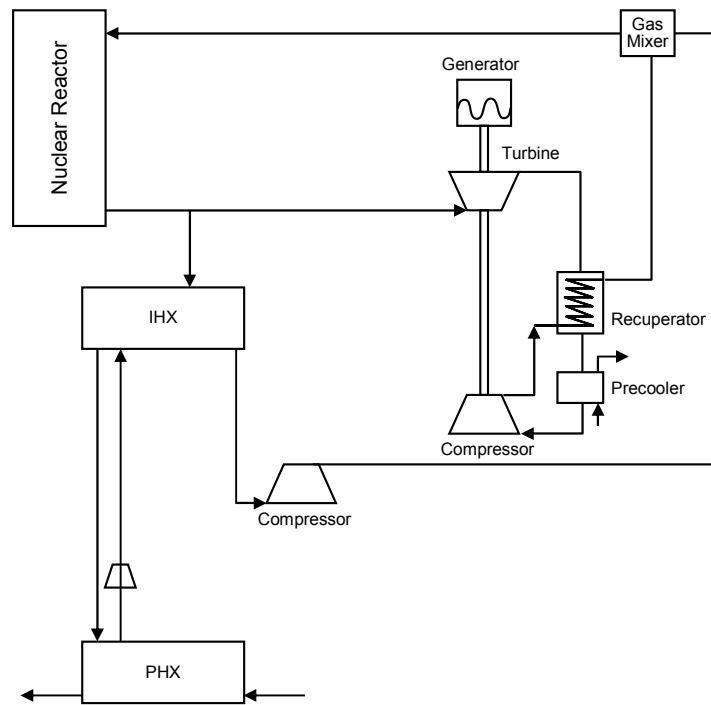
Figure 2. Configuration 2 (direct electrical cycle and a parallel IHX).
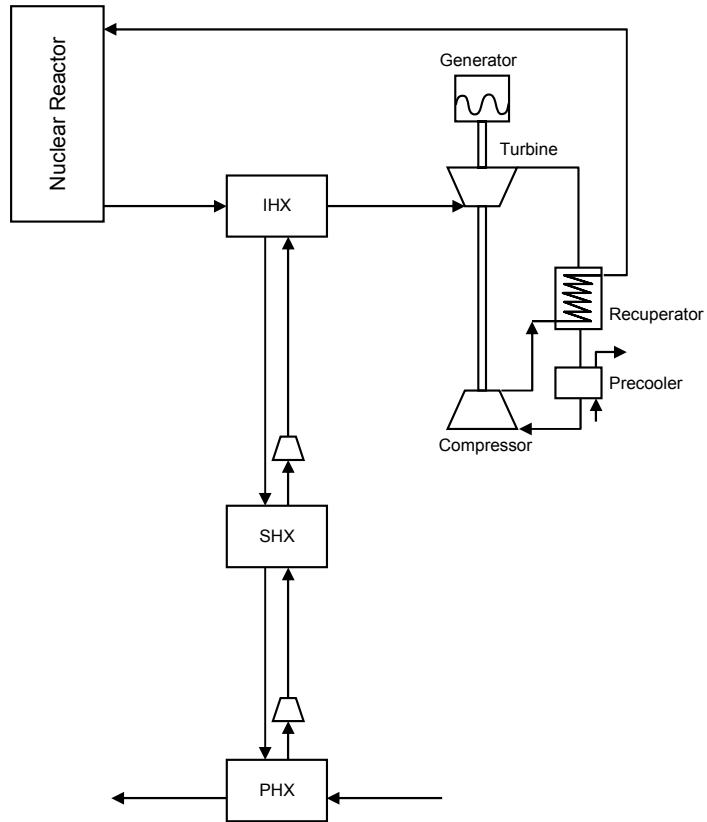
Figure 3. Configuration 3 (direct electrical cycle, serial IHX, and SHX).
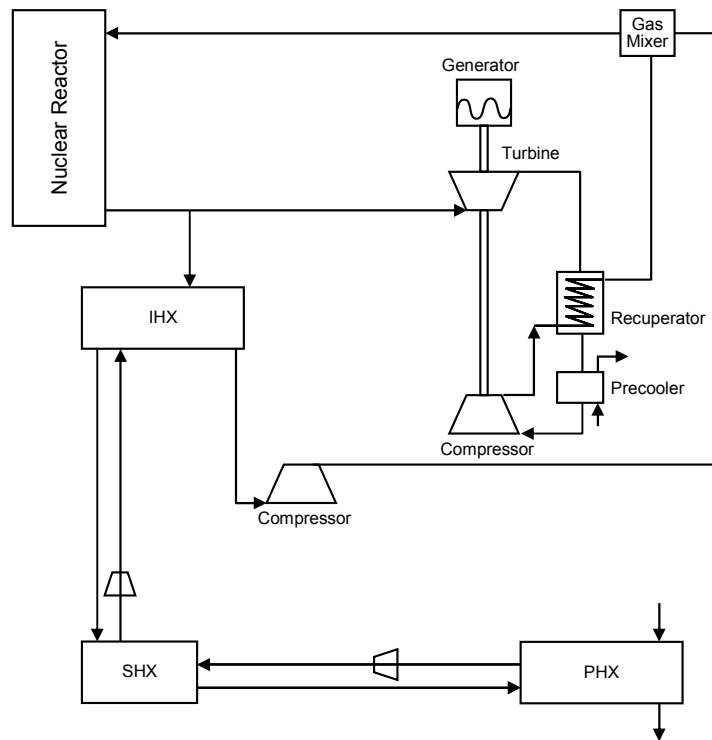
Figure 4. Configuration 4 (direct electrical cycle, parallel IHX, and SHX).
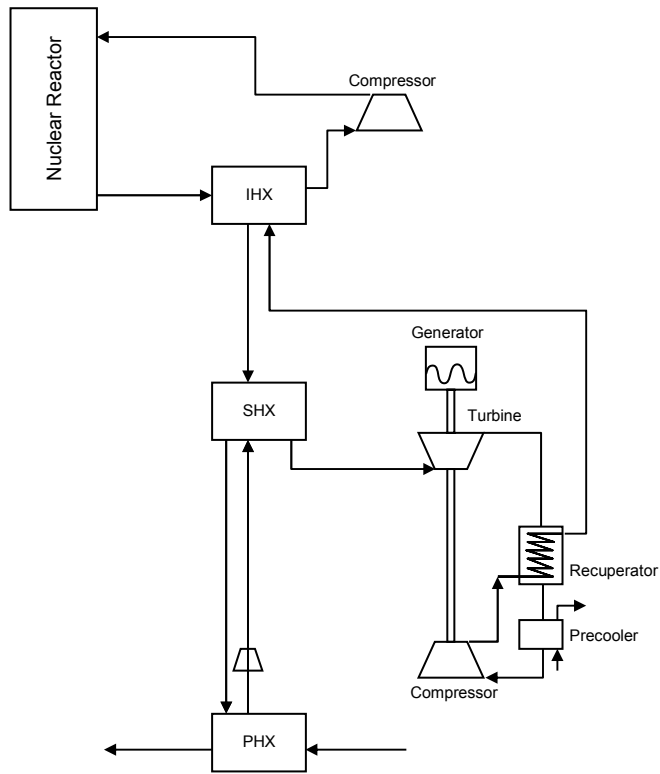
Figure 5. Configuration 5 (indirect electrical cycle and a serial SHX).
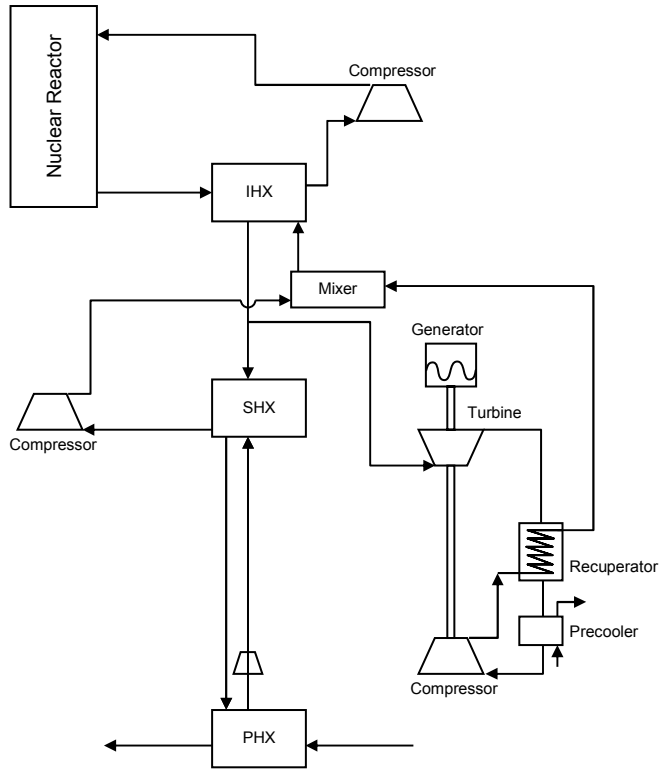
Figure 6. Configuration 6 (indirect electrical cycle and a parallel SHX).
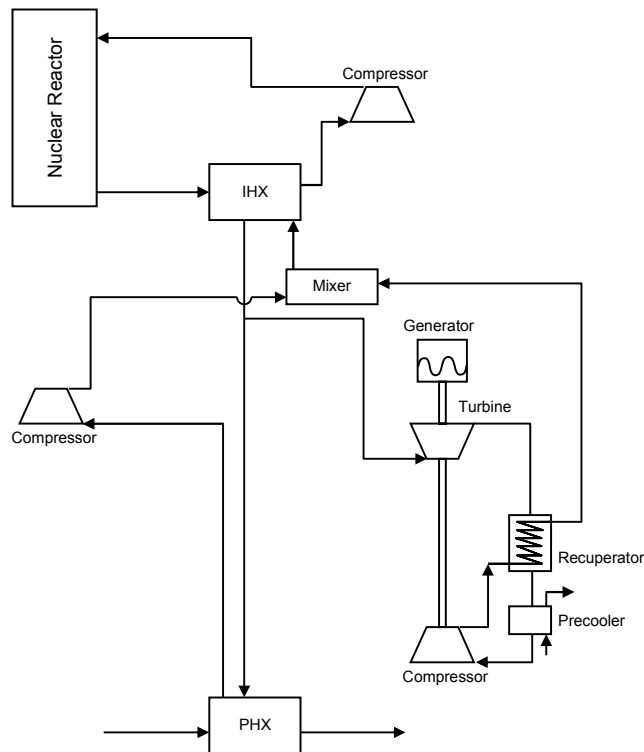
Figure 7. Configuration 7 (indirect electrical cycle and a parallel PHX).

The Independent Technology Review Group (2004) recommended the use of an indirect cycle for the NGNP because it was judged to be more practical for operation and to involve less developmental risk than a direct cycle.

4. METHODS

This section describes the methods used to perform the thermal-hydraulic and efficiency evaluations. The thermal hydraulic methods included a simple stress analysis that is described in Section 4.1 to determine the thickness of various components. The thicknesses were used in the component sizing analysis that is described in Section 4.2. The method used to estimate the overall cycle efficiency for each configuration is described in Section 4.3.

4.1 Simplified Stress Analysis

A simplified stress analysis was performed for different components in the various configurations. The analysis determined the thickness required so that the circumferential stress was less than or equal to an assumed allowable value. The use of consistent stresses allowed identification of limiting components and a fair comparison between different configurations.

The creep rupture strength of a material depends on the operating time at a given temperature.   Figure 8 shows that the rupture strength of Alloy 800 decreases sharply with temperature. At an operating time of 10^5 h (about 11 years), the rupture strength is 240 MPa at 500 °C, but decreases to 8 MPa at 900 °C. The rupture strength also depends on the time at temperature. At 900 °C, the rupture strength increases from 8 to 16 MPa when the operating time decreases from 10^5 to 10^4 h. The data presented in Figure 8 suggest

8

that the mechanical design of the heat transport loop will be a challenge because of the desired high temperature and the long lifetime, both of which act to reduce the rupture strength.
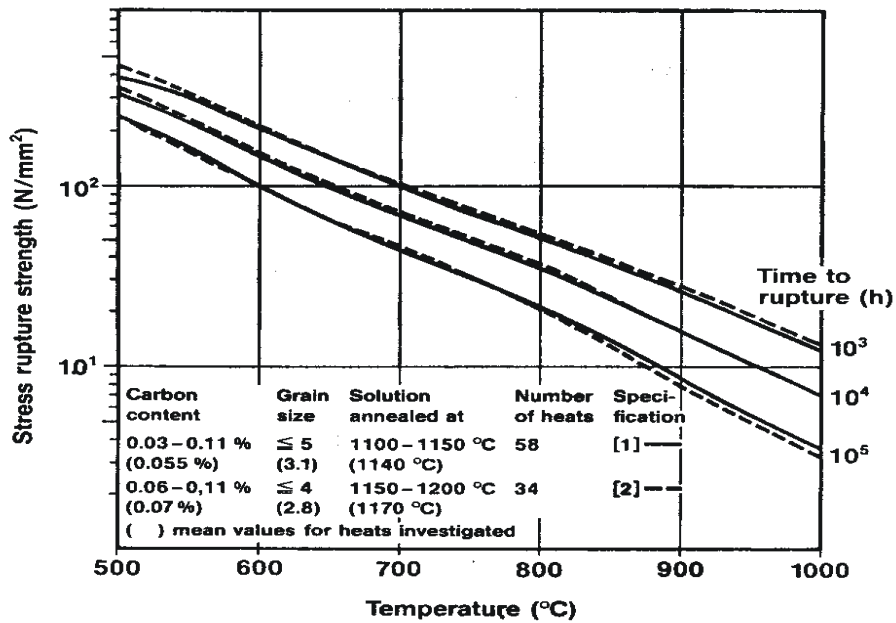
Figure 8. Creep rupture strength of Alloy 800 (from Diehl and Bodman 1990).

The creep rupture strengths of three candidate materials for the heat transport loop are shown in Figure 9 for a temperature of 900 °C. These three materials are Alloy 800HT, which is a high-temperature variation of Alloy 800 (Special Metals 2004a), Alloy 617 (Special Metals 2004b), and Hastelloy X (Haynes International 2005). Alloy 617 has the highest rupture strength of these three materials at 900 °C. The allowable stress will eventually be specified by an applicable code, but will be less than the strengths shown in Figure 9 to account for safety factors.   For this analysis, the allowable stress was assumed to be half of the creep rupture strength.
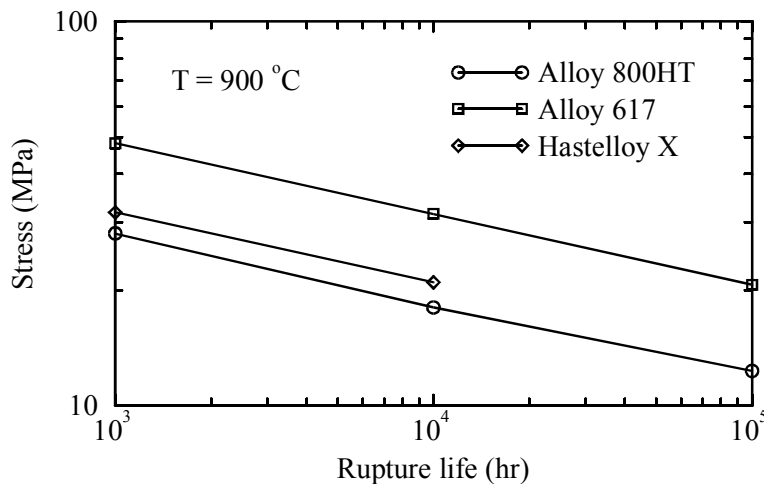
Figure 9. Creep rupture strengths of candidate materials.

A simple stress analysis was performed to determine the required thickness for the heat transport loop piping and the heat exchangers. For thick walled cylinders, the tangential stress, σ, is calculated as (Crandall et al. 1972)

$$\sigma = \frac{P_i[(r_o/r)^2 + 1] - P_o[(r_o/r_i)^2 + (r_o/r)^2]}{(r_o/r_i)^2 - 1} \quad , \tag{1}$$

where r is the radius, P is the pressure, and the subscripts i and o refer to the inner and outer surfaces, respectively. The stress is negative if the external pressure exceeds the internal pressure, but the maximum magnitude always occurs at the inner surface. The radius ratio that causes the maximum stress to be less than or equal to the allowable stress, σ_D, can be calculated from Equation (1). For cases where the internal pressure exceeds the external pressure, the limiting ratio is

$$\frac{r_o}{r_i} \geq \sqrt{\frac{\sigma_D + P_i}{\sigma_D + 2P_o - P_i}} \quad . \tag{2}$$

For cases where the external pressure exceeds the internal pressure, the maximum, absolute value of the stress will be less than or equal to the allowable stress when the radius ratio is

$$\frac{r_o}{r_i} \geq \sqrt{\frac{\sigma_D - P_i}{\sigma_D - 2P_o + P_i}} \quad . \tag{3}$$

A simple stress analysis was also performed for the IHX assuming that it is a compact heat exchanger of the type designed by Heatric (Dewson and Thonon 2003). The design of the heat exchanger channels is defined by the channel diameter, d, pitch, p, and plate thickness, t_p, as illustrated in Figure 10. Each plate contains either hot or cold fluid, but not both. Adjacent plates contain the other fluid. Following the method used by Dostal et al. (2004), the minimum wall thickness between channels, t_f, can be approximated as

$$t_f \geq \frac{p}{\dfrac{\sigma_D}{\Delta P} + 1} \quad , \tag{4}$$

where σ_D is the allowable stress and ΔP is the differential pressure between the hot and cold streams. Expressing Equation (4) in terms of pitch-to-diameter ratio yields

$$\frac{p}{d} \geq 1 + \frac{\Delta P}{\sigma_D} \quad . \tag{5}$$

10

04-GA50050-12
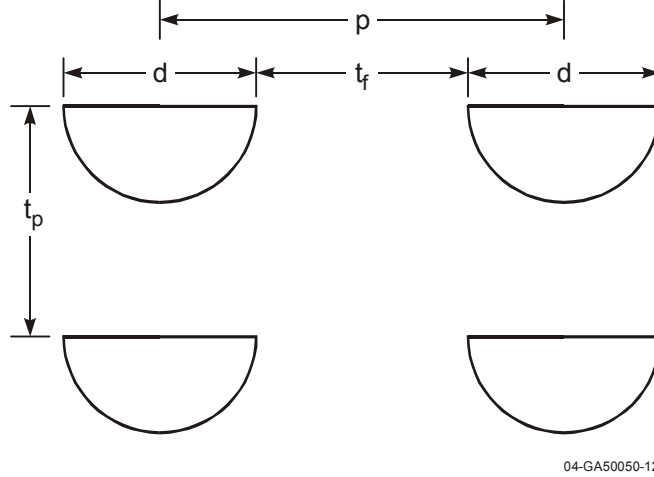
Figure 10. Illustration of IHX channels.

The required plate thickness can also be calculated based on the method of Dostal et al. (2004). The plate is assumed to be a thick-walled cylinder, with an inner radius of d/2 and an outer radius of t_p. Equations (2) and (5) can be used to calculate the thickness-to-diameter and pitch-to-diameter ratios for the IHX as a function of allowable stress and various pressures of the hot and cold streams. The allowable stress is assumed to be 10 MPa, which is approximately half of the rupture strength of Alloy 617 at 900 °C.

4.2 Component Sizing

The nominal temperature drop between the outlet of the NGNP and the maximum temperature delivered to the hydrogen production plant is assumed to be 50 °C. This temperature drop imposes requirements on the effectiveness of the heat exchangers that connect the NGNP and the production plant and the amount of heat loss than can be tolerated in the intermediate loop. Although the total temperature drop between the NGNP and the production plant is fixed by assumption, the distribution of the temperature drop between the heat exchangers and heat loss can be varied. For example, if the heat loss can be reduced, the temperature drops across the heat exchangers can be increased and smaller heat exchangers can be used. After accounting for heat loss, the remaining temperature drop between the outlet of the NGNP and the maximum temperature delivered to the hydrogen production plant is divided evenly between the IHX, PHX, and, if present, the SHX.

As mentioned previously, the temperature drop between the NGNP and the production plant imposes requirements on the heat exchangers. The effectiveness of a heat exchanger, ε, (Kreith 1964) can be calculated as

$$\varepsilon = \frac{(\dot{m}c_p)_h (T_{h\,in} - T_{h\,out})}{(\dot{m}c_p)_{min} (T_{h\,in} - T_{c\,in})} \tag{6}$$

where $\dot{m}$ is the mass flow rate, c_p is the specific heat capacity at constant pressure and is assumed constant, and T is the temperature. The subscripts h and c refer to the hot and cold sides of the heat exchanger, the subscripts in and out refer to the inlet and outlet ends of the heat exchanger, and the subscript min refers to the minimum value for the hot and cold sides.

The heat exchangers are assumed to be in counterflow, which requires less surface area than is required for parallel flow (Kreith 1964). Counterflow heat exchangers are therefore smaller, and presumably

11

cheaper, than corresponding heat exchangers in parallel flow. If the values of $\dot{m}c_p$ are the same for the hot and cold streams, the effectiveness depends only on the inlet and outlet temperatures.

Estimates are also made to size the heat exchangers. The required heat transfer area, A_{ht}, can be calculated from equations given by Krieth (1964)

$$A_{ht} = \frac{\varepsilon(\dot{m}c_p)_{min}(T_{h\,in} - T_{c\,in})}{U\Delta T} \quad , \tag{7}$$

where U is the overall heat transfer coefficient and ΔT is the log-mean temperature difference, which is calculated as

$$\Delta T = \frac{\Delta T_a - \Delta T_b}{\ln(\Delta T_a / \Delta T_b)} \quad , \tag{8}$$

where ΔT_a is the temperature difference between the hot and cold fluid streams at one end of the heat exchanger and ΔT_b is the temperature difference at the other end. The overall heat transfer coefficient is calculated from the heat transfer coefficients on both sides of the exchanger and the thermal conductivity and thickness of the metal. The heat transfer coefficients and the thermal conductivity are assumed constant over the length of the heat exchanger. For turbulent flow, the heat transfer coefficients are calculated using the Dittus-Boelter correlation, with a leading coefficient of 0.021 for gases and 0.023 for liquids (INEEL 2003a). For laminar flow, the heat transfer coefficients are calculated from the exact solution for fully developed flow with constant heating rate (Kayes and Crawford 1980). The thermal conductivity of the metal is calculated assuming Alloy 800, and varies between 18 and 26 W/m-K over the temperature range of interest.

The pressure drop across a component is calculated from either the Blausius equation (Bird et al. 1960) or the more accurate Zigrang-Sylvester correlation (INEEL 2003b) for turbulent flow and the exact solution for fully developed laminar flow in a tube (Bird et al. 1960).

The front face of the IHX is assumed to be square. Iterations are performed to determine the width of the IHX. First, a diameter of the semicircular flow channel is assumed. The plate thickness and pitch between channels are then calculated from the ratios given by Equations (2) and (5). A width of the IHX is then assumed. The flow areas of the hot and cold streams are then calculated from the width and geometries of the channels and plates. The mass flow rates for both streams are calculated from an energy balance and the assumed inlet and outlet temperatures. The overall heat transfer coefficient and effectiveness are then calculated. The required heat transfer area is then calculated from Equation (7). The length of the heat exchanger is then calculated from heat transfer area and the wetted perimeter of the channels, which allows the calculation of the pressure drop. The heat exchanger width is then varied until the desired pressure drop is obtained.

A similar method is used for the tube-in-shell PHX. First, the tube inner diameter is assumed. The tube thickness is then calculated from ratios determined in the stress analysis. The pitch-to-outer-diameter ratio of the tubes is set to 1.3, a typical value for tube bundles. The tube bundle is assumed to have a triangular pitch. Details on the heat transfer coefficients and fluid temperature distribution on the process side of the PHX are not yet available. Consequently, the heat transfer coefficient on the process side is assumed to be 2000 W/m^2-K, which is a representative value for the conditions being considered. The inlet and outlet fluid temperatures on the process side are also assumed. The inner diameter of the shell is then varied until the desired pressure drop is obtained.

The inner diameters of the hot and cold leg pipes in the heat transport loop are sized to produce a given pressure drop. The thickness of the piping is based on the results of the stress analysis. The heat loss is calculated using an overall heat transfer coefficient, which accounts for the thermal resistance of the heat transfer coefficient at the inner and outer surfaces, the pipe metal, and the insulation (Bird et al. 1960). Specifically,

$$U_0 = \frac{1}{r_0\left(\dfrac{1}{r_0 h_0} + \dfrac{\ln(r_1/r_0)}{k_1} + \dfrac{\ln(r_2/r_1)}{k_2} + \dfrac{1}{r_2 h_2}\right)} \ , \tag{9}$$

where U_0 is the overall heat transfer coefficient based on the inner surface area of the pipe, k_1 and k_2 are the thermal conductivities of the pipe metal and insulation, respectively, and r_0, r_1, and r_2 are the radii of the inner surface of the metal, the outer surface of the metal, and the other surface of the insulation, respectively. The heat transfer coefficient at the inner surface, h_0, is calculated using the Dittus-Boelter correlation (INEEL 2003a) as described previously. The heat transfer coefficient at the outer surface, h_2, accounts for natural convection and radiation. The convective contribution is calculated using the Churchill-Chu correlation for natural convection from a horizontal cylinder (Holman 1986). The radiation term is calculated assuming that the pipe is in a large enclosure (Homan 1986), such as in a buried conduit. The thermal conductivity of the metal is based on Alloy 800. The thermal conductivity of the insulation is assumed to be 0.1 W/m-K, which is a representative value for glasswool. The thickness of the insulation is varied to obtain the desired heat loss. In case an alternate insulation material is eventually selected, the required thickness can be approximated by the thickness value reported here multiplied by the ratio of the actual thermal conductivity to the assumed thermal conductivity.

Estimates of the pumping power, Q_p, are approximated using

$$Q_p = \frac{\dot{m}\Delta P}{\rho} \ , \tag{10}$$

where $\dot{m}$ is the mass flow rate, ΔP is the pressure drop, and ρ is the fluid density (Glasstone and Sesonske 1967). The fluid density is based on the temperature at the inlet to the reactor for the hot stream of the IHX and based on the temperature of the cold stream entering the IHX or the SHX for the intermediate and tertiary loops.

4.3 Efficiency Evaluation

The efficiency of each proposed configuration was estimated using HYSYS (Aspen Technology 2005a), a process optimization code used in the chemical and oil industries. Input models were developed for each of the configurations illustrated in Figures 1 through 7.

The PCU cycle efficiency, η_{PCU}, used in this study is defined as:

$$\eta_{PCU} = \frac{\text{Electric power output}}{\text{Reactor thermal power - H}_2 \text{ process power}} = \frac{\Sigma W_T - \Sigma W_C - W_S - \Sigma W_{CIR}}{Q_{th} - Q_{H2}} \ , \tag{11}$$

where ΣW_T is the total turbine workload, ΣW_C is the total compressor workload, W_S is the plant stationary load, ΣW_{CIR} is the circulator workload in the primary, intermediate, and, if present, tertiary loops, Q_{th} is the reactor thermal power, and Q_{H2} is the power supplied through the PHX to the hydrogen generating plant. For the efficiency calculations, we report the overall cycle efficiency, which is defined as

$$\eta_{overall} = \frac{\Sigma W_T - \Sigma W_C - W_S - \Sigma W_{CIR} + 0.5 * Q_{H2}}{Q_{th}}, \tag{12}$$

where the efficiency of the hydrogen generation process was assumed to be 50%. The plant stationary load was neglected in the current analysis.

The polytropic efficiency, rather than the isentropic efficiency, is used for representing the efficiency of the turbomachinery. The equations for the expansion and compression processes in a perfect gas are taken from Saravanamuttoo et al. (1996). For an expansion, the efficiency is calculated from

$$\frac{T_{0,ex}}{T_{0,in}} = \left(\frac{P_{0,ex}}{P_{0,in}}\right)^{\left(\frac{R}{C_P}\eta_{p,e}\right)}, \tag{13}$$

where R is the gas constant, C_p is the specific heat, $\eta_{p,e}$ is the turbine polytropic efficiency, T_0 is the stagnation temperature, and P_0 is the stagnation pressure. Subscripts *ex* and *in* refer to exit gas and inlet gas, respectively. For a compression, the efficiency is calculated from

$$\frac{T_{0,ex}}{T_{0,in}} = \left(\frac{P_{0,ex}}{P_{0,in}}\right)^{\left(\frac{R}{C_P}\frac{1}{\eta_{p,c}}\right)}. \tag{14}$$

HYSYS was used to develop an input model for each configuration and working fluid and to optimize the cycle efficiency. HYSYS uses the Peng-Robinson (1976) equation of state to determine the properties of the working fluids. However, HYSYS does not have thermal properties for molten salts. Therefore, the physical and thermal properties of Flinak and $NaBF_4$-NaF were input as hypothetical components in tabular form.

The efficiencies of the turbine and compressors were assumed to be 92% and 90%, respectively. Figures 1 through 7 show a single shaft connecting one turbine and one compressor. However, two compressors, a high-pressure compressor (HPC) and a low-pressure compressor (LPC), were used for better cycle efficiency. The pressure ratio, which is defined as the outlet pressure from the HPC divided by the inlet pressure to the LPC, was varied to optimize the overall cycle efficiency. Each compressor was assumed to provide half of the overall pumping power. Cooling was applied between compressors to reduce the power consumed by the HPC. Cooler components were used to simulate the heat loss and differential pressure along the hot and cold legs of the intermediate heat transport loop.

5. RESULTS

The methods described in Section 4 were applied to the configurations shown in Section 3 to evaluate their thermal-hydraulic and efficiency characteristics. Results from the simplified stress analysis are presented in Section 5.1. Results from the thermal-hydraulic analysis are presented in Section 5.2. Section 5.3 contains results from the evaluation of cycle efficiency.

5.1 Stress Evaluation

The maximum circumferential stress for the hot leg of the intermediate heat transport loop was calculated from Equation (1) for internal pressures between 2 MPa and 7 MPa assuming that the external pressure was 0 MPa. A pressure of 2 MPa corresponds to the use of either low-pressure helium or a liquid salt as the working fluid. A pressure of 7 MPa corresponds to the use of high-pressure helium as the working fluid.

The results of these calculations are shown in Figure 11 as a function of the thickness-to-diameter ratio, $t/d = (r_o - r_i)/(2r_i)$, of the hot leg pipe. The figure also shows the rupture strength of Alloy 800HT and Alloy 617 after 10^5 hours of operation at 900 °C (Special Metals 2004a, Special Metals 2004b). The maximum allowable stress would be decreased from the rupture strength to account for desired lifetimes greater than 10^5 hours (11 years) and required safety factors. For this analysis, the maximum allowable stress was assumed to be 10 MPa, which is approximately half of the rupture strength of Alloy 617. To achieve a maximum stress of 10 MPa, the required thickness-to-diameter ratios were calculated from Equation (2). The limiting ratios were 0.11 for an internal pressure of 2 MPa, 0.37 for 5 MPa, and 0.69 at 7 MPa. As a point of reference, the thickness-to diameter ratio for Schedule 160 pipe, the thickest commercially available in the size range of interest here (Crane 1979), is 0.14.
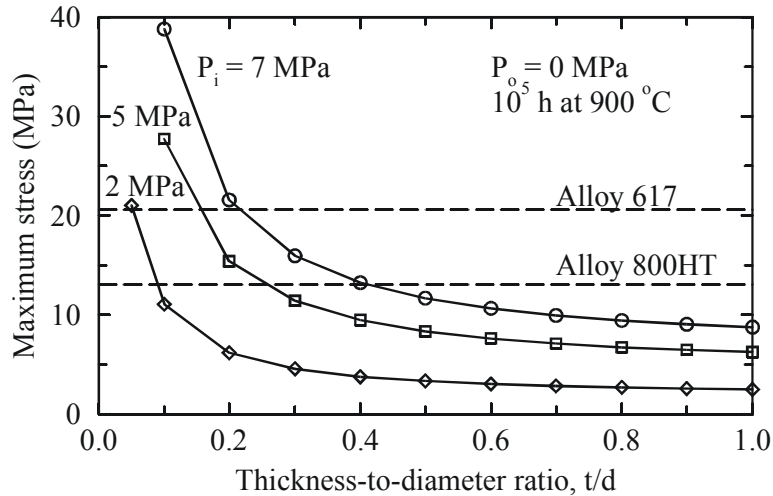
Figure 11. Circumferential stress as a function of thickness-to-diameter ratio.

These simple calculations suggest that a reasonable piping thickness can be obtained for operating pressures and temperatures of 2 MPa and 900 °C. However, the required thickness for operating pressures greater than 5 MPa are not reasonable given maximum values for commercially available pipe. Although these calculations assume separate hot and cold leg piping, and not the alternative (concentric) configurations that can be used to mitigate the stress, they provide a useful indication of the piping issues. If helium is the working fluid, it is desirable to keep the loop pressure high because the pumping power increases as the pressure decreases. Thus, cycle efficiency is degraded at low pressures. However, for configurations in which the heat transport loop is not connected to the PCU, the use of reduced pressure may be desirable to limit stresses in the hot leg. The liquid salts have a significant advantage compared to helium in terms of pipe thickness because they can be used more efficiently at low pressure.

These results suggest that reasonable thicknesses in the hot leg of the intermediate heat transport loop cannot be achieved with separate hot and cold legs if helium is the working fluid and a high pressure is desired to obtain a high efficiency. However, other options are available in order to obtain an acceptable mechanical design. These options include using stronger materials, such as oxide dispersion strengthened alloys or ceramics, insulating the inside surface of the pipe to limit the temperature during normal operating conditions, or using an annular arrangement, with the hot stream flowing in the inner pipe and the cold stream flowing in the other direction in the outer annulus.

The design of the cold leg piping is easier since the stress rupture strength is much higher at lower temperatures. According to Figure 8, the rupture strength of Alloy 800 is 240 MPa for 10^5 hours of operation at 500 °C and is 42 MPa at 700 °C. The allowable stress was assumed to be half of the rupture strength. Equation (2) was used to determine the required thickness-to-diameter ratio for several different cases involving different working fluids and pressure. The exterior pressure was assumed to be 0 MPa. The results for the hot and cold legs are summarized in Table 2.

Table 2. Summary of the stress calculations for the intermediate heat transport loop piping.

Leg	P_i (MPa) / T (°C)	σ_D (MPa)	t/d	Comments
Hot	2 / 900	10	0.11	Low-pressure helium or liquid salt
Hot	3.5 / 900	10	0.22	Intermediate pressure
Hot	5 / 900	10	0.37	Intermediate pressure
Hot	7 / 900	10	0.69	High-pressure helium
Cold	2 / 500	120	0.01	Low-pressure helium
Cold	2 / 700	42	0.05	Low-pressure liquid salt
Cold	7 / 500	120	0.03	High-pressure helium

A simple stress analysis was also performed for the IHX. Equations (2) and (5) were used to calculate the thickness-to-diameter and pitch-to-diameter ratios for the IHX as a function of allowable stress and various pressures of the hot and cold streams. The allowable stress was assumed to be 10 MPa.

The results of the stress calculations for the IHX are summarized in Table 3. Three cases were evaluated. The first case assumed that the inner and outer pressures were 7 and 0 MPa, respectively. This case required the largest pitch and plate thickness, but had the advantage that the pressure difference between the hot and cold streams would not have to be controlled closely during operation. The second case assumed that the inner and outer pressures were 7 and 5 MPa, respectively. This case assumes that a high pressure coolant is used on the cold side of the IHX. A pressure difference of 2 MPa between the hot and cold streams was assumed for flexibility during operation. The third case assumed that the outer pressure was 2 MPa, corresponding to the use of either low-pressure helium or liquid salt in the heat transport loop. The use of a low pressure coolant requires thicker plates and a larger pitch, which results in a larger heat exchanger.

Table 3. Summary of the stress calculations for the IHX.

P_i / P_o (MPa)	p/d	t_p/d	Comments
7 / 0	1.70	1.19	Maximum differential pressure
7 / 5	1.20	0.57	High-pressure helium
7 / 2	1.50	0.78	Low-pressure helium or liquid salt

The results shown in Figure 11 are also applicable to the shell of the PHX. However, the magnitude of the circumferential stress in the PHX tubes, which see a higher pressure on the outside of the tubes, is greater than that shown in Figure 11. The radius ratio that caused the maximum of the absolute value of the stress to be less than the allowable stress was calculated from Equation (3) as a function of the external pressure for an allowable stress of 10 MPa and an internal pressure of zero. The required thickness-to-diameter ratio was 0.15 for an external pressure of 2 MPa. However, for an external pressure of 7 MPa, the magnitude of the stress exceeded the allowable value for all ratios. The rupture strength for Alloy 617 after 10^4 hours of operation at 880 °C is about 48 MPa (Special Metals 2004b). Dividing the rupture strength by two yields an estimated allowable stress of 24 MPa. Using this allowable value, the required thickness-to-diameter ratio was 0.27 for an external pressure of 7 MPa. The use of high-pressure helium will require relatively thick PHX tubes and will result in a relatively short lifetime (a little over a year) using currently available materials. The results of these calculations are summarized in Table 4.

Table 4. Summary of the stress calculations for the PHX.

P_i / P_o (MPa)	σ_D (MPa)	t/d	Comments
0 /7	10	∞	High-pressure helium. Allowable stress based on Alloy 617 after 10^5 hours of operation at 900 °C.
0 / 7	24	0.27	High-pressure helium. Allowable stress based on Alloy 617 after 10^4 hours of operation at 900 °C.
0 / 2	10	0.15	Low-pressure helium or molten salt. Allowable stress based on Alloy 617 after 10^5 hours of operation at 900 °C.

The stress calculations indicate that a low-pressure fluid, either helium or liquid salt, is more attractive for the heat transport loop than high-pressure helium at the current time. Low pressure reduces the stresses in the PHX tubes, which are the limiting components in the heat transport loop, to manageable levels using existing materials. Although the use of low-pressure helium is considered viable for the NGNP, it probably is not viable for a plant in which the entire thermal output is used for hydrogen production because of pumping power requirements for a low-pressure gas. The use of high-pressure helium will require either new materials with higher rupture strengths or more sophisticated designs, such as a compact PHX, rather than a tube-in-shell design.

The simple stress analysis performed here will probably result in smaller components than would be obtained from a more rigorous analysis. For example, the finite element analysis performed by Peterson et al. (2004) showed that the maximum stress near the corners of the semi-circular channels was significantly greater than the average stress between channels of the IHX. Similarly, the stresses calculated for the hot legs of the intermediate heat transport loop did not include the effects of radial components, which become significant when the internal pressure approaches the allowable stress. The stresses for the hot and cold leg pipes did not account for the effects of fittings and bends. The size of the heat exchangers would also be increased by accounting for the distribution headers, which were neglected in the current study. The simple analyses performed here are considered adequate to evaluate the relative differences between configurations, but more detailed calculations will be required during the design process.

In summary, Alloy 617 has greater rupture strength at 900 °C than either Alloy 800HT or Hastelloy X. Thus, Alloy 617 is currently the preferred material for the high-temperature portions of the heat transport loop from strength considerations. The simplified stress analysis indicates that the PHX tubes are the most limiting components in the heat transport loop. Based on an allowable stress of 10 MPa, which is probably the highest that can be expected for Alloy 617 at 900 °C, the PHX can not be designed for a

long lifetime ($> 10^5$ h) if the operating pressure is 7 MPa. A reasonable tube thickness can be achieved if the pressure is reduced to 2 MPa. Thus, the PHX should be placed within a relatively low pressure loop. The stresses from the simple analysis described here will probably be less than would result from more rigorous calculations. Consequently, the component sizes calculated here will probably be less than actually required, but should be adequate for an evaluation of the relative differences between configurations.

5.2 Thermal-Hydraulic Evaluation

Evaluations were performed to determine various thermal-hydraulic parameters, such as the thermodynamic state, mass flow rate, etc., at various locations in the intermediate heat transport loop for the configurations illustrated in Figures 1 through 7. The nominal pressure in the intermediate heat transport loop was 2.0 MPa based on the results of the stress calculations presented in Section 5.1. The other thermal-hydraulic parameters were primarily a consequence of the assumptions and requirements described in Section 2 and the need to obtain relatively large log-mean temperature differences across the heat exchangers to reduce their size. For those cases using liquid salts as coolants, the thermal-hydraulic parameters were also affected by the need to achieve a reasonable amount of margin between the minimum temperature in the loop and the freezing temperature of the salt. Although freezing is not of concern with helium, similar temperatures were generally assumed with all coolants so that consistent comparisons between coolants were obtained.

Scoping calculations were also performed to estimate the relative sizes of the various components using the methods described in Section 4.2. The thermal-hydraulic evaluations for the seven configurations are described in Sections 5.2.1 through 5.2.7. The thermal-hydraulic performances of the seven configurations are compared in Section 5.2.8.

5.2.1 Configuration 1

Configuration 1, which is illustrated in Figure 1, utilizes a direct electrical cycle. The IHX, which removes less than 10% of the reactor power and directs it towards the hydrogen production plant, is located upstream of the PCU. This configuration is the simplest configuration in terms of equipment and may be especially suitable for the demonstration of hydrogen production. However, the overall efficiency of the electrical production process is reduced because the PCU receives a lower temperature fluid. Based on the results of the stress analysis, the pressure in the heat transport loop is assumed to be relatively low, 2 MPa. Calculations were performed to size the IHX, the hot and cold legs of the loop piping, and the PHX assuming that the working fluid is either helium or a liquid salt.

The IHX was assumed to be a printed circuit heat exchanger (PCHE) with straight semi-circular flow channels. Based on the results presented in Section 5.1, the pitch-to-diameter ratio of the channels was set to 1.50 and the plate thickness-to-diameter ratio was set to 0.78. The diameter of the semi-circular fluid channels was assumed to be 1.5 mm, which is a representative value. For example, Dostal et al. (2004) used 2.0 mm while Peterson et al. (2004) used 1.0 and 3.0 mm. The pressure drop across the hot side of the IHX was assumed to be 0.05 MPa. Since this pressure drop is the same as that across the core in the GT-MHR, the required pumping power for the hot side of the IHX will be the same as that required for the core. The temperature drop across the cold side of the IHX was assumed to be 400 °C when the working fluid was helium and 200 °C when the working fluid was a liquid salt. The smaller temperature rise with the liquid salt increases the margin between the minimum temperature in the loop at normal operating conditions and the freezing temperatures of 454 and 385 °C for Flinak and NaBF$_4$-NaF, respectively.

Table 5 shows the effect of the working fluid in the heat transport loop on various IHX parameters. The IHX operated in the turbulent regime on the hot side and in the laminar regime on the cold side. Design values were chosen so that neither side operated in the transition region between the turbulent and laminar regimes. Even though the log-mean temperature difference was 60% greater with helium as the working fluid, which would result in a significantly smaller heat exchanger according to Equation (7), the better heat transport properties of the liquid salts compensated for much of the difference in temperature. The total volume of the IHX was actually reduced by about 10% with Flinak and increased by about 20% with $NaBF_4$-NaF. Since the capital cost of the IHX can be expected to be roughly proportional to its size, it is expected that the use of Flinak would reduce the capital cost of the IHX by about 10% compared to low-pressure helium whereas the cost would increase by about 20% with $NaBF_4$-NaF. The pumping powers for the liquid salts were orders of magnitude lower than for helium.

Table 5. IHX parameters for Configuration 1.

Parameter	He/He	He/Flinak	He/NaBF$_4$-NaF
Log-mean temperature difference, °C	124	78	78
Hot / cold fluid pressure drop, Pa	5.0E4 / 3.3E3	5.0E4 / 4.3E2	5.0E4 / 2.4E2
Hot / cold fluid pumping power, W	3.4E6 / 6.2E4	3.4E6 / 2.8E1	3.4E6 / 1.9E1
Hot /cold fluid Reynolds number	5510 / 530	5800 / 64	5130 / 200
Width, m	2.37	2.31	2.45
Length, m	0.076	0.070	0.086
Volume, m^3	0.42	0.37	0.52

Table 5 shows that the width of the front face of the IHX is much bigger than the length of the channels. The resulting small aspect ratio will complicate the design and construction of the heat exchanger. For example, if the heat exchanger contains counterflow and crossflow regions such as illustrated by Dewson and Thonon (2003), the length of the crossflow region will greatly exceed the length of the counterflow region and the pressure drop will greatly exceed the value reported here, which accounts only for the counterflow region. According to Dostal et al. (2004), the maximum width currently available for a Heatric heat exchanger module is 0.6 m. Thus, either several modules would have to be combined in parallel to obtain the required number of channels, which would complicate the design of the headers, or the height of the heat exchanger will have to greatly exceed its width, which would cause the heat exchanger to be less compact. The relatively long length of the headers may also cause flow distribution problems between channels.

Table 5 shows that the pressure drop on the cold side of the IHX is much less than on the hot side even when the working fluid is low-pressure helium. The smaller pressure drop is partially caused by a much lower velocity of the cold stream compared to that of the hot stream. Preliminary calculations suggest that the velocity of the cold stream can be increased to nearer that of the hot stream by allowing the hot fluid to flow through two thirds of the plates rather than every other plate as assumed previously. Preliminary calculations show that the total volume of the IHX could be reduced by about 30% by using this technique with either low-pressure helium or a liquid salt as the working fluid. Since reducing the size of the IHX should lower the capital cost, there appears to be a clear benefit in using two layers of hot plates per cold layer and this approach should be considered further. Peterson et al. (2004) describe an alternate approach where a smaller diameter was applied to the semi-circular channel of the low-velocity fluid.

The PHX was assumed to consist of tubes in a shell with the process fluid flowing inside the tubes and the working fluid of the intermediate heat transport loop flowing inside the shell. This configuration is

convenient for hydrogen production because it allows the catalysts to be placed inside the tubes. The inner diameter of the tube was assumed to be 1.0 cm. The thickness-to-inner-diameter ratio of the tubes was 0.15 based on the results presented in Table 4. The pitch-to-outer-diameter ratio of the tubes was set to 1.3, a typical value for tube bundles. The tube bundle was assumed to have a triangular pitch. The inlet and outlet temperatures of the hot stream were based on those used previously for the IHX after accounting for the heat losses in the hot and cold legs. The difference between the inlet and outlet temperatures of the cold stream was 100 °C more than that of the hot stream to increase the log-mean temperature difference and reduce the size of the PHX. Because details on the heat transfer coefficient and fluid temperature distributions for the process side of the PHX are not yet available, results for the PHX are considered more uncertain than for the other components in the intermediate heat transport loop.

Table 6 shows the effect of the working fluid in the intermediate heat transport loop on various PHX parameters. The PHX operated in the turbulent regime on the hot side of the heat exchanger for all three fluids. The larger log-mean temperature differences and better heat transport properties of the liquid salts resulted in significantly smaller heat exchangers. For example, the PHX volumes with Flinak and $NaBF_4$-NaF were about 30% of that obtained with helium as the working fluid.   Since the capital cost of the PHX can be expected to be roughly proportional to its size, it is expected that the use of a liquid salt would reduce the capital cost of the PHX substantially compared to low-pressure helium. The pumping powers of the liquid salts were much smaller than for helium.

Table 6. PHX parameters for Configuration 1.

Parameter	He	Flinak	$NaBF_4$-NaF
Log-mean temperature difference, °C	56	117	117
Hot fluid pressure drop, Pa	5.0E4	1.0E4	1.0E4
Hot fluid pumping power, W	9.5E5	6.5E2	9.4E2
Hot fluid Reynolds number	1.6E4	5.8E3	1.9E4
Shell inner diameter, m	1.02	0.58	0.60
Length, m	10.2	10.0	8.82
Volume, m^3	8.40	2.61	2.49
Number of tubes	3320	1050	1140

Parametric calculations were performed to investigate the effects of tube inner diameter, the pitch-to-diameter ratio, and the pressure drop across the hot stream for the option with helium as the working fluid. Increasing the tube inner diameter by a factor of two increased the total volume by a factor of 2.2, primarily because of an increase in the tube length. Decreasing the pitch-to-diameter ratio from 1.3 to 1.2 decreased the total volume by 17% and the length by 35%.   Increasing the pressure drop across the hot stream by a factor of two, which also increases the pumping power by a factor of two, decreased the total volume by 11% and increased the length by 20%.

The configuration of the intermediate loop piping consisted of separate hot and cold legs.   The length of the legs was assumed to be 90 m, the average of the values recommended by Smith et al. (2005). Somewhat different assumptions were made depending on the working fluid. With helium as the working fluid, the inner diameters of the hot and cold legs were sized to provide pressure drops of 0.05 MPa, the same as assumed previously for the hot stream of the IHX. The heat loss from the piping was assumed to cause a 10 °C temperature drop in fluid temperature across the hot leg and a 4.3 °C drop across the cold leg. The same heat losses were assumed with the liquid salts, but these heat losses caused half of the temperature change assumed with helium because the overall temperature change across the loop was half of that with helium. The inner diameters of the hot and cold legs were sized to provide a pressure drop of 0.30 MPa with the liquid salts. The thickness-to-diameter ratios were obtained from the stress analysis

summarized in Table 2. For the hot leg, the thickness-to-diameter ratio was 0.11. For the cold leg, the thickness-to-diameter ratio was 0.01 for helium and 0.05 for liquid salt. The thickness of the insulation was adjusted to obtain the desired heat loss.

Calculated parameters for the hot and cold legs are summarized in Table 7. The use of liquid salts results in several benefits relative to the piping. First, the pipes are much smaller, roughly 35% of the diameter, with a salt as the working fluid. Second, the smaller diameter results in much less metal volume. Even accounting for the thinner cold leg resulting from the lower cold leg temperature with helium, the total metal volume with the salts is only 15% of that with helium. The reduction in metal volume will reduce the capital cost of the system. Third, the amount of insulation required to achieve the same heat loss was reduced significantly with salt because of the reduced pipe diameter and the corresponding reduction in heat transfer area. The thickness of insulation required with the salts varied between 14% and 47% of that required with helium. Finally, the pumping power was much less with the salts, about 0.05 MW versus 1.9 MW with helium. The pipe diameters were about 10% larger with $NaBF_4$-NaF compared to Flinak.

Table 7. Hot/cold leg parameters for Configuration 1.

Parameter	He	Flinak	$NaBF_4$-NaF
Hot / cold legs			
Inner diameter, m	0.422 / 0.387	0.130 / 0.129	0.145 / 0.143
Insulation thickness, m	5.5E-3 / 4.1E-3	7.9E-4 / 1.6E-3	9.9E-4 / 1.9E-3
Differential pressure, Pa	5.0E4 / 5.0E4	3.0E5 / 3.0E5	3.0E5 / 3.0E5
Pumping power, W	9.5E5 / 9.5E5	2.0E4 / 2.0E4	2.8E4 / 2.8E4
Heat loss, W	1.25E6 / 5.4E5	1.25E6 / 5.4E5	1.25E6 / 5.4E5
Reynolds number	1.4E6 / 2.1E6	8.6E5 / 4.1E5	2.4E6 / 1.6E6

The effects of hot leg pipe diameter on normalized pumping power are shown in Figure 12 for low-pressure helium, high-pressure helium, Flinak, and $NaBF_4$-NaF. The use of low-pressure helium caused the required diameter to increase by 60% compared to high-pressure helium. Thus, a substantial reduction in piping size could be achieved by using a stronger material that could withstand the stresses associated with higher pressure.   Figure 12 also shows that the use of liquid salts results in significantly smaller pipes and pumping powers. The highest pumping powers and smallest diameters for the liquid salts correspond to a pressure drop of 1.0 MPa in the hot leg. Any further decrease in diameter would cause the maximum pressure in the heat transport loop to exceed the 2-MPa value used in the stress analysis. For a given normalized pumping power, the required pipe diameter increased by 19% when Flinak was replaced by $NaBF_4$-NaF.

Figure 12. Hot leg diameter versus normalized pumping power for Configuration 1.

The thermal-hydraulic conditions in the intermediate heat transport loop for Configuration 1 are summarized in Figures 13, 14, and 15 assuming that low-pressure helium, Flinak, and NaBF$_4$-NaF are the working fluids, respectively.

Figure 13. Thermal-hydraulic conditions for Configuration 1 with low-pressure helium.

Figure 14. Thermal-hydraulic conditions for Configuration 1 with Flinak.

Figure 15. Thermal-hydraulic conditions for Configuration 1 with $NaBF_4$-NaF.

The total pumping power for the intermediate heat transport loop was between 50 and 100 times smaller when liquid salts were used as the working fluid rather than helium. The lower pumping power will improve the overall efficiency of the cycle. However, the improvement is relatively small for the dual-purpose facility evaluated here because the pumping power for the entire loop is only 0.5% of the reactor power even with low-pressure helium as the working fluid.

Calculations were performed to investigate the effects of various parameters on component sizes in the intermediate heat transport loop. These parametric calculations are described below.

Effects of Separation Distance

The effects of separation distance between the nuclear and hydrogen plants on the required inner diameters for the hot and cold legs are shown in Figure 16 for low-pressure helium. The required diameters decreased by 8% when the separation distance was decreased from 90 to 60 m. The required diameters increased by 52% when the separation distance increased from 90 to 500 m. Almost identical percentage changes were obtained for Flinak. Thus, the separation distance has a significant effect on the required diameters of the hot and cold legs of the intermediate heat transport loop.
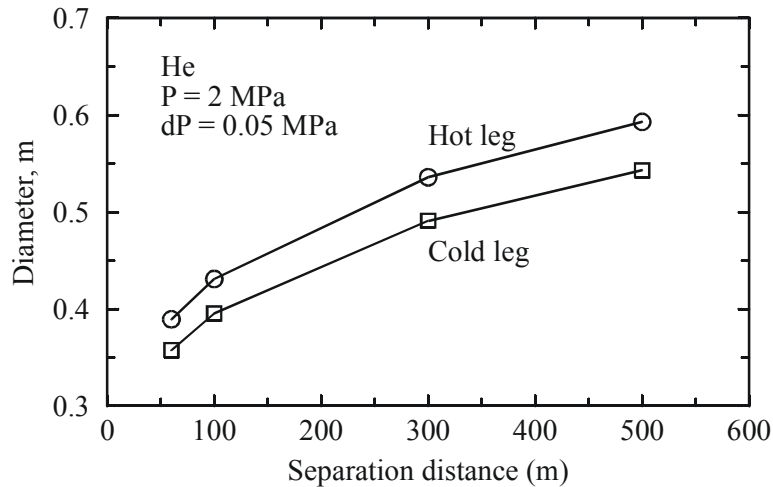
Figure 16. The effects of separation distance on pipe diameters for Configuration 1.

The separation distance also affects the maximum velocity of the fluid in the intermediate heat transport loop because it affects the pipe diameter and flow area. The maximum velocity with low-pressure helium varies between 240 and 100 m/s as the separation distance varies between 60 and 500 m. At the nominal length of 90 m, the maximum velocity is 200 m/s. Although this large velocity might be of concern relative to erosion damage in the loop, the density of the helium is small and its dynamic head is less than that in the steam lines of existing nuclear reactors. Thus, erosion should not be of concern unless the piping material is much more susceptible to erosion than the materials used in existing plants. In any case, the velocity in the hot leg can always be reduced by using a larger pipe.

Parametric calculations related to heat loss were performed. Without insulation, the combined heat loss from the hot and cold legs was 15% of the total thermal power applied to the loop for low-pressure helium. For the liquid salts, the heat loss was about 8% of the total thermal power. Between 0.1 and 0.5 cm of insulation were sufficient to reduce the combined heat loss to less than 4% of the total thermal power applied to the loop for a separation distance of 90 m. As shown in Figure 17, more insulation was required when the separation distance increased. The figure also shows that the amount of insulation required is much less with either liquid salt than with low-pressure helium. However, the heat loss appears to be manageable with a reasonable amount of insulation with any of the working fluids evaluated. The insulation will experience a high service temperature, with a maximum value near 870 °C.

24
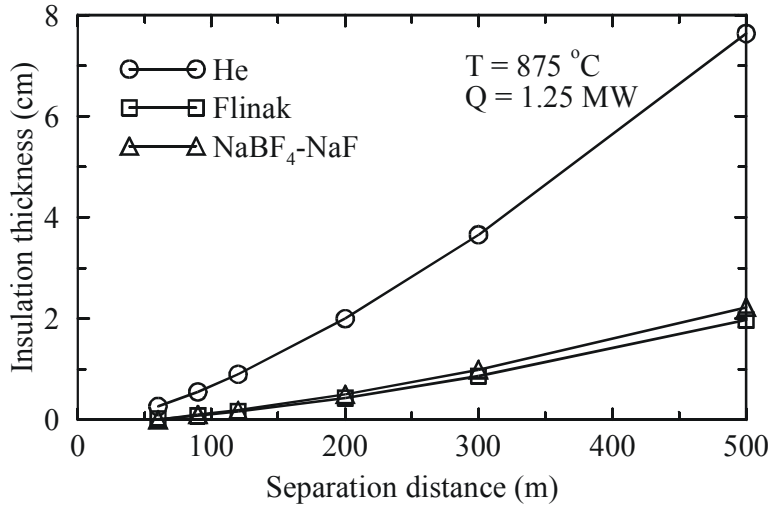
Figure 17. The effect of separation distance on required insulation thickness in the hot leg of Configuration 1.

Effects of Heat Loss

The results shown previously were obtained with a total heat loss of 1.79 MW in the intermediate loop piping. Parametric calculations were performed assuming that there was no heat loss. Without heat loss, the log-mean differential temperature across the IHX was larger than in the original calculation, resulting in a 7% smaller heat exchanger. The PHX was nearly the same size as in the original calculation because the increased log-mean differential temperature was compensated for an increase in the power removed by the heat exchanger. The increased power delivered to the hydrogen production plant was estimated to cause a 0.15% increase in the overall efficiency of the cycle.

Effects of Power

An evaluation was performed in which the entire thermal output of the NGNP was directed towards the hydrogen production plant. For this case, the IHX and intermediate heat transport loop were sized to transport 600 MW, rather than the 50 MW assumed previously. The method was the same as that used previously except that the temperature rise across the hot stream of the IHX was increased slightly, from 400 to 405 °C, to account for pumping power in the primary coolant system. In the previous calculations, the pumping power was assumed to be removed by the PCU, but the pumping power had to be removed through the IHX in this case. The temperature rise of the cold stream of the IHX was also assumed to be 405 °C. Calculations were performed with low-pressure helium and $NaBF_4$-NaF working fluids. The margin between the minimum temperature in the loop and the freezing temperature was 86 °C with $NaBF_4$-NaF. The corresponding margin with Flinak was 17 °C, which was judged to be insufficient. Consequently, calculations were not performed with Flinak as the working fluid. The parameters for the loop piping and the PHX were the same as those used previously except that the same thickness-to-diameter ratio (0.01) of the cold leg was applied for both fluids because their cold leg temperatures were the same.

The effects of the working fluid on various parameters are summarized in Table 8. The volumes of the IHX and PHX were 15 and 35% smaller, respectively, when the working fluid was $NaBF_4$-NaF than when it was helium. The relative effect of the working fluid was different between the two heat exchangers because of variations in the log-mean temperature difference between heat exchangers. In the IHX, the

25

log-mean temperature difference was the same for both working fluids, and the difference in size was a consequence of the better heat transport properties of the liquid salt. The log-mean temperature difference across the PHX was smaller with helium as the working fluid because the larger pumping power resulted in a significant temperature rise across the compressor. Thus, the effect of the working fluid on the PHX volume was a consequence of the better heat transport properties of the liquid salt coupled with the larger temperature difference.

Table 8. Intermediate heat transport loop parameters for Configuration 1 at high power.

Parameter	He/He	He/ $NaBF_4$-NaF
IHX:		
Log-mean temperature difference, °C	26	26
Hot / cold fluid pressure drop, Pa	5.0E4 / 1.7E5	5.0E4 / 6.9E3
Hot / cold fluid pumping power, W	3.4E6 / 3.72E7	3.4E6 / 3.6E3
Hot /cold fluid Reynolds number	1330 / 1356	1440 / 240
Width, m	5.12	4.92
Length, m	1.52	1.40
Volume, m³	39.8	33.9
PHX:		
Log-mean temperature difference, °C	48	63
Hot fluid pressure drop, Pa	5.0E4	2.0E3
Hot fluid pumping power, W	1.12E7	1.0E3
Hot fluid Reynolds number	1.5E4	4.4E3
Shell inner diameter, m	3.73	2.72
Length, m	12.4	15.1
Volume, m³	135	87.7
Number of tubes	4.4E4	2.4E4
Hot / cold legs:		
Inner diameter, m	1.09 / 1.00	0.29 / 0.28
Insulation thickness, m	0.019 / 0.017	0.0032 / 0.0020
Differential pressure, Pa	5.0E4 / 5.0E4	3.0E5 / 3.0E5
Pumping power, W	1.12E7 / 1.12E7	1.6E5 / 1.6E5
Heat loss, W	1.25E6 / 5.4E5	1.25E6 / 5.4E5
Reynolds number	6.6E6 / 9.8E6	7.1E6 / 2.5E6

The effect of the working fluid is more significant on the size and insulation requirements for the hot and cold legs. Similar to the results presented previously in Table 7, the diameters of the hot and cold leg pipes are about 70% smaller with the liquid salt as the working fluid. The smaller diameter results in much less metal volume and insulation.

The working fluid significantly affected the pumping power for the heat transport loop. The pumping power for the heat transport loop was 70.8 MW when the working fluid was low-pressure helium and 0.3 MW when it was $NaBF_4$-NaF. Assuming an efficiency of 50% for the hydrogen production process, the additional pumping power required for low-pressure helium would reduce the overall cycle efficiency by 5.9%. Although the additional pumping power required for low-pressure helium did not affect the overall cycle efficiency significantly when 50 MW were applied to the heat transport loop, the effect on cycle efficiency becomes significant when the entire reactor power is applied to hydrogen production.

The thermal-hydraulic states in the intermediate heat transport loop are summarized in Figures 18 and 19 for helium and $NaBF_4$-NaF, as the working fluids, respectively. Although the figures show various components of the PCU, only the compressor would actually be needed for this configuration because all of the reactor power was transported to the hydrogen production plant, with none left for electricity generation.
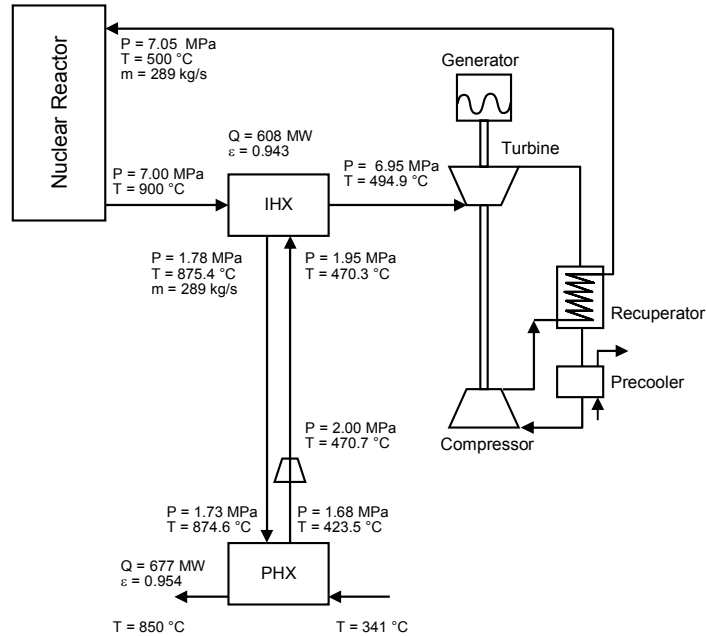
Figure 18. Thermal-hydraulic states for Configuration 1 at high power with low-pressure helium.
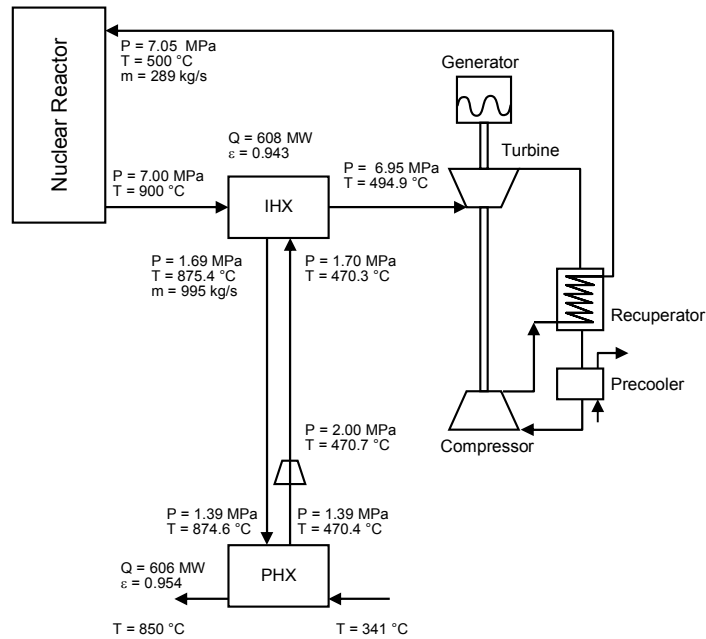
Figure 19. Thermal-hydraulic states for Configuration 1 at high power with $NaBF_4$-NaF.

Effects of Reactor Outlet Temperature

An evaluation was performed to determine the effects of increasing the outlet temperature of the NGNP from 900 to 1000 °C on the heat transport loop. The other parameters were the same as used previously. This evaluation assumed that low-pressure helium was the working fluid in the intermediate heat transport loop. The higher inlet temperature to the IHX in this case would increase the margin to freezing and hence would improve the relative performance of liquid salt. This evaluation implicitly assumed that stronger materials than those considered in Section 4.1 were available to meet the creep rupture strength requirements.

The increased outlet temperature allowed a larger temperature drop across each heat exchanger to still achieve an outlet temperature of 850 °C on the process side of the PHX. Assuming a 10 °C temperature drop across the hot leg, the allowed temperature drop for each heat exchanger was 70 °C (= [1000 – 850 – 10]/2 °C).

The effect of the NGNP outlet temperature on various parameters in the intermediate heat transport loop is presented in Table 9. The principal effect of the higher outlet temperature was to increase the log-mean temperature difference, which reduced the size of the heat exchangers by from 40 to 55%. The higher outlet temperature required the diameters of the hot and cold legs to increase by about 1%. The insulation thickness required in the hot and cold legs increased by from 10 to 30% because the legs were operating at higher temperature. These results show that an increase in the outlet temperature of the NGNP could be used to reduce the size and capital cost of the heat exchangers. An alternate approach would be to keep the size of components as described previously and to supply an increased temperature to the hydrogen production plant to increase the efficiency of the cycle.

Table 9. The effect of NGNP outlet temperature on intermediate heat transport loop parameters for Configuration 1.

Parameter	900 °C	1000 °C
IHX:		
Log-mean temperature difference, °C	124	200
Hot / cold fluid pressure drop, Pa	5.0E4 / 3.3E3	5.0E4 / 2.9E3
Hot / cold fluid pumping power, W	3.4E6 / 6.2E4	3.8E6 / 5.9E4
Hot /cold fluid Reynolds number	5510 / 530	6110 / 600
Width, m	2.37	2.18
Length, m	0.076	0.052
Volume, m^3	0.42	0.25
PHX:		
Log-mean temperature difference, °C	56	112
Hot fluid pressure drop, Pa	5.0E4	5.0E4
Hot fluid pumping power, W	9.5E5	1.0E6
Hot fluid Reynolds number	1.6E4	2.0E4
Shell inner diameter, m	1.02	0.89
Length, m	10.2	6.00
Volume, m^3	8.40	3.76
Number of tubes	3320	2530
Hot / cold legs:		
Inner diameter, m	0.422 / 0.387	0.426 / 0.392
Insulation thickness, m	0.0055 / 0.0041	0.0062 / 0.0053

Differential pressure, Pa	5.0E4 / 5.0E4	5.0E4 / 5.0E4
Pumping power, W	9.5E5 / 9.5E5	1.0E6 / 1.0E6
Heat loss, W	1.25E6 / 5.4E5	1.25E6 / 5.4E5
Reynolds number	1.4E6 / 2.1E6	1.4E6 / 2.0E6

The thermal-hydraulic states in the intermediate heat transport loop for this configuration are summarized in Figure 20. The higher outlet temperature of the reactor increased the operating temperature of the intermediate heat transport loop by about 50 °C. The other parameters were generally similar to those shown in Figure 13.
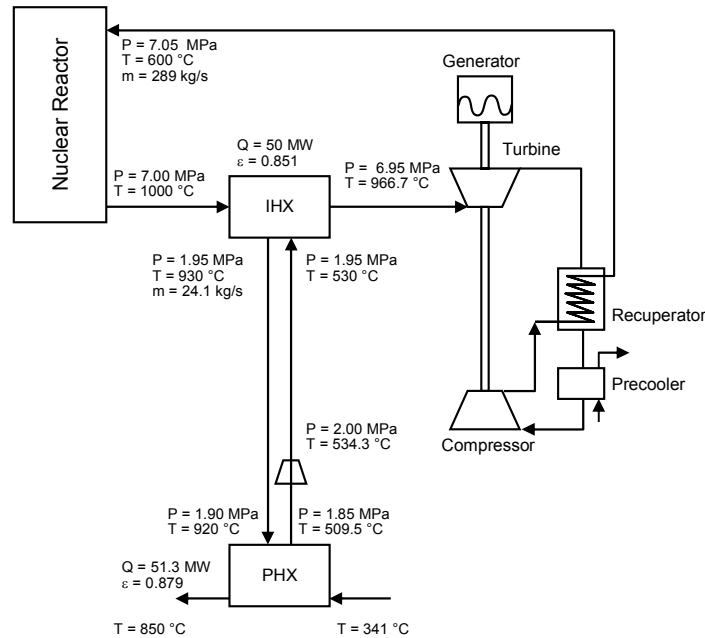
Figure 20. Thermal-hydraulic states for Configuration 1 with a reactor outlet temperature of 1000 °C.

Effects of Pressure

An evaluation was performed to determine the effect of increasing the pressure in the intermediate heat transport loop from 2 to 7 MPa with helium as the working fluid. The parameters for this evaluation were the same as used previously. This evaluation implicitly assumed that stronger materials than those considered in Section 4.1 were available to meet the creep rupture strength requirements.

Table 10 shows that the use of high-pressure helium did not significantly affect the IHX, but reduced the size of the PHX and the piping. The volume of the PHX was reduced by 30% with high-pressure helium. The diameters of the hot and cold legs were reduced by 22%. The reduced diameters of the legs resulted in less insulation to obtain the desired heat loss. The higher pressure increased the density of the helium and reduced the pumping power by 2.1 MW. Thus, significant benefits can be achieved if the strong enough materials are available to increase the operating pressure of the helium.

Table 10. The effect of operating pressure on intermediate heat transport loop parameters for Configuration 1.

Parameter	2 MPa	7 MPa
IHX:		
Log-mean temperature difference, °C	124	124
Hot / cold fluid pressure drop, Pa	5.0E4 / 3.3E3	5.0E4 / 9.4E2
Hot / cold fluid pumping power, W	3.4E6 / 6.2E4	3.4E6 / 5.2E3
Hot /cold fluid Reynolds number	5510 / 530	5540 / 530
Width, m	2.37	2.36
Length, m	0.076	0.075
Volume, m^3	0.42	0.42
PHX:		
Log-mean temperature difference, °C	56	61
Hot fluid pressure drop, Pa	5.0E4	5.0E4
Hot fluid pumping power, W	9.5E5	2.7E5
Hot fluid Reynolds number	1.6E4	2.8E4
Shell inner diameter, m	1.02	0.77
Length, m	10.2	12.9
Volume, m^3	8.40	5.98
Number of tubes	3320	1870
Hot / cold legs:		
Inner diameter, m	0.422 / 0.387	0.330 / 0.304
Insulation thickness, m	0.0055 / 0.0041	0.0039 / 0.0026
Differential pressure, Pa	5.0E4 / 5.0E4	5.0E4 / 5.0E4
Pumping power, W	9.5E5 / 9.5E5	2.7E5 / 2.7E5
Heat loss, W	1.25E6 / 5.4E5	1.25E6 / 5.4E5
Reynolds number	1.4E6 / 2.1E6	1.8E6 / 2.7E6

RELAP5 Calculations

The results presented previously for Configuration 1 were generated with a spreadsheet.   Calculations were also performed with the RELAP5-3D computer code (INEEL 2003a, INEEL 2003b) to validate the results obtained with the spreadsheet. RELAP5 models of the IHX, hot and cold legs, and the PHX were developed. The computer code was used to simulate the nominal configuration illustrated in Tables 5 through 7 with low-pressure helium as the working fluid. Boundary conditions of inlet temperature, mass flow rate, and outlet pressure were applied to each component.

Table 11 compares the results of the spreadsheet with those calculated from RELAP5. The power removed by the IHX and PHX agreed to within 2%. The heat loss from the hot and cold legs agreed within 0.4%. The pressure drops agreed within 3% except for the cold side of the IHX, where the agreement was within 22%. The poorer agreement for this case was primarily due to the difference between the distributions of fluid properties calculated by the code versus the average values assumed in the spreadsheet. Overall, the results were in reasonable agreement, which validates the results obtained from the spreadsheet.

Table 11. Validation comparisons for Configuration 1.

Parameter	Spreadsheet	RELAP5
IHX:		
Power, W	50.0E6	49.3E6
Hot / cold fluid pressure drop, Pa	4.97E4 / 3.28E3	4.90E4 / 4.01E3
PHX:		
Power, W	51.1E6	50.0E6
Hot fluid pressure drop, Pa	5.00E4	4.88E4
Hot /cold leg:		
Heat loss, W	1.25E6 / 0.54E6	1.25E6 / 0.54E6
Pressure drop, Pa	5.00E4 / 5.00E4	5.12E4 / 5.13E4

RELAP5 was also used to investigate the time required to freeze the salt coolant during two transients. The RELAP5 model for Configuration 1 is illustrated in Figure 21. The first transient simulated a loss-of-offsite power with Flinak as the working fluid. The flows in the hot side of the IHX, the cold side of the PHX, and the intermediate heat transport loop were reduced to zero over 10 seconds.   The fluid temperatures then decreased due to heat loss. As shown in Figure 22, the minimum fluid temperature reached 454 °C, the freezing point of Flinak, at 3900 s. Based on the difference in melting temperatures, the onset of freezing would have been delayed by about 1500 s if the salt had been $NaBF_4$-NaF. Thus, there is substantial time available to bring an auxiliary heat source online to prevent freezing in the intermediate heat transport loop following a loss-of-offsite power.
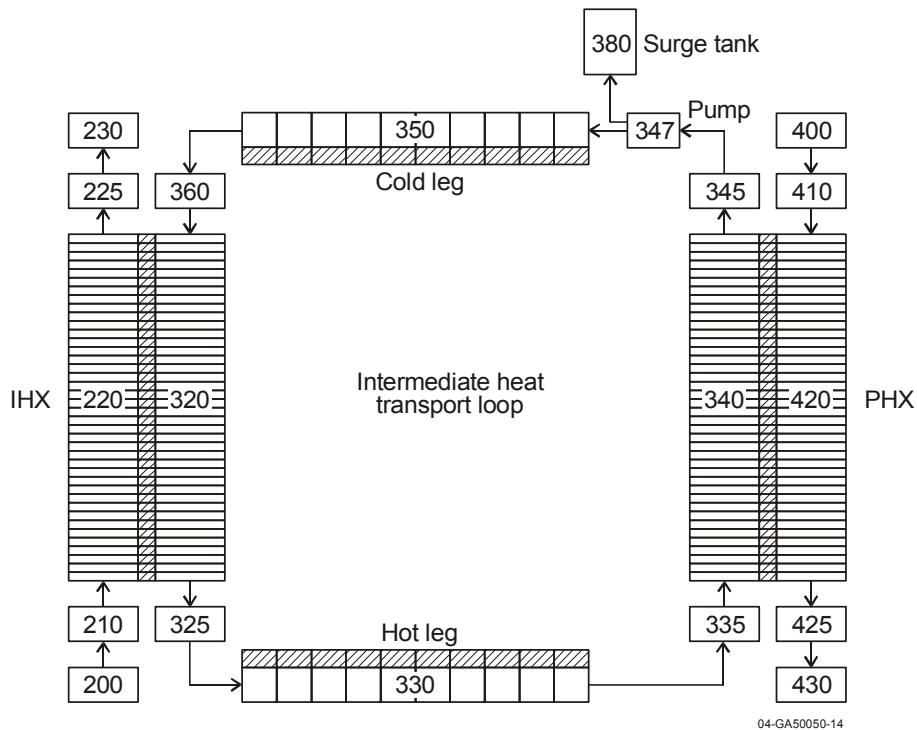
Figure 21. RELAP5 model of the intermediate heat transport loop.
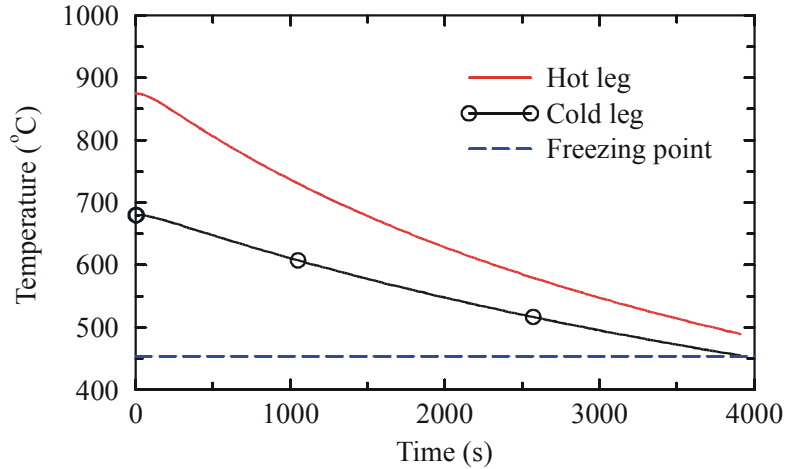
Figure 22. Fluid temperatures following a loss-of-offsite power.

The second transient simulated a loss-of-heat source, such as might occur following a reactor trip. The flow in the hot side of the IHX was reduced to zero over 10 seconds, but the flows in the intermediate loop and the cold side of the PHX continued. The continued flow in the cold side of the PHX resulted in a rapid cooling of the intermediate loop as shown in Figure 23. The freezing temperature of Flinak was reached at 300 s. Based on the difference in melting temperatures, the onset of freezing would have been delayed by about 140 s if the salt had been NaBF$_4$-NaF. Although the onset of freezing occurs much earlier for this transient, there is probably adequate time to bring the auxiliary heat source online. The starting of the auxiliary heat source could be delayed substantially if the flow through the cold side of the PHX were terminated quickly by closing an isolation valve.
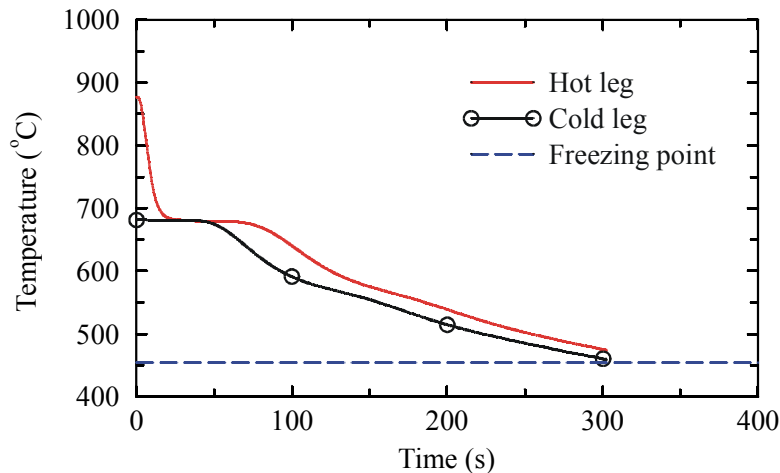
Figure 23. Fluid temperatures following a loss-of-heat source.

A surge tank will be required to accommodate the contraction and expansion of the liquid salt during cooling and heating transients. The RELAP5 calculations indicated that the liquid volume stored in the surge tank would have to exceed 10% of the total volume of the loop to prevent the tank from emptying during the transient.

5.2.2 Configuration 2

Configuration 2, which is illustrated in Figure 2, utilizes a direct electrical cycle. The IHX, which removes less than 10% of the reactor power and directs it towards the hydrogen production plant, is located in parallel with the PCU. Thus, both the PCU and the hydrogen production plant receive the maximum possible temperature. However, the PCU receives less flow than in Configuration 1. Based on the results of the stress analysis, the pressure in the heat transport loop is assumed to be relatively low, 2 MPa. Calculations were performed to size the components of the intermediate loop assuming that the working fluid was either helium or $NaBF_4$-NaF.

The IHX, hot and cold legs, and the PHX were sized based on the methods described previously. The fluid differential temperatures across the hot and cold sides of the IHX were assumed to be 300 and 350 °C, respectively. These temperatures resulted in a minimum temperature in the intermediate heat transport loop that was nearly 150 °C above the freezing temperature of $NaBF_4$-NaF. The same differential temperatures were used with helium to allow consistent comparisons between working fluids. Because the temperature in the cold leg was similar with both fluids, the same thickness-to-diameter ratio (0.01) was used for both fluids. The inlet temperature of the cold fluid in the PHX was set to 341 °C, the same value used in Configuration 1, to allow for a consistent determination of heat exchanger sizes. The thickness of the insulation was varied to determine the same heat loss values as obtained previously for Configuration 1. Other parameters were the same as used for Configuration 1.

Table 12 shows the effect of the working fluid in the heat transport loop on various parameters. The components were consistently smaller with $NaBF_4$-NaF as the coolant. The better heat transport properties of $NaBF_4$-NaF compared to helium resulted in a 14% reduction in the total volume of the IHX and a 30% reduction in the total volume of the PHX. The diameters and thicknesses of the hot and cold legs were reduced by more than 70% with the liquid salt. The thicknesses of the insulation were reduced by more than 80% with the liquid salt. Based on the reduction in component sizes, the use of a liquid salt has the potential to significantly reduce the capital cost of the intermediate heat transport loop. The operating cost should also be less with the liquid salt because the pumping power for the intermediate heat transport loop was reduced from 6.7 MW to 0.03 MW.

Table 12. Intermediate heat transport loop parameters for Configuration 2.

Parameter	He/He	He/ NaBF$_4$-NaF
IHX		
Log-mean temperature difference, °C	40	40
Hot / cold fluid pressure drop, Pa	5.0E4 / 1.4E5	5.0E4 / 5.0E3
Hot / cold fluid pumping power, W	3.7E5 / 3.2E6	3.7E5 / 2.5E2
Hot /cold fluid Reynolds number	1800 / 1600	1950 / 310
Width, m	1.44	1.39
Length, m	0.99	0.92
Volume, m^3	2.05	1.76
PHX		
Log-mean temperature difference, °C	65	78
Hot fluid pressure drop, Pa	5.0E4	2.0E3
Hot fluid pumping power, W	1.2E6	1.0E2
Hot fluid Reynolds number	1.7E4	5.6E3
Shell inner diameter, m	1.05	0.77
Length, m	8.68	11.2
Volume, m^3	7.50	5.22
Number of tubes	3490	1880
Hot / cold legs		
Inner diameter, m	0.444 / 0.413	0.117 / 0.114
Insulation thickness, m	0.0059 / 0.0058	0.0006 / 0.0001
Differential pressure, Pa	5.0E4 / 5.0E4	3.0E5 / 3.0E5
Pumping power, W	1.2E6 / 1.2E6	1.5E4 / 1.5E4
Heat loss, W	1.25E6 / 5.4E5	1.25E6 / 5.4E5
Reynolds number	1.6E6 / 2.1E6	1.7E6 / 7.5E5

Table 12 shows that the width of the front face of the IHX is about the same size as the length of the channels, which results in an aspect ratio near unity. This aspect ratio is much bigger than was obtained previously for Configuration 1. Consequently, the design and construction of the headers should be much easier for Configuration 2 than for Configuration 1, which results in a significant advantage for Configuration 2. However, there will still probably be design issues relative to attaching the hot and cold headers to the IHX and flow distribution between channels.

The volume of the IHX shown in Table 12 is about one tenth of the 21-m^3 value reported by Peterson et al. (2004) for a helium-to-helium heat exchanger. The difference in results is due to different assumptions. The diameter of the semi-circular channels used here is half that used by Peterson et al. (2004), which leads to a factor of four difference in volume for laminar flow. The log-mean temperature difference is also twice that used by Peterson et al. (2004), which reduces the size by another factor of two. The pitch-to-diameter and thickness-to-diameter ratios obtained from the simple stress evaluation described in Section 5.1 are smaller than the values obtained from the finite element analysis performed by Peterson et al. (2004), which also leads to a smaller volume. The ratios obtained from the finite element analysis are expected to be more accurate than those obtained here.

The volume of the PHX was 30% less with NaBF$_4$-NaF, but the tubes were about 30% longer. Parametric calculations showed that the geometry of the PHX was sensitive to the assumed pressure drop. For example, increasing the pressure drop by a factor of five reduced the volume by about 20% while increasing the length by about 60%. Since the pumping power is proportional to the pressure drop, large

changes in pressure drop result in large changes in the pumping power. Because the pumping power is orders of magnitude smaller with the salt, large changes in pumping power can be more easily accommodated with salt as the working fluid, which means that the geometrical shape of the heat exchanger can be changed more easily with salt as the coolant.

The thermal-hydraulic conditions in the intermediate heat transport loop are summarized in Figure 24 for Configuration 2 assuming that low-pressure helium is the working fluid. Figure 25 presents corresponding results assuming that $NaBF_4$-NaF is the working fluid.
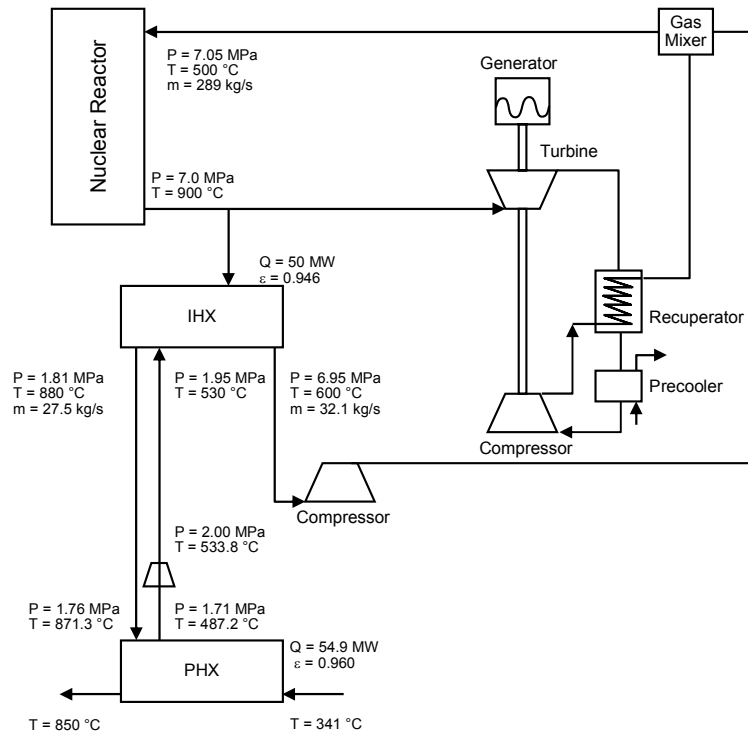
Figure 24. Thermal-hydraulic conditions for Configuration 2 with low-pressure helium.
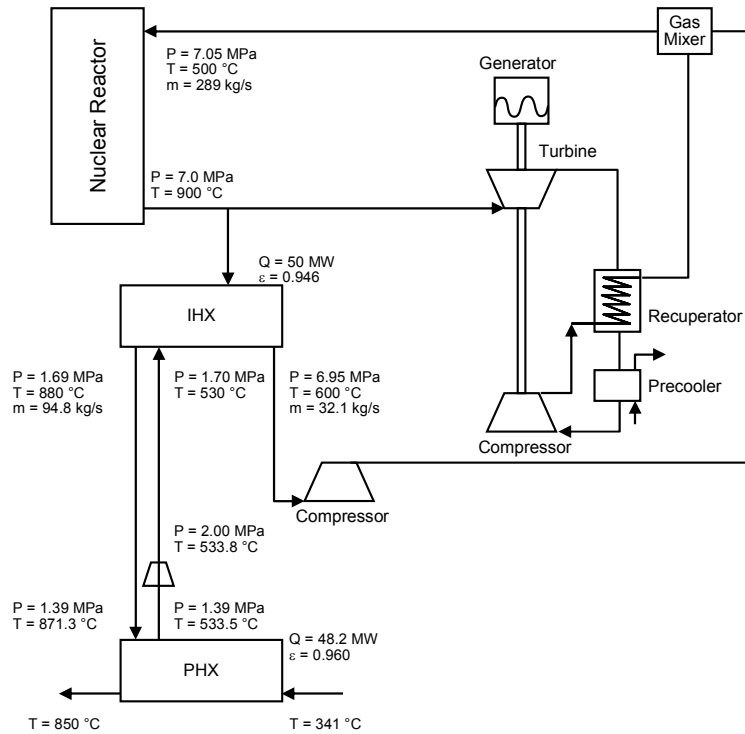
Figure 25. Thermal-hydraulic conditions for Configuration 2 with NaBF$_4$-NaF.

Although the use of a liquid salt as the coolant in the intermediate heat transport loop results in significant advantages as discussed previously, the potential for freezing causes significant disadvantages. First, an auxiliary heating system will probably be required to prevent freezing during reactor shutdowns and other transients. The auxiliary heating system would add to the capital cost of the plant. Second, loop parameters must be constrained to provide adequate margin to freezing during normal operation. For example, the differential fluid temperatures across the hot and cold sides of the IHX assumed here were 300 and 350 °C, respectively, to provide margin from freezing during normal operation. Calculations with the HYSYS model indicate that the overall efficiency of the plant could be increased by 0.5% if the differential fluid temperatures were increased to 400 and 450 °C with helium as the working fluid. The overall cycle efficiency was estimated to increase by an additional 0.4% if the helium were replaced with a salt. However, the margin to freezing of the salt during normal operation would decrease from 145 to 46 °C, which intuitively seems too small. The increase in the differential fluid temperatures across the IHX requires larger heat exchangers for a fixed inlet temperature on the cold side of the PHX. Thus, the increased operating efficiency is balanced by an increased capital cost with either fluid. However, an additional constraint exists with salt because of a to-be-determined requirement on the minimum margin to freezing. Although the operating efficiency is higher with salt than helium for given loop temperatures, higher efficiencies can potentially be achieved with helium because it can operate at lower minimum loop temperatures. This advantage of helium exists primarily at relatively low loop powers, such as the 50 MW assumed here. As mentioned previously, salt coolant has a significant advantage relative to operating efficiency if the entire thermal output of the NGNP is directed towards the hydrogen production plant.

36

Effect of PHX Inlet Temperature

A parametric calculation was performed to determine the effect of the inlet temperature on the cold side of the PHX. The inlet temperature was increased from the 341 to 441 °C. The working fluid in the intermediate heat transport loop was assumed to be low-pressure helium.

The increased inlet temperature on the cold side of the PHX reduced the log-mean temperature difference across the heat exchanger by about a factor of two. The volume of the PHX was increased by a factor of 2.3 from the value shown in Table 12. The parameters for the IHX, hot leg, and cold leg were identical to those shown previously in Table 12 and Figure 24.

5.2.3 Configuration 3

Configuration 3, which is illustrated in Figure 3, utilizes a direct electrical cycle. The configuration is identical to Configuration 1, except that it contains an additional loop that connects the intermediate heat transport loop with the PHX. This tertiary loop, which contains a SHX, provides additional separation of the nuclear and hydrogen plants compared to Configuration 1. This additional separation should increase the safety of both plants and may make the nuclear plant easier to license. However, the tertiary loop increases the capital cost and lowers the overall efficiency of the plant. Scoping calculations were performed to estimate the effects of the tertiary loop on component sizes.

For these scoping calculations, the intermediate heat transport loop was connected to the primary coolant system of the nuclear plant through the IHX. The intermediate heat transport loop was assumed to have the same length and heat loss as described previously for Configuration 1. The tertiary loop was assumed to be short. Consequently, the heat loss and pressure drop across the hot and cold legs in the tertiary loop were neglected. The working fluid in both loops was low-pressure helium. For Configuration 1, the differential fluid temperature on the cold side of the IHX was 400 °C. The differential temperature on the hot side of the PHX was slightly larger because of pumping power. The differential temperature on the cold side of the PHX was 100 °C higher than on the hot side to increase the log-mean temperature difference for the heat exchanger, resulting in a fluid temperature difference of about 500 °C. For Configuration 3, the differential fluid temperatures were assumed to be approximately 300 °C in the intermediate loop, 400 °C in the tertiary loop, and 500 °C on the cold side of the PHX. The inlet temperature on the process side of the PHX was the same value as used in Configuration 1 to minimize the differences between configurations.

The SHX was assumed to be a compact heat exchanger. Assuming an internal pressure of 2 MPa and an external pressure of 0 MPa, the method described in Section 4.1 yielded values of 1.2 and 0.61, for the pitch-to-diameter and plate thickness-to-diameter ratios, respectively. Both values were less than those obtained for the IHX because of the lower maximum pressure. The channel diameter was 1.5 mm, the same value as used previously.

The method described in Section 4.2 was used to calculate component sizes and thermal-hydraulic states for Configuration 3. Table 13 compares various parameters for Configurations 1 and 3. The thermal-hydraulic states for Configuration 3 are summarized in Figure 26. The IHX and PHX were 40 to 50% larger in Configuration 3. The overall temperature drop between the nuclear plant and the inlet of the cold stream of the PHX was the same in both configurations. However, this overall temperature drop was divided between three heat exchangers in Configuration 3 versus two in Configuration 1. The log-mean temperature differences across the IHX and PHX were smaller in Configuration 3, resulting in larger heat exchangers. The mass flow rate in the intermediate loop was about 30% higher in Configuration 3 to achieve the smaller temperature drop between the nuclear plant and the IHX. The larger mass flow rate in

Configuration 3 will require a larger, and presumably more costly, compressor or blower. The increased mass flow rate in Configuration 3 required the hot and cold legs in the intermediate loop to be 12 to 15% larger than in Configuration 1 to achieve the same differential pressure. Depending on the relative cost of components, the capital cost of the intermediate loop should be between 12 and 50% higher in Configuration 3. After accounting for the additional components in the tertiary loop, the relative capital cost should be even higher. The operating cost will also be higher for Configuration 3 because the total pumping power was 3.0 MW higher.

Table 13. A comparison of loop parameters for Configurations 1 and 3.

Parameter	Configuration 1	Configuration 3
IHX		
Log-mean temperature difference, °C	124	89
Hot / cold fluid pressure drop, Pa	5.0E4 / 3.3E3	5.0E4 / 5.2E3
Hot / cold fluid pumping power, W	3.4E6 / 6.2E4	3.4E6 / 1.5E5
Hot /cold fluid Reynolds number	5510 / 530	4930 / 600
Width, m	2.37	2.50
Length, m	0.076	0.092
Volume, m^3	0.42	0.58
SHX[1]		
Log-mean temperature difference, °C		48
Hot / cold fluid pressure drop, Pa		5.0E4 / 3.4E4
Hot / cold fluid pumping power, W		1.4E6 / 6.2E5
Hot /cold fluid Reynolds number		1070 / 850
Width, m		1.49
Length, m		0.51
Volume, m^3		1.15
PHX		
Log-mean temperature difference, °C	56	42
Hot fluid pressure drop, Pa	5.0E4	5.0E4
Hot fluid pumping power, W	9.5E5	9.2E5
Hot fluid Reynolds number	1.6E4	1.4E4
Shell inner diameter, m	1.02	1.10
Length, m	10.2	13.2
Volume, m^3	8.40	12.6
Number of tubes	3320	3860
Intermediate loop hot / cold legs		
Inner diameter, m	0.422 / 0.387	0.471 / 0.444
Insulation thickness, m	5.5E-3 / 4.1E-3	6.5E-3 / 7.8E-3
Differential pressure, Pa	5.0E4 / 5.0E4	5.0E4 / 5.0E4
Pumping power, W	9.5E5 / 9.5E5	1.4E6 / 1.4E6
Heat loss, W	1.25E6 / 5.4E5	1.25E6 / 5.4E5
Reynolds number	1.4E6 / 2.1E6	1.7E6 / 2.2E6

1. Not applicable for Configuration 1.

Figure 26. Thermal-hydraulic states for Configuration 3 with low-pressure helium.

5.2.4 Configuration 4

Configuration 4, which is illustrated in Figure 4, utilizes a direct electrical cycle. The configuration is identical to Configuration 2, except that it contains a tertiary loop that connects the intermediate heat transport loop with the PHX. This tertiary loop, which contains a SHX, provides additional separation of the nuclear and hydrogen plants compared to Configuration 2. This additional separation should increase the safety of both plants and may make the nuclear plant easier to license. However, the tertiary loop increases the capital cost and lowers the overall efficiency of the plant. Calculations were performed to estimate the effects of the tertiary loop on component sizes.

For these scoping calculations, the intermediate heat transport loop was connected to the primary coolant system of the nuclear plant through the IHX. The intermediate heat transport loop was assumed to have the same length and heat loss as assumed previously for Configuration 2. The tertiary loop was assumed to be short. Consequently, the heat loss and pressure drop across the hot and cold legs in the tertiary loop were neglected. The working fluid in both loops was low-pressure helium. The differential fluid temperatures on the hot and cold sides of the IHX were the same for both configurations. The inlet and outlet temperatures on the process side of the PHX were the same as used in Configuration 2 to minimize the differences between configurations. For Configuration 4, the differential fluid temperatures were assumed to be approximately 350 °C in the intermediate loop, 400 °C in the tertiary loop, and 500 °C on the cold side of the PHX.

The geometrical parameters for the IHX, PHX, and hot and cold legs were the same as assumed previously for Configurations 1, 2, and 3. For the SHX, these parameters were the same as used previously for Configuration 3.

The method described in Section 4 was used to calculate component sizes and thermal-hydraulic states for Configuration 4. Table 14 compares various parameters for Configurations 2 and 4. The thermal-hydraulic states for Configuration 4 are summarized in Figure 27. The overall temperature drop between the nuclear plant and the inlet of the cold stream of the PHX was the same in both configurations. However, this overall temperature drop was divided between three heat exchangers in Configuration 4 versus two in Configuration 2. The log-mean temperature differences across the IHX and PHX were smaller in Configuration 4, resulting in larger heat exchangers. The IHX and PHX were 20 and 60% larger in Configuration 4. The total volume of the compact heat exchangers, including the IHX and the SHX for Configuration 4, was 160% greater in Configuration 4.

Table 14. A comparison of loop parameters for Configurations 2 and 4.

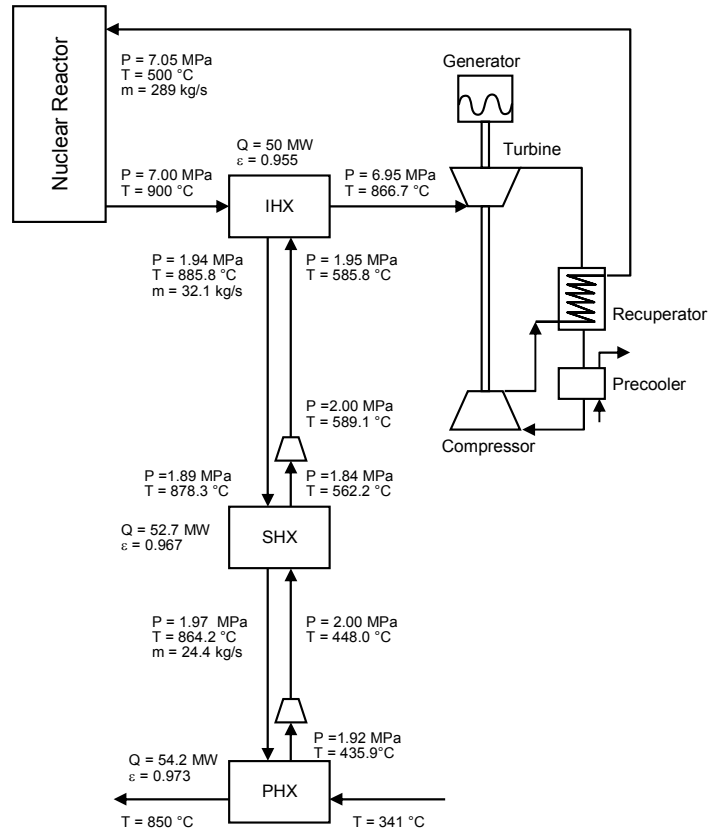| Parameter	Configuration 2	Configuration 4
IHX		
Log-mean temperature difference, °C	40	33
Hot / cold fluid pressure drop, Pa	5.0E4 / 1.4E5	5.0E4 / 1.4E5
Hot / cold fluid pumping power, W	3.7E5 / 3.2E6	3.7E5 / 3.3E6
Hot /cold fluid Reynolds number	1800 / 1600	1630 / 1440
Width, m	1.44	1.51
Length, m	0.99	1.09
Volume, m^3	2.05	2.50
SHX[1]		
Log-mean temperature difference, °C		20
Hot / cold fluid pressure drop, Pa		5.0E4 / 4.6E4
Hot / cold fluid pumping power, W		1.2E6 / 9.4E5
Hot /cold fluid Reynolds number		670 / 650
Width, m		1.77
Length, m		0.90
Volume, m^3		2.83
PHX		
Log-mean temperature difference, °C	65	46
Hot fluid pressure drop, Pa	5.0E4	5.0E4
Hot fluid pumping power, W	1.2E6	1.0E6
Hot fluid Reynolds number	1.7E4	1.5E4
Shell inner diameter, m	1.05	1.12
Length, m	8.68	12.0
Volume, m^3	7.50	11.8
Number of tubes	3490	3980
Intermediate loop hot / cold legs		
Inner diameter, m	0.444 / 0.413	0.444 / 0.413
Insulation thickness, m	5.9E-3 / 5.8E-3	6.0E-3 / 5.9E-3
Differential pressure, Pa	5.0E4 / 5.0E4	5.0E4 / 5.0E4
Pumping power, W	1.2E6 / 1.2E6	1.2E6 / 1.2E6
Heat loss, W	1.25E6 / 5.4E5	1.25E6 / 5.4E5
Reynolds number	1.5E6 / 2.1E6	1.5E6 / 2.1E6

1. Not applicable for Configuration 2.

A comparison of Figures 24 and 27 shows that the intermediate loop operated at about 6 °C higher temperature in Configuration 4 than in Configuration 2. The higher operating temperature was caused by the additional heat exchanger between the IHX and the PHX. The other operating conditions were nearly identical for Conditions 2 and 4. Consequently, the diameters of the hot and cold legs and the insulation requirements were nearly identical for the two configurations. The total pumping power was about 2.0 MW higher in Configuration 4 because of the tertiary loop.
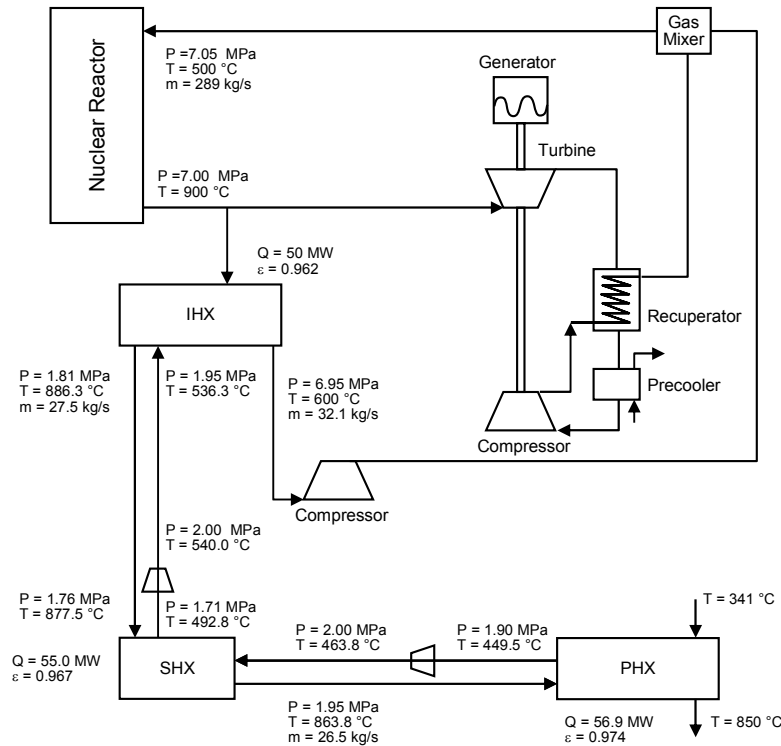
Figure 27. Thermal-hydraulic states for Configuration 4 with low-pressure helium.

5.2.5 Configuration 5

Configuration 5, which is illustrated in Figure 5, utilizes an indirect electrical cycle. The configuration is similar to Configuration 1 in that the heat exchanger that directs heat towards the hydrogen production plant, in this case the SHX, is located upstream of the PCU. This makes Configuration 5 relatively simple in terms of the equipment required. However, the overall efficiency of the plant should be lowered because the PCU receives fluid at a lower temperature. Configuration 5 is also similar to Configuration 3 in that there are three heat exchangers between the nuclear reactor and the hydrogen production plant. Thus, Configuration 5 provides a similar amount of separation between the nuclear and hydrogen plants as Configuration 3. This additional separation should increase the safety of both plants and may make the nuclear plant easier to license. However, the additional separation will also increase the capital cost and lower the overall efficiency of the plant. Scoping calculations were performed to estimate the component sizes for Configuration 5.

This configuration contains three coolant loops. The primary coolant system contains the nuclear reactor, the hot side of the IHX, and a compressor. The secondary coolant system contains the cold side of the IHX, the hot side of the SHX, the PCU, and connecting piping, which is assumed to be short. Hence, heat loss and pressure drop across the connecting piping were neglected. The intermediate heat transport loop

41

connects the secondary coolant system to the hydrogen production plant. The intermediate heat transport loop was assumed to have the same length and heat loss as assumed previously for Configuration 1. The working fluid in the secondary coolant system was assumed to be high-pressure helium to achieve efficient production of electricity. The working fluid in the heat transport loop was assumed to be low-pressure helium.

Parameters for Configuration 5 were generally the same as used previously for the analysis of Configuration 1 to allow a fair comparison between configurations. Specifically, the differential fluid temperature across the reactor core was 400 °C, the same as in previous calculations. The differential fluid temperature across the hot stream of the IHX was slightly greater because of pumping power in the primary coolant system. The differential fluid temperature across the cold side of the IHX was initially assumed to be 400 °C to achieve a high mass flow rate and high efficiency in the production of electricity. The differential fluid temperature across the cold stream of the SHX was 400 °C, consistent with that used previously for Configuration 1. The inlet and outlet fluid temperatures on the cold side of the PHX were also the same as used previously for Configuration 1, which resulted in a differential fluid temperature of about 500 °C.

The diameter of the semi-circular channels in the IHX and the SHX was 1.5 mm, the same value as used previously. The pitch-to-diameter and plate thickness-to-diameter ratios of the IHX were set at 1.20 and 0.57 based on the results shown in Table 3. These values correspond to interior and exterior pressures of 7 and 5 MPa, respectively, which conservatively bound the values expected during normal operation. For the SHX, these parameters were set to 1.50 and 0.78, consistent with the values used previously. The tube diameter, thickness-to-diameter ratio, and pitch-to-diameter ratio of the PHX were also as assumed previously. Similarly, the thickness-to-diameter ratios for the hot and cold legs of the intermediate loop were 0.11 and 0.01, respectively, the same values as used previously.

The method described in Section 4.2 was used to calculate component sizes and thermal-hydraulic states for Configuration 5. Table 15 compares various parameters for Configurations 1 and 5. The thermal-hydraulic states for Configuration 5 are summarized in Figure 28. The IHX was more that 100 times bigger in Configuration 5 than in Configuration 1 because it was sized to remove 100% of reactor power rather than 8%. The IHX was also bigger in Configuration 5 because its log-mean temperature difference was more than ten times smaller than in Configuration 1. The smaller log-mean temperature difference was a consequence of assuming approximately the same differential fluid temperature on both sides of the IHX. A parametric study to investigate the effects of differential fluid temperature on the cold side of the IHX is described later.

Table 15. A comparison of loop parameters for Configurations 1 and 5.

Parameter	Configuration 1	Configuration 5
IHX		
Log-mean temperature difference, °C	124	11
Hot / cold fluid pressure drop, Pa	5.0E4 / 3.3E3	5.0E4 / 5.0E4
Hot / cold fluid pumping power, W	3.4E6 / 6.2E4	3.4E6 / 3.3E6
Hot /cold fluid Reynolds number	5510 / 530	880 / 900
Width, m	2.37	4.82
Length, m	0.076	2.23
Volume, m^3	0.42	53.3
SHX[1]		
Log-mean temperature difference, °C		110
Hot / cold fluid pressure drop, Pa		5.0E4 / 3.4E3
Hot / cold fluid pumping power, W		3.3E6 / 6.3E4
Hot /cold fluid Reynolds number		5360 / 505
Width, m		2.42
Length, m		0.082
Volume, m^3		0.48
PHX		
Log-mean temperature difference, °C	56	47
Hot fluid pressure drop, Pa	5.0E4	5.0E4
Hot fluid pumping power, W	9.5E5	9.4E5
Hot fluid Reynolds number	1.6E4	1.5E4
Shell inner diameter, m	1.02	1.06
Length, m	10.2	11.7
Volume, m^3	8.40	10.3
Number of tubes	3320	3570
Intermediate loop hot / cold legs		
Inner diameter, m	0.422 / 0.387	0.421 / 0.386
Insulation thickness, m	5.5E-3 / 4.1E-3	5.4E-3 / 4.0E-3
Differential pressure, Pa	5.0E4 / 5.0E4	5.0E4 / 5.0E4
Pumping power, W	9.5E5 / 9.5E5	9.4E5 / 9.4E5
Heat loss, W	1.25E6 / 5.4E5	1.25E6 / 5.4E5
Reynolds number	1.4E6 / 2.1E6	1.4E6 / 2.1E6

1.   Not present in Configuration 1.

The SHX in Configuration 5 was generally similar to the IHX in Configuration 1 because both heat exchangers were sized to remove 50 MW of power and operated at similar conditions. The use of the indirect cycle in Configuration 5 added an additional heat exchanger between the nuclear and hydrogen plants and reduced the log-mean differential temperature across the SHX. As a result, the SHX in Configuration 5 was 14% bigger than the IHX in Configuration 1. The PHX in Configuration 5 was 23% bigger than in Configuration 1 for the same reason. The hot and cold legs of the intermediate loop were similar in both configurations. The total pumping power was 6.6 MW higher in Configuration 5.
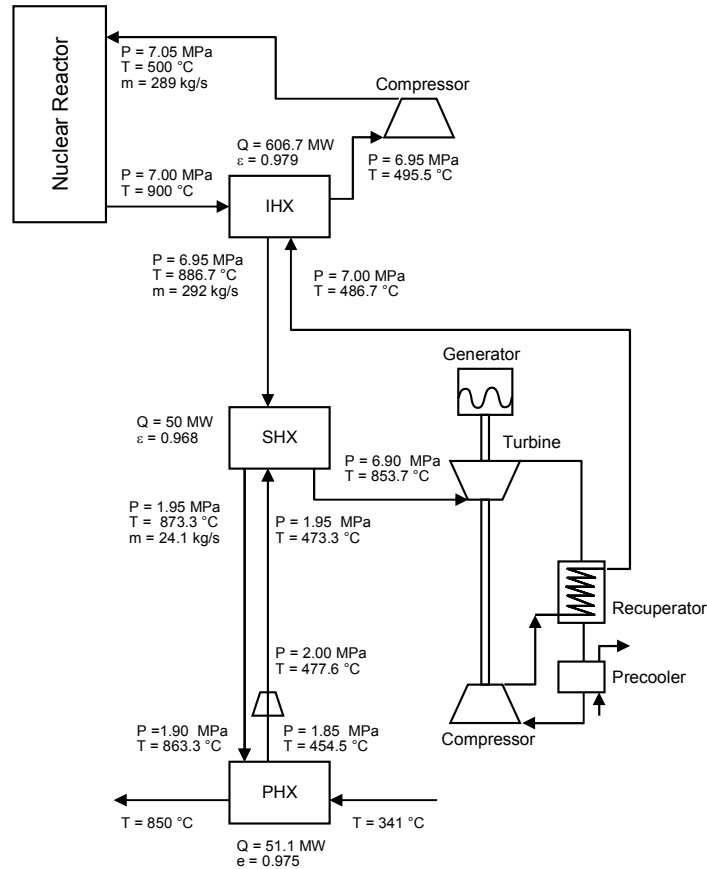
Figure 28. Thermal-hydraulic states for Configuration 5 with low-pressure helium.

For the results shown in Table 15, the differential fluid temperature on the cold side of the IHX was set to 400 °C to obtain a relatively high flow rate through the PCU and a correspondingly high efficiency for electricity production. However, the use of similar differential fluid temperatures on both sides of the IHX resulted in a relatively small log-mean temperature difference and a relatively large heat exchanger. Consequently, a sensitivity study was performed to investigate the effects of increasing the differential fluid temperature on the cold side of the IHX to 450 °C. This change decreased the flow rate through the PCU by 11% and reduced the overall efficiency of the cycle by 1.5%. However, the log-mean temperature difference increased almost three times resulting in a 64% reduction in the volume of the IHX. The volumes of the SHX and PHX were increased by 1.4 and 0.1%, respectively. Since the IHX constituted the vast majority of the heat exchanger volume, decreasing the flow rate in the secondary coolant system would significantly lower the capital cost of the system at the expense of reducing the cycle efficiency. Economic calculations would have to be performed to optimize the competing effects of capital and operating costs.

Table 15 shows that the log-mean temperature difference across the PHX was about half the corresponding value for the SHX. The PHX was also about twenty times larger than the SHX. A second sensitivity calculation was performed in which the differential fluid temperature across the cold side of the SHX was decreased from 400 to 264 °C. This change resulted in a log-mean temperature difference of about 80 °C for both heat exchangers. This change increased the volume of the SHX by 31% and decreased the volume of the PHX by 48%. Because the PHX was much larger, the combined heat exchanger volume was reduced by 44%. Because the reduced fluid differential temperature caused an increase in the mass flow rate in the intermediate loop, the diameters of the hot and cold legs had to be

44

increased by about 20% to keep the same differential pressures. These results indicate that the differential fluid temperature (and mass flow rate) in the intermediate loop has a significant impact on component sizes. An optimal design would require economic calculations based on the relative costs of the various components.

5.2.6 Configuration 6

Configuration 6, which is illustrated in Figure 6, utilizes an indirect electrical cycle. The flow in the secondary coolant system is divided, with most of the flow going towards the PCU and the remainder going through the SHX to direct heat towards the hydrogen production plant. The flow through the hot side of the SHX is then mixed with the flow from the PCU to feed the cold side of the IHX. The division of flow in the secondary loop is similar to that occurring in the primary loop of Configuration 2. Configuration 6 is also similar to Configuration 5 in that it contains three coolant loops and thus achieves a relatively high degree of separation between the nuclear and hydrogen plants. Configuration 6 provides a higher fluid temperature to the PCU than Configuration 5, which acts to increase the efficiency of the cycle. However, some of the flow is diverted away from the PCU which acts to decrease the efficiency of the cycle. Calculations were performed to estimate the component sizes for Configuration 6.

Configuration 6 contains three coolant loops. The primary coolant system contains the nuclear reactor, the hot side of the IHX, and a compressor. The secondary coolant system contains the cold side of the IHX, the hot side of the SHX, the PCU, and connecting piping, which is assumed to be short. Hence, heat loss and pressure drop across the connecting piping were neglected. The intermediate heat transport loop connects the secondary coolant system to the hydrogen production plant. The intermediate heat transport loop was assumed to have the same length and heat loss as assumed previously for Configuration 2. The working fluid in the secondary coolant system was assumed to be high-pressure helium to achieve efficient production of electricity. The working fluid in the heat transport loop was assumed to be low-pressure helium.

Parameters for Configuration 6 were generally the same as used previously for the analysis of Configuration 2 to allow a fair comparison between configurations. Specifically, the differential fluid temperature across the reactor core was 400 °C, the same as in previous calculations. The differential fluid temperature across the hot stream of the IHX was slightly greater because of pumping power in the primary coolant system. The differential fluid temperature across the cold side of the IHX was assumed to be 400 °C to achieve a high mass flow rate and high efficiency in the production of electricity. The differential fluid temperature across the cold stream of the SHX was 350 °C, consistent with that used previously for the IHX in Configuration 2. The inlet and outlet fluid temperatures on the cold side of the PHX were also the same as used previously for Configuration 2, which resulted in a differential fluid temperature of about 500 °C.

The diameter of the semi-circular channels in the IHX and the SHX was 1.5 mm, the same value as used previously. The pitch-to-diameter and plate thickness-to-diameter ratios of the IHX were set at 1.20 and 0.57 based on the results shown in Table 3. These values correspond to interior and exterior pressures of 7 and 5 MPa, respectively, which conservatively bound the values expected during normal operation. For the SHX, these parameters were set to 1.50 and 0.78, also based on the results shown in Table 3. The tube diameter, thickness-to-diameter ratio, and pitch-to-diameter ratio of the PHX were also as assumed previously. Similarly, the thickness-to-diameter ratios for the hot and cold legs of the intermediate loop were 0.11 and 0.01, respectively, the same values as used previously.

The method described in Section 4 was used to calculate component sizes and thermal-hydraulic states for Configuration 6. Table 16 compares various parameters for Configurations 2 and 6. The thermal-hydraulic states for Configuration 6 are summarized in Figure 29. The IHX was 25 times bigger in Configuration 6 than in Configuration 2 because it was sized to remove 100% of reactor power rather

45

than 8% and because its log-mean temperature difference was more than three times smaller. The smaller log-mean temperature difference was a consequence of assuming approximately the same differential fluid temperature on both sides of the IHX. A sensitivity study to investigate the effects of differential fluid temperature on the cold side of the IHX was described previously in Section 5.2.5 for Configuration 5.

Table 16. A comparison of loop parameters for Configurations 2 and 6.

Parameter	Configuration 2	Configuration 6
IHX		
Log-mean temperature difference, °C	40	11
Hot / cold fluid pressure drop, Pa	5.0E4 / 1.4E5	5.0E4 / 5.0E4
Hot / cold fluid pumping power, W	3.7E5 / 3.2E6	3.4E6 / 3.3E6
Hot /cold fluid Reynolds number	1800 / 1600	900 / 910
Width, m	1.44	4.77
Length, m	0.99	2.26
Volume, m^3	2.05	51.3
SHX[1]		
Log-mean temperature difference, °C		33
Hot / cold fluid pressure drop, Pa		5.0E4 / 1.4E5
Hot / cold fluid pumping power, W		3.7E5 / 3.2E6
Hot /cold fluid Reynolds number		1660 / 1460
Width, m		1.51
Length, m		1.11
Volume, m^3		2.52
PHX		
Log-mean temperature difference, °C	65	54
Hot fluid pressure drop, Pa	5.0E4	5.0E4
Hot fluid pumping power, W	1.2E6	1.1E6
Hot fluid Reynolds number	1.7E4	1.6E4
Shell inner diameter, m	1.05	1.09
Length, m	8.68	9.95
Volume, m^3	7.50	9.24
Number of tubes	3490	3760
Hot / cold legs		
Inner diameter, m	0.444 / 0.413	0.443 / 0.412
Insulation thickness, m	5.9E-3/ 5.8E-3	5.8E-3 / 5.6E-3
Differential pressure, Pa	5.0E4 / 5.0E4	5.0E4 / 5.0E4
Pumping power, W	1.2E6 / 1.2E6	1.1E6 / 1.1E6
Heat loss, W	1.25E6 / 5.4E5	1.25E6 / 5.4E5
Reynolds number	1.6E6 / 2.1E6	1.6E6 / 2.2E6

    1.   Not present in Configuration 2.

The SHX in Configuration 6 was generally similar to the IHX in Configuration 2 because both heat exchangers were sized to remove 50 MW of power and operated at similar conditions. The use of the indirect cycle in Configuration 6 added an additional heat exchanger between the nuclear and hydrogen plants and reduced the log-mean differential temperature across the SHX. As a result, the SHX in Configuration 6 was 23% bigger than the IHX in Configuration 2. The PHX in Configuration 6 was 23% bigger than in Configuration 2 for the same reason. The hot and cold legs of the intermediate loop were similar in both configurations. The total pumping power was 6.6 MW higher in Configuration 6.
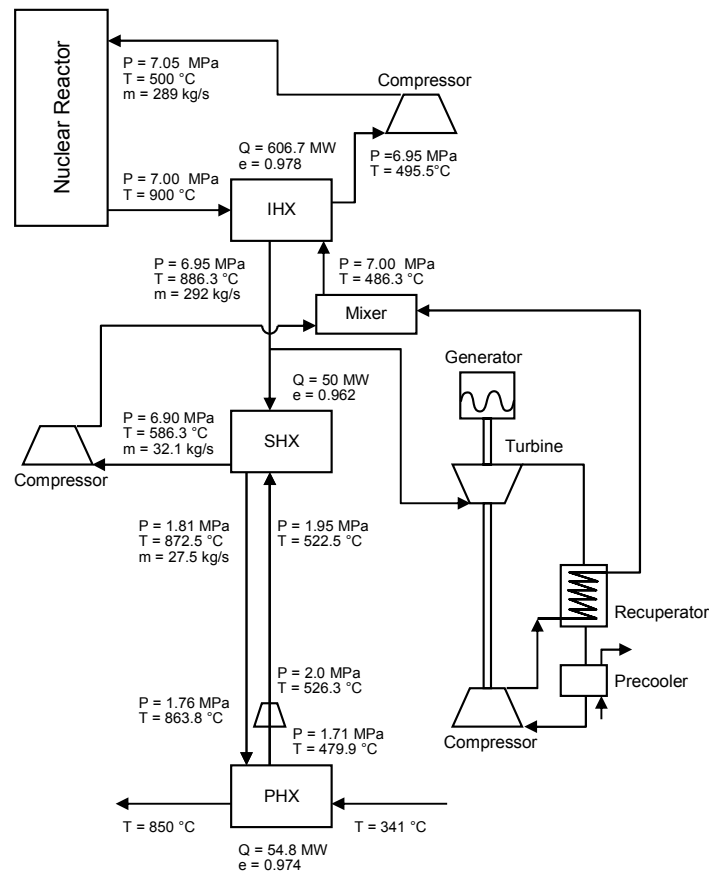
Figure 29. Thermal-hydraulic states for Configuration 6 with low-pressure helium.

The results shown previously for Configuration 6 were as consistent as possible with those obtained for Configuration 2. A sensitivity calculation was performed in which the differential fluid temperature across the cold side of the SHX was increased from 350 to 400 °C to be consistent with Configuration 5. The SHX was nearly 270% larger in Configuration 6. The smaller differential temperature across the hot stream of the SHX in Configuration 5 resulted in a large differential temperature at the cold end of the SHX, which increased the log-mean differential temperature and reduced the size of the heat exchanger compared to Configuration 6. The PHX was 19% greater in Configuration 6, primarily because of a larger log-mean differential temperature. Although the SHX and PHX were larger in Configuration 6 than in Configuration 5, the combined volume of the IHX, SHX, and PHX, which is a better measure of the total capital cost, was only 5% greater in Configuration 6 because the IHX was the largest heat exchanger. The aspect ratio of the SHX was much greater in Configuration 6 than in Configuration 5. The larger aspect ratio indicates that the heat exchanger would be easier to design relative to constructing the headers and distributing flow between the channels. The hot and cold legs of the intermediate heat transport loop were nearly identical in both configurations. The total pumping power was 0.8 MW less in Configuration 6.

5.2.7 Configuration 7

Configuration 7, which is illustrated in Figure 7, utilizes an indirect electrical cycle. This configuration contains two coolant loops. The primary coolant system contains the nuclear reactor, the hot side of the IHX, and a compressor. The secondary coolant system contains the cold side of the IHX, the PCU, and intermediate heat transport loop. The flow in the secondary coolant system is divided, with most of the

47

flow going towards the PCU and the remainder going through intermediate heat transport loop to the PHX. The two streams are recombined upstream of the IHX. This configuration is similar to Configuration 6 except that it does not contain a SHX. Consequently, Configuration 7 has the potential to have a lower capital cost than Configuration 6. However, Configuration 7 has less separation between the nuclear and hydrogen plants, which may make the nuclear plant more difficult to license. Another disadvantage of this configuration is that a salt cannot be used as the working fluid because the turbine cannot utilize liquid.

The intermediate heat transport loop was assumed to have the same length and heat loss as assumed previously for Configuration 6. The working fluid in the secondary coolant system was assumed to be low-pressure helium based on the results of the simplified stress analysis presented in Section 4.1. Other parameters for Configuration 7 were generally the same as used previously for the analysis of Configuration 6 to allow a fair comparison between configurations. Specifically, the differential fluid temperature across the reactor core was 400 °C, the same as in previous calculations. The differential fluid temperature across the hot stream of the IHX was slightly greater because of pumping power in the primary coolant system. The differential fluid temperature across the cold side of the IHX was assumed to be 400 °C to achieve a high mass flow rate and high efficiency in the production of electricity. The inlet and outlet fluid temperatures on the cold side of the PHX were also the same as used previously for Configuration 6, which resulted in a differential fluid temperature of about 500 °C. One difference from Configuration 6 was that the mass flow rate in the intermediate heat transport loop was about 20% lower, and was in closer agreement to the sensitivity calculation performed for Configuration 6 than the base case.

The diameter of the semi-circular channels in the IHX was 1.5 mm, the same value as used previously. The pitch-to-diameter and plate thickness-to-diameter ratios of the IHX were set at 1.50 and 0.78 based on the results shown in Table 3. These values correspond to interior and exterior pressures of 7 and 2 MPa, respectively, which conservatively bound the values expected during normal operation. The tube diameter, thickness-to-diameter ratio, and pitch-to-diameter ratio of the PHX were also as assumed previously. Similarly, the thickness-to-diameter ratios for the hot and cold legs of the intermediate loop were 0.11 and 0.01, respectively, the same values as used previously.

The method described in Section 4.2 was used to calculate component sizes and thermal-hydraulic states for Configuration 7. Table 17 compares various parameters for Configurations 6 and 7. The thermal-hydraulic states for Configuration 7 are summarized in Figure 30. The IHX was 15% bigger in Configuration 7 than in Configuration 6. The increased size was caused by the larger pitch-to-diameter and plate thickness-to-diameter ratios needed in Configuration 7 because of the larger pressure drop between the hot and cold fluids in the IHX. The effects of the larger ratios were partially offset by the increased log-mean temperature difference across the IHX in Configuration 7 due to the lack of a SHX and a tertiary loop. Although the mass flow rate on the cold side of the IHX was the same in both configurations, the pressure drop was three times higher and the pumping power was more than ten times higher because of the reduced pressure in Configuration 7. The increased pumping power corresponds to 5.3% of the rated core power, and would reduce the overall cycle efficiency by about 2.65%. The increased pumping power in Configuration 7 is a significant disadvantage compared to Configuration 6.

48

Table 17. A comparison of loop parameters for Configurations 6 and 7.

Parameter	Configuration 6	Configuration 7
IHX		
Log-mean temperature difference, °C	11	17
Hot / cold fluid pressure drop, Pa	5.0E4 / 5.0E4	5.0E4 / 1.7E5
Hot / cold fluid pumping power, W	3.4E6 / 3.3E6	3.4E6 / 3.9E7
Hot /cold fluid Reynolds number	900 / 910	1090 / 1120
Width, m	4.77	5.65
Length, m	2.26	1.85
Volume, m^3	51.3	58.9
SHX[1]		
Log-mean temperature difference, °C	33	NA
Hot / cold fluid pressure drop, Pa	5.0E4 / 1.4E5	
Hot / cold fluid pumping power, W	3.7E5 / 3.2E6	
Hot /cold fluid Reynolds number	1660 / 1460	
Width, m	1.51	
Length, m	1.11	
Volume, m^3	2.52	
PHX		
Log-mean temperature difference, °C	54	48
Hot fluid pressure drop, Pa	5.0E4	5.0E4
Hot fluid pumping power, W	1.1E6	8.8E5
Hot fluid Reynolds number	1.6E4	1.5E4
Shell inner diameter, m	1.09	1.03
Length, m	9.95	12.03
Volume, m^3	9.24	9.93
Number of tubes	3760	3340
Hot / cold legs		
Inner diameter, m	0.443 / 0.412	0.409 / 0.376
Insulation thickness, m	5.8E-3 / 5.6E-3	5.3E-3 / 3.9E-3
Differential pressure, Pa	5.0E4 / 5.0E4	5.0E4 / 5.0E4
Pumping power, W	1.1E6 / 1.1E6	8.7E5 / 8.7E5
Heat loss, W	1.25E6 / 5.4E5	1.25E6 / 5.4E5
Reynolds number	1.6E6 / 2.2E6	1.4E6 / 2.0E6

1. Not present in Configuration 7.

Calculations described in Section 5.3 show that the overall efficiency of the cycle decreases sharply as the pressure in the secondary coolant system decreases. The cycle efficiency drops below 45% at a pressure near 3 MPa. Therefore, the pressure supplying the turbine must exceed 3 MPa in order to obtain a reasonable efficiency. However, the stress analysis indicates that the pressure cannot be much higher than 2 MPa at 900 °C with currently available materials and a reasonable pipe thickness. The maximum reasonable thickness-to-diameter ratio is considered to be 0.20, which substantially exceeds the 0.14 value for Schedule 160 pipe, the thickest commercially available (Crane 1979), in the size range of interest here. An extrapolation of the results given in Table 2 for the hot leg shows that if the pressure exceeds 3.2 MPa, the required thickness-to-diameter ratio exceeds 0.2 for an allowable stress of 10 MPa.   The situation is even worse with respect to the tube-in-shell PHX, where the required thickness-to-diameter ratio will exceed 0.2 if the pressure outside of the tubes exceeds 2.4 MPa. Although the stress in the hot legs can be reduced using an annular arrangement of the hot and cold legs, such a technique cannot be

readily applied to the PHX tubes. The stress on the tubes can be reduced by increasing the inner pressure, but at the cost of reducing the efficiency of the hydrogen production process.
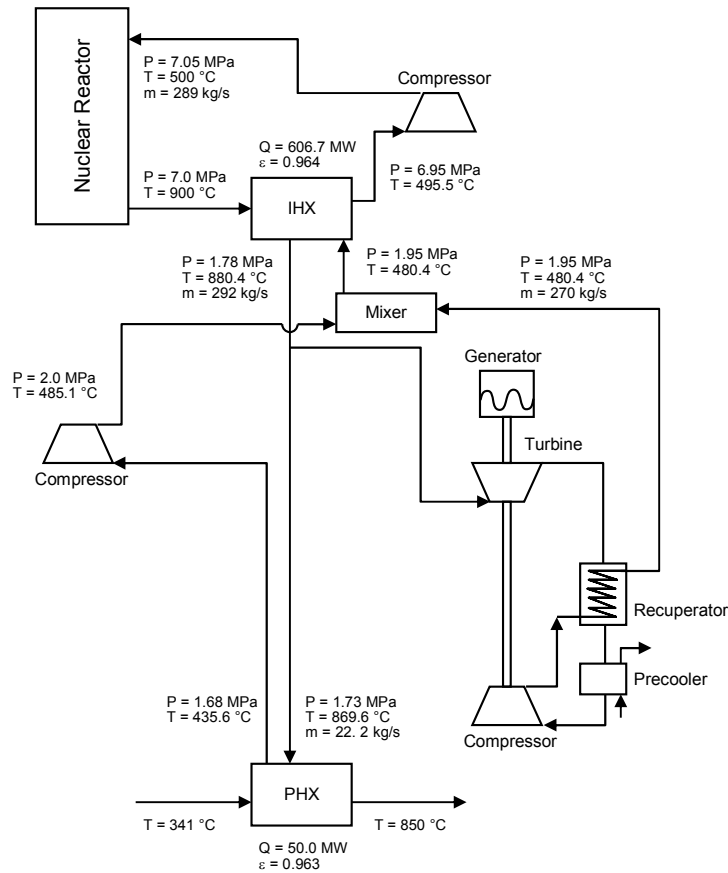
Figure 30. Thermal-hydraulic states for Configuration 7 with low-pressure helium.

5.2.8 Comparison of Configurations and Options

The diameters and insulation thicknesses of the hot leg of the intermediate loop are compared in Figures 31 and 32 for each configuration. The variations in hot leg diameter and insulation thickness were generally small with helium as the working fluid and were primarily due to differences in the assumed flow rates. The figures also show that the diameter and insulation thickness were much smaller when the helium coolant was replaced by liquid salt.
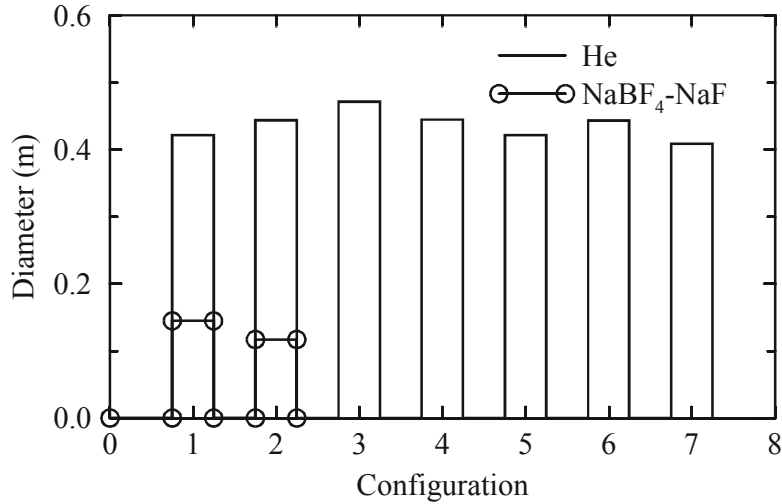
Figure 31. A comparison of hot leg diameters in the various configurations of the intermediate heat transport loop.
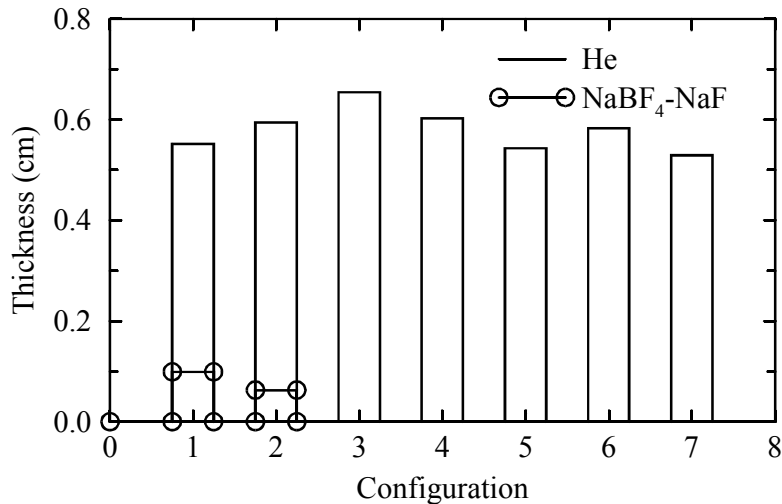
Figure 32. A comparison of insulation thicknesses in the hot leg for the various configurations of the intermediate heat transport loop.

The relative sizes of the configurations are illustrated in Figure 33, which is based on the calculated metal volume in the intermediate heat transport loop, and, if present, the SHX and the tertiary loop. The volume includes that of the fluid in the compact heat exchangers because their cost would presumably include the metal that was etched away during construction. The volume does not include that of equipment in the PCU, such as the recuperator and the precooler, but does include the IHX.

Figure 33 shows that the smallest size was obtained with Configuration 1. The components that contained the most metal in Configuration 1 were the hot leg, the PHX shell, and the PHX tubes. The metal volumes for Configurations 3 and 4, which contained a SHX, were 40 to 60% greater than for Configurations 1 and 2, which did not contain a SHX. In addition to its volume, the presence of the SHX required the other heat exchangers to be larger to achieve the necessary effectiveness. The total metal volumes for the configurations with an indirect electrical cycle were significantly larger than for those with a direct cycle. For example, the total volume for Configuration 5, which utilized an indirect cycle, was five times greater than for Configuration 1, which utilized a direct cycle. The large increase in

51

volume was a consequence of the IHX being designed to remove 600 MW of thermal power for the indirect cycles versus 50 MW for the direct cycles. However, the costs of the indirect and direct options will not differ by a factor of five because of the relatively large components, such as the recuperator and precooler, that are present in both options but are not included in Figure 33.
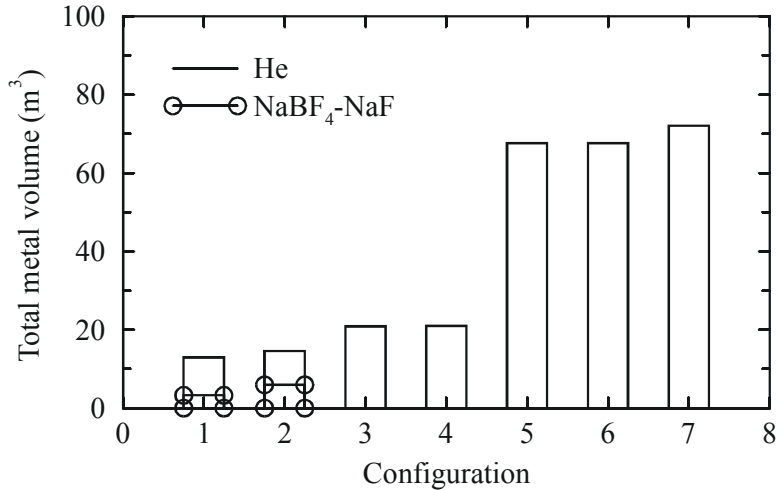
Figure 33. Relative sizes of the intermediate heat transport loop in each configuration.

The pumping powers required for the various configurations with helium coolant are shown in Figure 34. The pumping power includes the reactor core, both sides of the IHX, both sides of the SHX if it is present, the hot side of the PHX, and the hot and cold legs in the intermediate heat transport loop. The pumping power does not include that required for the PCU, but its pumping power is included within the efficiency calculations described in Section 5.3. The minimum pumping power was obtained for Configuration 1. The pumping power for Configuration 2 was 8% higher than for Configuration 1. The addition of a SHX and tertiary loop caused the pumping power in Configurations 3 and 4 to be about 30% larger than in Configuration 1. The use of an indirect cycle in Configurations 5 and 6 caused the pumping power to increase by about 70% compared to Configuration 1, but the difference in pumping powers was relatively small compared to the core power. Consequently, the difference in pumping powers between Configurations 1 and 5 corresponds to a 0.6% change in cycle efficiency assuming that the efficiency of the hydrogen production process is 50%. The pumping power was much larger for Configuration 7 because of the power required for the cold, low-pressure side of the IHX.
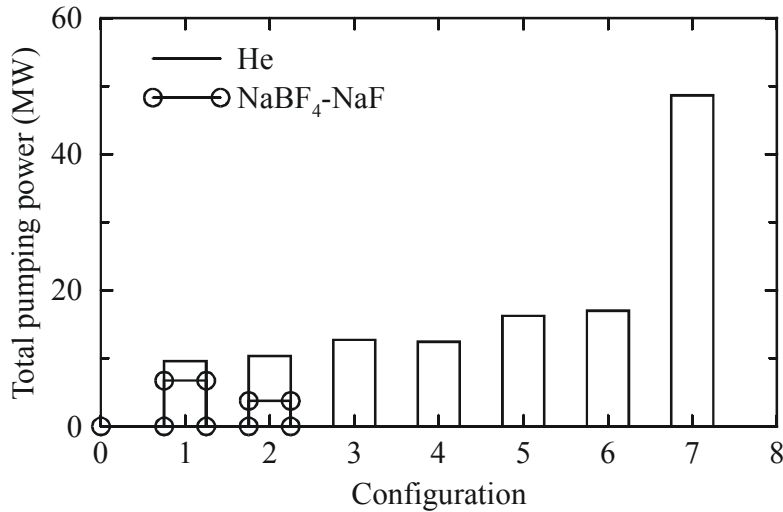
Figure 34. Relative pumping powers in the intermediate heat transport loop for each configuration.

Figures 33 and 34 also show the effect of coolant on the metal volume and pumping power for Configurations 1 and 2. The total metal volume of the intermediate heat transport loop was reduced by 60 to 70% with the liquid salt compared to helium. The total pumping power was reduced between 30 and 60%. The reduction in the pumping power of the intermediate heat transport loop itself was far larger, but the total pumping power accounted for the reactor core and the hot side of the IHX, which were cooled by helium. Thus, the use of a liquid salt can significantly reduce the size and pumping power of the intermediate heat transport loop. Both of these factors have the potential to reduce the cost of the system.

Significant benefits can also be obtained if the operating pressure of the helium in the intermediate heat transport loop can be increased. Assuming that strong enough materials are available, increasing the pressure in the intermediate loop from 2 to 7 MPa would decrease the metal volume by 30% and reduce the pumping power by 20% for Configuration 1. The use of high-pressure helium results in smaller benefits than are obtained by using a liquid salt.

The use of low-pressure helium as the working fluid in the intermediate heat transport loop mitigates the creep rupture problems that are described in Section 5.1. Although the pumping power increases as the pressure is decreased, the use of low-pressure helium as the working fluid results in a relatively small decrease in efficiency for an intermediate loop sized to deliver 50 MW of power to the hydrogen production plant. For example, the difference in overall cycle efficiency between low- and high-pressure helium is less than 0.2% for Configuration 1 assuming that the efficiency of the hydrogen production process is 50%. However, the use of low-pressure helium becomes unattractive when more power is delivered to the hydrogen production plant. For example, the difference in efficiency between low- and high-pressure helium for a single-purpose plant in which the entire 600-MW output of the nuclear plant is delivered to the hydrogen production plant is estimated to be 4.2%. The overall cycle efficiency could be increased by another 1.7% by using a liquid salt as the working fluid.

The compact heat exchangers will be easier to design and construct if they are arranged in parallel with the PCU rather than in series. The width of the front face of the compact heat exchangers significantly exceeded the length of the channels for those configurations using the serial option, including Configurations 1 and 3 for the IHX and Configuration 5 for the SHX. For these configurations, the length of the crossflow region will significantly exceed the length of the counterflow region, which would hurt the thermal performance of the heat exchanger and would cause the pressure drop to greatly exceed the values reported here. This option will result in relatively large headers and would probably result in flow

53

mal-distribution between channels. The parallel option results in much larger aspect ratios. However, there will still probably be design issues relative to attaching the hot and cold headers to the IHX and flow distribution between channels. More detailed evaluations, such as those being performed by Peterson et al. (2004), are required to address these issues.

5.3 Cycle Efficiency Evaluation

The HYSYS (Aspen Technology 2005a) computer code was used to calculate the overall cycle efficiency for the configurations illustrated in Figures 1 through 7. The thermal-hydraulic states for the reactor, IHX, and intermediate heat transport loop were based on the values presented in Section 5.2. The states for the PCU were optimized as described in Section 4.3.

The HYSYS results were validated by comparison with results from two other methods, including the ASPEN PLUS computer code (Aspen Technology 2005b) and a Visual-Basic model developed by MIT and revised by INL (Oh and Moore 2005). The results from all three codes were compared for Configuration 7 with preliminary values for the thermal-hydraulic states. Helium was used as the working fluid for these validation calculations.

Schematics of the HYSYS, Aspen Plus, and Visual-Basic models for Configuration 7 with preliminary thermal-hydraulic parameters are shown in Figures 35 through 37.
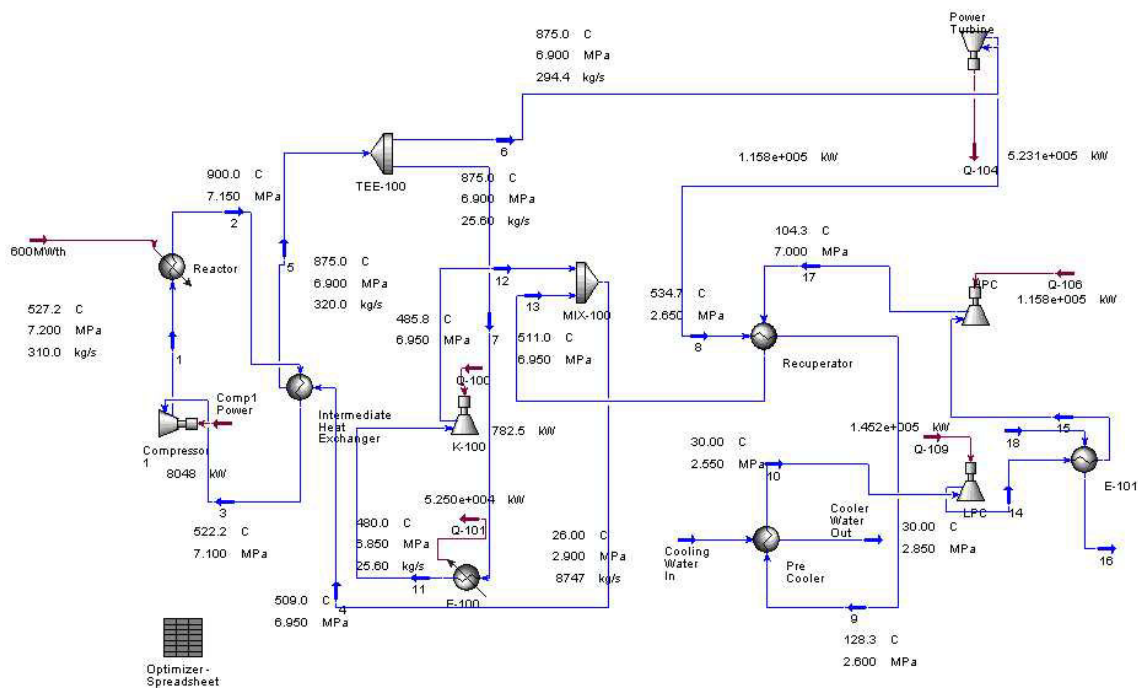
Figure 35. Schematic of the HYSYS model.

Figure 36. Schematic of the Aspen Plus model.

Figure 37. Calculation logic for the Visual-Basic model.

Results from the validation calculations are summarized in Table 18. The agreement is excellent. The overall efficiency is 49.7% using all three codes.

Table 18. Summary of validation calculations for cycle efficiency.

	HYSYS	Aspen Plus	V-B Model
Reactor power	600 MW-thermal	600 MW-thermal	600 MW-thermal
Number of shafts	1	1	1
Reactor inlet	527 °C	527 °C	527 °C
	7.2 MPa	7.2 MPa	7.2 MPa
Reactor outlet	900 °C	899.7 °C	900 °C
	7.15 MPa	7.15 MPa	7.15 MPa
Helium mass flow	310 kg/s	310 kg/s	310 kg/s
Turbine inlet	875 °C	875 °C	875 °C
	6.9 MPa	6.9 MPa	6.9 MPa
HPC outlet	104.3 °C	104.6 °C	104.3 °C
	7 MPa	7 MPa	7 MPa
Pressure ratio	2.74	2.74	2.74
Net cycle efficiency	49.7%	49.7%	49.7%

The overall efficiency of each configuration was evaluated using the HYSYS model. Figure 38 shows a snapshot of the HYSYS simulation of Configuration 1. Table 19 summarizes the important parameters in the simulation. The overall cycle efficiency calculated from Equation (12) was 50.6%.
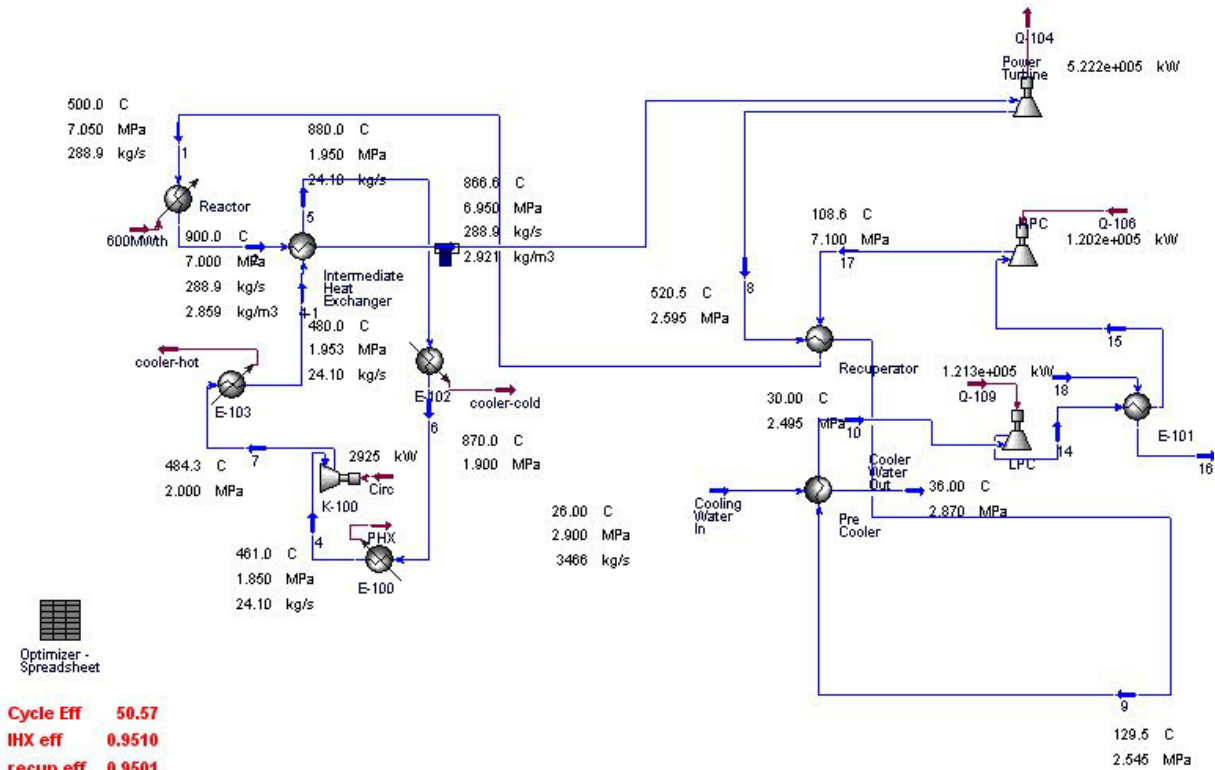
Figure 38. Snapshot of the HYSYS model of Configuration 1.

Table 19. PCU parameters for Configuration 1.

	HYSYS Results
Reactor power	600 MW-thermal
Reactor inlet	500 °C
	7.05 MPa
Reactor outlet	900 °C
	7.0 MPa
Helium mass flow to PCU	288.9 kg/s
Turbine inlet	866.6 °C
	6.95 MPa
HPC outlet	108.6 °C
	7.1 MPa
Flow rate of intermediate loop	24.1 kg/s
Pressure ratio	2.85
Overall cycle efficiency	50.6%

Configuration 2 utilizes a direct electrical cycle and a parallel IHX. The helium from the reactor is split with 88.9% flowing towards the PCU and the rest towards the IHX. As a result, the inlet temperature of helium (900 °C) to the turbine is higher than that of Configuration 1 (866.7 °C). However, the mass flow rate was reduced from 288.9 kg/s to 256.8 kg/s. Both the temperature and the mass flow rate affect the cycle efficiency. The higher temperature results in a higher efficiency, but the reduced mass flow results in a lower efficiency. The overall cycle efficiency is slightly higher than that of the Configuration 1, which indicates that the effect of temperature was larger than the effect of mass flow. The overall efficiency for Configuration 2 is 50.7 %, which is the highest efficiency among the cycles evaluated.

Configuration 3 is similar to Configuration 1 except that it utilizes a SHX and a short tertiary loop to provide better separation of the nuclear and hydrogen plants. The overall efficiency is 50.3% which is slightly less than that of Configuration 1. Configuration 4 is similar to Configuration 2 except that it also utilizes a SHX and a short tertiary loop. Again, the use of the SHX resulted in only a slight decrease in overall efficiency.

Configurations 5 and 6 utilize an indirect cycle. The efficiencies of Configurations 5 and 6 are 1.1% lower than for Configurations 1 and 2, respectively, which utilized a direct cycle.

Configuration 7 utilizes an indirect cycle with the intermediate heat transport loop and the PCU arranged in parallel. Because a low pressure of 2 MPa was used to limit the stress in the PHX, the PCU also operated at a low pressure. The lower pressure reduced the efficiency of this configuration to 38.6%. This configuration is not considered to be a viable option because of its low efficiency.

Table 20 summarizes the results for all seven configurations with helium coolant.

Table 20. Efficiency parameters for Configurations 1 through 7.

	Conf-1	Conf-2	Conf-3	Conf-4
PCU configuration	Direct	Direct	Direct	Direct
IHX	Serial	Parallel	Serial	Parallel
SHX	N/A	N/A		
Turbine inlet	866.6 °C	900 °C	866.6 °C	900 °C
	288.9 kg/s	256.8 kg/s	288.9 kg/s	256.8 kg/s
HPC outlet	108.6 °C	119.8 °C	108.6 °C	119.8 °C
	7.1 MPa	7.1 MPa	7.1 MPa	7.1 MPa
Flow rate to IHX (cold side)	24.1 kg/s He	27.5 kg/s He	32.1 kg/s He	27.5 kg/s He
Flow rate to SHX	N/A	N/A	24.38 kg/s He	26.5 kg/s He
Pressure ratio	2.85	3.23	2.83	3.23
Overall cycle efficiency	50.6%	50.7%	50.3%	50.6%
	Conf-5	Conf-6	Conf-7	
PCU configuration	Indirect	Indirect	Indirect	
IHX				
SHX	Serial	Parallel	N/A	
Turbine inlet	853.7 °C	886.3 °C	880.4 °C	
	292. kg/s	260.1 kg/s	270. kg/s	
HPC outlet	110.3 °C	121.2 °C	144.7 °C	
	7.1 MPa	7.1 MPa	2.0 MPa	
Flow rate to IHX (cold side)	292. kg/s He	292.2 kg/s He	22. kg/s He	
Flow rate to SHX	24.1 kg/s He	27.5 kg/s He	22. kg/s He	
Pressure ratio	2.90	3.29	4.10	
Overall cycle efficiency	49.5%	49.6%	38.6%	

Calculations were performed to investigate the sensitivity of the overall efficiency to various parameters, including reactor outlet temperature, mass flow rate to the PCU, and pressure.

The sensitivity of the calculated results to variations in reactor outlet temperature between 900 and 1000 °C was determined. In order to maintain the mass flow rate through the core, the reactor inlet temperature was also raised. The results are summarized below for Configuration 1.

Table 21. Sensitivity of overall efficiency to reactor outlet temperature.

	900 °C	**950 °C**	**1000 °C**
Reactor power	600 MW thermal	600 MW thermal	600 MW thermal
Reactor inlet / outlet temperature	500 °C / 900 °C	550 °C / 950 °C	600 °C / 1000 °C
Turbine inlet	866.6 °C	916.6 °C	966.6 °C
	288.9 kg/s	288.9 kg/s	288.9 kg/s
HPC outlet	108.6 °C	103.9 °C	99.5 °C
	7.1 MPa	7.1 MPa	7.1 MPa
Flow rate to IHX	24.1 kg/s He	24.1 kg/s He	24.1 kg/s He
Pressure ratio	2.85	2.71	2.54
Cycle efficiency	50.6%	52.3%	53.9%

The mass flow rate is an important parameter for the cycle efficiency. Using Configuration 5, the mass flow rate to the PCU was varied between 260 kg/s and 292 kg/s. An increase in mass flow causes an increase in cycle efficiency as summarized in Table 22. The mass flow also affects the size of the components, such as the recuperator and precooler, required to achieve a constant pressure drop.

Table 22. Sensitivity of overall efficiency to mass flow rate through the PCU.

	260 kg/s	**276 kg/s**	**292 kg/s**
Reactor power	600 MW thermal	600 MW thermal	600 MW thermal
Reactor inlet / outlet temperature	500 °C / 900 °C	500 °C / 900 °C	500 °C / 900 °C
Turbine inlet	849.1 °C	852.0 °C	853.7 °C
	260 kg/s	276 kg/s	292 kg/s
HPC outlet	125.2 °C	117.3 °C	110.3 °C
	7.0 MPa	7.0 MPa	7.0 MPa
Flow rate to IHX	24.1 kg/s He	24.1 kg/s He	24.1 kg/s He
Pressure ratio	3.50	3.16	2.90
Cycle efficiency	48.0%	48.9%	49.5%

The system pressure also affects the cycle efficiency. Using Configuration 6, the compressor outlet pressure was varied from 2 to 7 MPa while the pressure ratio was adjusted to maximize cycle efficiency. Lower system pressure will reduce material stresses, reducing the size of the components, while higher pressure increases overall cycle efficiency. Therefore, a trade-off study between component size and cycle efficiency needs to be performed to determine the optimal design. The effects of system pressure on various parameters are summarized in Table 23. The effects on overall efficiency are presented in Figure 39.

Table 23. Sensitivity of overall efficiency to pressure.

|	2 MPa	3 MPa	4 MPa
Reactor power	600 MW thermal	600 MW thermal	600 MW thermal
Reactor inlet / outlet temperature	500 °C / 900 °C	500 °C / 900 °C	500 °C / 900 °C
Turbine inlet	866.6 °C	886.6 °C	866.6 °C
	259.9 kg/s	259.9 kg/s	259.9 kg/s
HPC outlet	137.5 °C	132.9 °C	129.7 °C
	2 MPa	3 MPa	4 MPa
Flow rate to SHX	27.5 kg/s He	27.5 kg/s He	27.5 kg/s He
Pressure ratio	3.94	3.61	3.47
Cycle efficiency	41.4%	45.4%	47.3%
	5 MPa	6 MPa	7 MPa
Reactor power	600 MW thermal	600 MW thermal	600 MW thermal
Reactor inlet / outlet temperature	500 °C / 900 °C	500 °C / 900 °C	500 °C / 900 °C
Turbine inlet	866.6 °C	886.6 °C	866.6 °C
	259.9 kg/s	259.9 kg/s	259.9 kg/s
HPC outlet	128.6 °C	126.7 °C	126.3 °C
	5 MPa	6 MPa	7 MPa
Flow rate to SHX	27.5 kg/s He	27.5 kg/s He	27.5 kg/s He
Pressure ratio	3.39	3.33	3.30
Cycle efficiency	48.4%	49.1%	49.6%
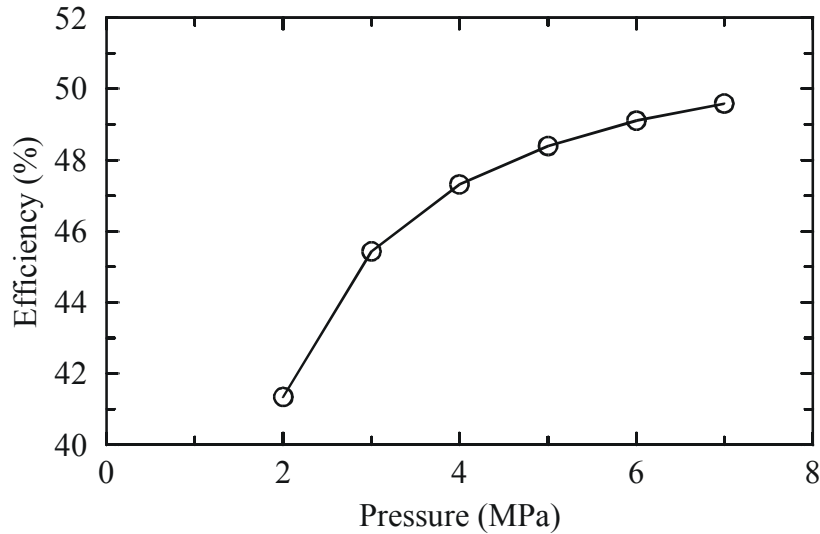
Figure 39. Sensitivity of overall efficiency to pressure.

Calculations were also performed to investigate the sensitivity of the calculated results to the working fluid. The working fluid affects the cycle operating condition, the efficiency, and the size of the plant components, which will be a major factor for the system cost. The previously reported results utilized helium as the working fluid. Sensitivity calculations were performed using the liquid salts Flinak and NaBF$_4$-NaF.

Using Configuration 1, the helium in the intermediate heat transport loop was replaced with Flinak in the HYSYS model. The results are compared in Table 24. The pumping power in the intermediate heat transport loop was significantly smaller with Flinak as the working fluid. However, the difference in cycle efficiency was relatively small (0.2%) because the pumping power was small compared to the reactor power even with helium as the working fluid.

Table 24. The effect of working fluid on the overall efficiency for Configuration 1.

	Helium	**Flinak**
Reactor power	600 MW-thermal	600 MW-thermal
Configuration	Direct and serial IHX	Direct and serial IHX
Reactor inlet	500 °C	500 °C
	7.05 MPa	7.05 MPa
Reactor outlet	900 °C	900 °C
	7.0 MPa	7.0 MPa
Helium mass flow to PCU	288.9 kg/s	288.9 kg/s
Turbine inlet	866.6 °C	866.6 °C
	6.95 MPa	6.95 MPa
HPC outlet	108.6 °C	108.6 °C
	7.1 MPa	7.1 MPa
Flow rate of intermediate loop	24.1 kg/s He	133 kg/s Flinak
Pressure ratio	2.85	2.85
Pump power	3.2 MW	47.9 kW
Cycle efficiency	50.6%	50.8%

Table 25 shows that similar results were obtained for Configuration 2 when helium in the intermediate heat transport loop was replaced with NaBF$_4$-NaF.

Table 25. The effect of working fluid on the overall efficiency for Configuration 2.

	Helium	NaBF$_4$-NaF
Reactor power	600 MW-thermal	600 MW-thermal
Configuration	Direct and parallel IHX	Direct and parallel IHX
Reactor inlet	500 °C	500 °C
	7.05 MPa	7.05 MPa
Reactor outlet	900 °C	900 °C
	7.0 MPa	7.0 MPa
Helium mass flow to PCU	256.8 kg/s	256.8 kg/s
Turbine inlet	900 °C	900 °C
	7.0 MPa	7.0 MPa
HPC outlet	119.8 °C	119.8 °C
	7.1 MPa	7.1 MPa
Flow rate of intermediate loop	27.5 kg/s He	94.8 kg/s NaBF$_4$-NaF
Pressure ratio	3.23	3.23
Pump power	6.7 MW	35.9 kW
Cycle efficiency	50.7%	51.3 %

6. SUMMARY

Stress Evaluation

The intermediate heat transport loop will likely be limited by the creep rupture strength of available materials. The creep rupture strength decreases with temperature and operating time while the stresses increase with pressure.   The mechanical design of the intermediate heat transport loop will be a challenge because of the desire to operate for a long time at elevated pressure and temperature. The following points summarize the results of the stress evaluation.

- Alloy 617 has greater rupture strength than either Alloy 800HT or Hastelloy X at 900 °C. Of the three materials evaluated, Alloy 617 is currently preferred for the high-temperature portions of the intermediate heat transport loop from strength considerations.

- The creep rupture strength of Alloy 617 is about 20 MPa for 10^5 hours (about 11 years) of operation at 900 °C. For this analysis, the allowable stress was assumed to be 10 MPa, half of the creep rupture strength of Alloy 617. Ultimately, the allowable stress will be determined by an applicable code.

- A simplified stress analysis indicates that the PHX tubes are the most limiting components in the intermediate heat transport loop. Based on an allowable stress of 10 MPa, the PHX can not be designed for a long lifetime ($> 10^5$ h) if the operating pressure is 7 MPa. A reasonable tube thickness can be achieved if the pressure is reduced to 2 MPa. Thus, a tube-in-shell PHX needs to be placed within a relatively low-pressure loop.

- The stresses from the simple analysis described here will probably be less than would result from more rigorous calculations. Consequently, the component sizes calculated here will probably be less than actually required, but should be adequate for evaluating the relative differences between configurations.

Thermal-Hydraulic Evaluation

The parametric studies described in Section 5.2 provide an overview of the effects of various configurations and options on the thermal-hydraulic characteristics of single- and dual-purpose facilities. The effects of these parameters on various thermal-hydraulic characteristics are summarized below.

- The use of low-pressure (2 MPa) helium as the working fluid in the intermediate heat transport loop mitigates the creep rupture problems that are encountered when using high-pressure (7 MPa) helium and results in a relatively small (0.2%) decrease in overall efficiency for a loop sized to deliver 50 MW of power to the hydrogen production plant. However, the decrease in efficiency becomes much larger (4.2%) when the entire 600-MW output of the nuclear plant is delivered to the hydrogen production plant. Thus, the use of low-pressure helium is judged to be a viable option for the dual-purpose NGNP, but is not attractive for a single-purpose facility dedicated to hydrogen production.

- Significant benefits can be obtained if the operating pressure of the helium in the intermediate heat transport loop can be increased. Assuming that strong enough materials are available, increasing the pressure in the intermediate loop from 2 to 7 MPa would decrease the size of the loop by 30% and reduce the pumping power by 20% for Configuration 1.

- The compact heat exchangers will be easier to design and construct if they are arranged in parallel with the PCU rather than in series. The parallel option results in much larger aspect ratios, which will reduce problems with flow distribution between channels.

- The addition of a tertiary loop will provide more separation between the nuclear and hydrogen plants, which should make both plants easier to operate and license. However, the addition of a tertiary loop also increases the overall cost of the plant. The metal volumes of the intermediate and tertiary loops for Configurations 3 and 4 were 40 to 60% greater than for the intermediate loop in Configurations 1 and 2. The increase in size can be used to estimate the difference in capital cost for this portion of the plant.

- The use of an indirect electrical cycle will reduce radiation levels in the PCU and make its maintenance easier. However, the use of an indirect electrical cycle will increase the size and cost of the plant. The IHX for an indirect cycle is much larger than for a direct cycle because it is designed to remove 600 MW of thermal power rather than 50 MW.

- The use of a liquid salt as a coolant results in several advantages compared to helium. First, the liquid salt allows the efficient transport of heat at relatively low pressure, which mitigates the problems associated with creep rupture. Second, the use of a liquid salt reduces the total metal volume of the intermediate heat transport loop by 60 to 70% compared with low-pressure helium. Third, the total pumping power is reduced between 30 and 60%. Fourth, the thickness of the insulation required to obtain a given heat loss is reduced by about 80%. All of these factors have the potential to reduce the cost of the NGNP. The use of a liquid salt in a single-purpose plant

63

dedicated to the production of hydrogen is estimated to increase the overall efficiency by 1.7 and 5.9% compared to high- and low-pressure helium, respectively.

- The use of a liquid salt also results in several disadvantages compared to helium. First, the material compatibility issues associated with the liquid salts are not as well known as they are for helium (see Appendix A). Second, the use of a liquid salt requires additional components that are not required with helium coolant. These additional components, which include an auxiliary heating system and a surge tank to accommodate the contraction and expansion of the liquid salt during transients, will tend to increase the capital cost of the system. Third, a liquid salt has the potential to freeze during transients. RELAP5-3D calculations were performed to estimate when freezing would occur during two transients without any mitigation. The time at which freezing occurred varied between 5 and 65 minutes, depending on whether the transient was initiated by a loss-of-reactor heat source with continued cooling from the cold side of the PHX or by a loss-of-offsite power in which the cooling was due to heat loss. Fourth, the use of salt places a constraint on the design of the hydrogen production plant that does not exist with helium as a coolant. Based on the transient calculations, it is desirable that the inlet temperature on the cold side of the PHX exceed the freezing temperature of the salt during normal operation so that freezing cannot occur quickly following a reactor trip.

- Heat losses from the intermediate loop appear to be manageable with a reasonable amount of insulation.

Cycle Efficiency Evaluation

The parametric studies described in Section 5.3 provide an overview of the effects of configuration, operating pressure, temperature, mass flow, and coolant on the efficiency of dual-purpose plants that generate both hydrogen and electricity. The effects of these parameters on the overall efficiency of the plant are summarized below.

- The use of an indirect cycle causes the overall efficiency of the plant to decrease by 1.1% compared to a direct cycle based on the temperature drop assumptions used for this analysis.

- The use of a liquid salt as the working fluid in the intermediate heat transport loop of the dual-purpose facility analyzed here causes the overall efficiency to increase by 0.2 – 0.6% compared to low-pressure helium because of reduced pumping power.

- The use of a heat exchanger that is arranged in parallel with the PCU causes the overall efficiency to increase by 0.1 – 0.3% compared to the use a heat exchanger that is arranged in series.

- The variations in overall efficiency were generally small between configurations, except for Configuration 7, where the efficiency was significantly less because of the relatively low operating pressure for this configuration.

- An increase in the reactor outlet temperature of 100 °C caused the overall efficiency to increase by 3.3%.

- An 11% decrease in the flow rate through the turbine caused the overall efficiency to decrease by 1.5%.

Conclusions and Recommendations

The following conclusions and recommendations are drawn from this study.

- The use of a low-pressure working fluid (either helium or liquid salt) allows for a relatively simple mechanical design for the intermediate heat transport loop based on currently available materials. The use of high-pressure helium as a working fluid requires more elegant designs than those considered here and precludes the use of a tube-in-shell PHX based on currently available materials.

- The heat exchanger in the intermediate heat transport loop should be arranged in parallel with the PCU rather than in series. The parallel arrangement results in a longer aspect ratio that should make the heat exchanger easier to design and construct and also increases the overall efficiency of the cycle.

- Configurations 1, 3, and 5 should be eliminated from further study because they use a serial heat exchanger arrangement. Configuration 7 should be eliminated from further study because of its low efficiency.

- The best options to consider further are Configurations 2, 4, and 6. Of these, Configuration 2, which utilizes a direct electrical cycle, is the smallest and has the highest efficiency. Configuration 6 is the largest and has the lowest efficiency, but the operational benefits of using an indirect electrical cycle may outweigh these disadvantages.

- The advantages of liquid salt as a coolant in the intermediate heat transport loop become more pronounced as additional power is delivered to the hydrogen production facility. Although low-pressure helium is an attractive option for the dual-purpose NGNP, it is not suitable for a single-purpose facility dedicated to hydrogen production. The use of a liquid salt coolant in the intermediate loop of the NGNP causes extra developmental risk compared to helium, but would provide valuable experience relative to its use in a single-purpose facility.

Research and Development Needs

Several key research and development needs were identified during this study. Programs to address these needs are generally underway, but the needs are included here for completeness.

- An applicable code that specifies the allowable stress for the desired operating conditions of the intermediate heat transport loop is required. The allowable stress is required input for the mechanical design of the loop.

- The development of stronger materials would simplify the design of the intermediate loop and is required before raising the outlet temperature of the NGNP can be realistically considered.

- More detailed stress evaluations of the various components in the intermediate loop are required. Better values for the channel pitch-to-diameter ratio and the plate thickness-to-diameter ratio need to be determined for the compact heat exchangers based on these more detailed evaluations.

- An appropriate material for insulating the intermediate loop needs to be identified along with its thermal properties.

- The compatibility of the candidate materials for structures and working fluids need to be determined at the desired operating conditions of the intermediate loop.

- The effects of freezing of a liquid salt in the intermediate loop need to be evaluated. Methods to prevent and/or recover from freezing need to be developed. A reasonable criterion for the required margin between the freezing point and the minimum operating temperature in the loop should be developed.

- A helium-recuperated PCU with a single shaft connecting the turbine and compressors was evaluated during this study. Other PCU configurations that include a reheat cycle, a combined cycle, and multiple-shaft designs should be evaluated. Other working fluids in the PCU, such as carbon dioxide, also need to be considered.

- Transient analyses of the PCU during start up, load changes, and grid separation need to be performed. Efficient control systems need to be developed and evaluated.

- This study represented the hydrogen production plant with temperature boundary conditions on the cold side of the PHX. More detailed modeling of the coupling between the hydrogen production plant and the PCU needs to be performed.

7. REFERENCES

ANLW, 2004, *Reactor/Process Interface Requirements*, ANL W7500-0001-ES-00, Revision 0, July 2004.

Aspen Technology, 2005a, "HYSYS Process Version 2.2.2," www.aspentech.com.

Aspen Technology, 2005b, "Aspen Plus Version 11.1," www.aspentech.com.

Bird, R. B., W. E. Stewart, and E. N. Lightfoot, 1960, *Transport Phenomena*, John Wiley & Sons, Inc., New York.

Crandall, S. H, N. C. Dahl, and T. J. Lardner, 1972, *An Introduction to the Mechanics of Solids*, Second Edition, McGraw-Hill Book Company, New York.

Crane, 1979, *Flow of Fluids through Valves, Fittings, and Pipe*, Technical Paper 410.

Dewson, S. J and B. Thonon, 2003, "The Development of High Efficiency Heat Exchangers for Helium Gas Cooled Reactors," Paper 3213, ICAPP03.

Diehl, H. and E. Bodman, 1990, "Alloy 800 Specifications in Compliance with Component Requirements," *Journal of Nuclear Materials*, 171, pp. 63-70.

Dostal, V., M. J. Driscoll, and P. Hejzlar, 2004, *A Supercritical Carbon Dioxide Cycle for Next Generation Nuclear Reactors*, MIT-ANP-TR-100, March 2004.

Krieth, F., 1964, *Principles of Heat Transfer*, International Textbook Company, Scranton.

General Atomics, 1996, *Gas Turbine-Modular Helium Reactor (GT-MHR) Conceptual Design Description Report*, GA Project No. 7658, 910720 Revision 1, July 1996.

Glasstone, S. and A. Sesonske, 1967, *Nuclear Reactor Engineering*, Van Nostrand Reinhold Co., New York.

Haynes International, 2005, http://www.haynesintl.comXsite/Xcsrs.html.

Holman, J. P., 1986, *Heat Transfer*, Sixth Edition, McGraw-Hill Book Company, New York.

Independent Technology Review Group, 2004, *Design Features and Technology Uncertainties for the Next Generation Nuclear Plant*, INEEL/EXT-04-01816, June 2004.

INEEL, 2005, *Next Generation Nuclear Plant Research and Development Program Plan*, INEEL/EXT-05-02581, January 2005.

INEEL, 2003a, *RELAP5-3D Code Manual Volume 4: Models and Correlations*, INEEL-98-00834, Revision 2.2, October 2003.

INEEL, 2003b, *RELAP5-3D Code Manual Volume 1: Code Structure, System Models and Solution Methods*, INEEL-98-00834, Revision 2.2, October 2003.

Kayes, W. M. and M. E. Crawford, 1980, *Convective Heat and Mass Transfer*, Second Edition, McGraw-Hill Book Company, New York.

MacDonald, P. E., J. W. Sterbentz, R. L. Sant, P. D. Bayless, R. R. Schultz, H. D. Gougar, R. L. Moore, A. M. Ougouag, and W. K. Terry, 2003, *NGNP Preliminary Point Design – Results of the Initial Neutronics and Thermal-Hydraulic Assessments*, INEEL/EXT-03-00870, July 2003.

Oh, C. and R. Moore, 2005, "Brayton Cycle for High Temperature Gas-Cooled Reactors," *Nuclear Technology*, Vol. 149, pp. 324-336.

Peng, D.Y. and Robinson, D.B., 1976, "A Two Constant Equation of State," *I.E.C. Fundamentals*, 15, pp. 59-64.

Peterson, P. F., H. Zhao, D. Huang, and G. Fukuda, 2004, *Conceptual Design for a 50 MW(t) Metallic Intermediate Heat Exchanger for the Next Generation Nuclear Plant*, UCBTH-04-001, Draft, December 20, 2004.

Saravanamuttoo, H. et al., 1996, *Gas Turbine Theory*, Fifth Edition, Prentice Hall.

Sochet, I., J. L. Rouyer, and P. Hemmerich, 2004, "Safe Hydrogen Generation by Nuclear HTR," Paper 4261, *Proceedings of ICAPP '04, Pittsburgh, PA, USA, June 13-17*.

Special Metals, 2004a, http://www.specialmetals.com/products/incoloyalloy800h&ht.htm, September.

Special Metals, 2004b, http://www.specialmetals.com/products/incoloyalloy617.htm, September.

Smith, C., S. Beck, and B. Galyean, 2005, *An Engineering Analysis for Separation Requirements of a Hydrogen Production Plant and High-Temperature Nuclear Reactor*, INL/EXT-05-00137 Rev 0, March 2005.

Vernondern, K. and T. Nishihara, 2004, *Valuation of the Safety Concept of the Combined Nuclear/Chemical Complex for Hydrogen Production with HTTR*, JUEL-4135.

APPENDIX A – Candidate Materials for a High Temperature Intermediate Loop with Molten Salt Working Fluids

Dane Wilson (ORNL)

A1. INTRODUCTION

The Nuclear Hydrogen Initiative is investigating both thermochemical cycles and high temperature electrolysis as methods for the production of hydrogen using nuclear energy. These production methods require heat inputs at elevated temperatures and hence, high temperature interfaces between the reactor heat source and the process fluid. High temperature electrolysis requires steam generation in the temperature range of 750 to 900 °C. The baseline thermochemical cycles (Sulfur-Iodine (SI) and Hybrid sulfur) require heat transfer to process fluids in the temperature range of 750 to 950 °C. The SI cycle consists of three coupled chemical reactions,[1] as shown in Fig. A1. Sulfuric acid and hydrogen iodide are generated in the low temperature Bunsen reaction, and the reaction products, sulfuric acid and hydrogen iodide, are decomposed at higher temperatures.
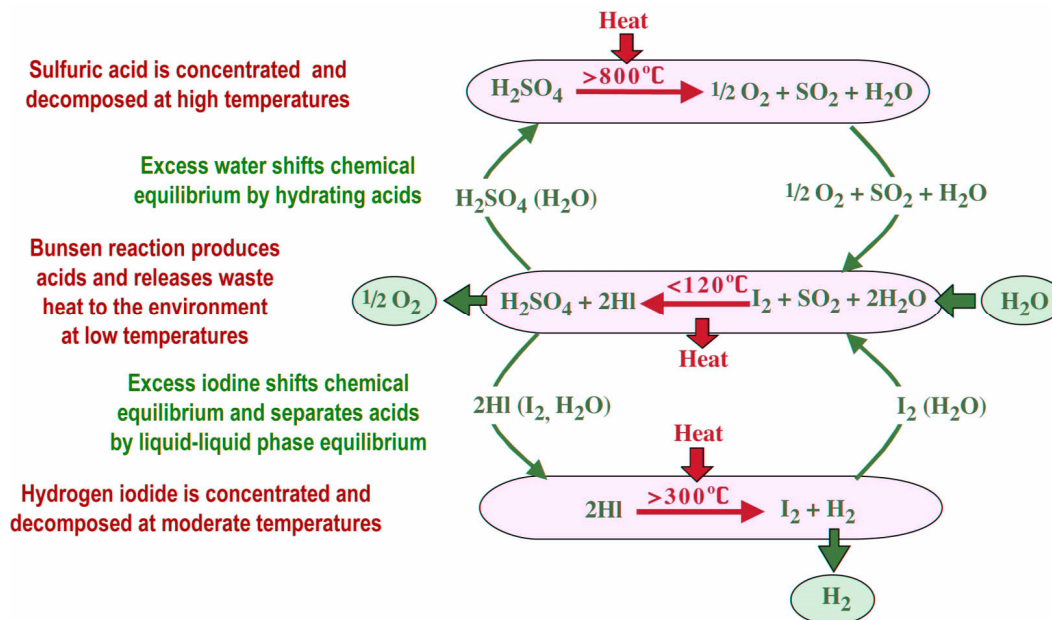
Figure A1. Reaction summary for the SI cycle.

The materials compatibility issues associated with heat transfer can be readily demonstrated with the SI cycle. The secondary side of the intermediate heat exchanger (IHX) is an incoming mixture of approximately 71 wt% H_2SO_4, 22 wt% SO_3, and 7 wt% H_2O in the temperature range of 803 to 838 K (530 to 565° C); and an outgoing mixture of approximately 40 wt% SO_2, 20 wt% H_2SO_4, 16 wt% H_2O, 13

wt% SO_3, and 10 wt% O_2 in the temperature range of 1173 to 1223 K (900 to 950 °C). The system has been modeled with operating pressures of 1.5 and 7 MPa (15 and 70 bar) on the secondary side. The primary side of the IHX will be exposed to either helium at approximately 7 MPa (70 bar) or a molten salt at 0.1 MPa (1 bar). With either heat transfer medium, the incoming temperature is estimated to be in the range of 1273 to 1223 K (1000 to 950 °C) and the outgoing temperature in the range of 1073 to 873 K (800 to 600 °C). While, as much as possible, operating pressures will be used that minimize the stress across the heat exchanger, the efficiency of the decomposition process is reduced when the decomposition reactions are performed at high pressures. While the choice of a molten salt will depend on the design and desired operating conditions, it is anticipated that a fluoride molten salt will be employed.

A2. APPROACH

High temperature heat transfer to vaporize and decompose the thermochemical cycle process fluid will require an efficient and corrosion resistant heat exchanger. This intermediate loop will have to be designed to be efficient (low heat losses), have the required acceptable pumping power, and be corrosion resistant to the working fluid. While the SI cycle is a leading candidate for hydrogen production, other thermochemical cycles and high temperature electrolysis are being considered. As such, the environment on the process side of the intermediate heat exchange has not been established. Thus, this initial report looks only at compatibility issues associated with the intermediate heat exchanger working fluid.

Two candidate working fluids are being considered: helium and molten salts. Helium poses relatively better known compatibility issues and requires higher pumping powers and pressures than molten salts. Further, the compatibility issues associated with high temperature helium are being addressed for the Next Generation Nuclear Plant (NGNP) high temperature gas-cooled reactor. Molten salts provide for much better heat transfer characteristics, lower pumping powers, and allow for the use of low pressure loops. However, the use of molten salts results in less well understood materials compatibility issues at these temperatures and presents issues associated with freezing due to the salts relatively high (~400 °C) melting points. For example, LiF-NaF-KF melts at 454 °C, KF-ZrF_4 melts at 390 °C, and LiF-BeF_2 melts at 460 °C.[2] In order to determine the viability of molten salts as a heat transfer medium for nuclear hydrogen production and take advantage of their better heat transfer and lower pumping power characteristics, the materials compatibility and mechanical properties issues of possible structural materials must be addressed.

This study was undertaken to:

- Identify candidate structural materials (alloys, composites, and other advanced materials) for a molten salt intermediate loop at temperatures in the range of 750 to 950 °C.
- Review available compatibility and mechanical property data to determine current limits of performance for candidate salts.
- Select the most promising structural materials for the molten salt intermediate loop.
- Develop a preliminary test matrix for evaluation of these materials.

A3. PAST EXPERIENCE

After several years of research and development (R&D) activities on molten salt reactor systems, the Aircraft Reactor Experiment began operation in 1954 at Oak Ridge National Laboratory (ORNL) to demonstrate the feasibility of operating a molten-salt fueled reactor at high temperature; fuel entered the core at 649 °C and exited at 816 °C when the reactor power level was 2.5 MW. A second demonstration, the Aircraft Reactor Test, was under development for several years before it was discontinued upon termination of the Aircraft Nuclear Propulsion Program in 1957-58. Subsequently, the Molten Salt

Reactor Experiment (MSRE) was carried out at ORNL to demonstrate that the desirable features of the molten salt concept could be incorporated into a safe and reliable civilian power reactor. The 7.4 MW(t) MSRE, which operated at 549 to 649 °C, went critical in 1965 and was shut down in 1969 after a successful operating history. Because of the success of the MSRE, additional R&D was carried out in support of a molten salt breeder concept.

Areas such as salt chemistry, including phase behavior, purity requirements, radiation stability, etc. and materials for salt-containing structures, including physical and mechanical properties, corrosion, irradiation effects, etc. were thoroughly investigated. The majority of these studies were in support of applications at ≤700 °C; however, the available data base affords useful technical support for applications at >700 °C.

Based on early R&D, the nickel-base alloy Hastelloy N was developed by ORNL for use in the MSRE. Several hundred thousand hours of corrosion experience with Hastelloy N and fluoride salts were obtained in thermal convection loop tests[3-5] and pumped loop tests[6] in addition to experience from the MSRE. Corrosion studies also included graphite as well as stainless steels and some refractory metal alloys, (e.g., TZM).

A4. UNDERSTANDING DERIVED FROM PAST EXPERIENCE

Two general mechanisms of corrosion, metal dissolution and oxidation of metal to ions, can occur in molten salt systems. Because of low solubilities of most structural metals in salt systems, one mechanism, metal dissolution due to solubility in the melt, is not a common form of attack. The second mechanism, oxidation of metal to ions, is more likely. This oxidation is manifest in forms akin to those observed in aqueous systems, including stress corrosion, galvanic corrosion, erosion-corrosion and fretting corrosion. Many of the principles that apply to aqueous corrosion also apply to molten salt corrosion such as anodic dissolution and cathodic reduction of an oxidant. However, there are also major differences from aqueous systems especially if the salts are electronic as well as ionic conductors. Reduction reactions can occur in the melt as well as at the metal-melt interface. In many molten salt systems the rate controlling step is ion diffusion into the bulk solution, not the charge transfer that is typical of aqueous systems.

Thermodynamic stability of the fluoride salt components versus alloy constituents is quite important because molten-salt corrosion is usually induced by reduction/oxidation (redox) reactions. In work leading to operation of the MSRE, ORNL demonstrated the excellent compatibility of Hastelloy N with fluoride salts containing LiF, BeF_2, ThF_4, and UF_4. If the salt is pure and the metal clean, UF_4 is the strongest oxidant in a fuel-salt system. The reaction,

$$UF_4 \text{ (d)} + \frac{1}{2} Cr \text{ (s)} \rightarrow UF_3 \text{ (d)} + \frac{1}{2} CrF_2 \text{ (d)},$$
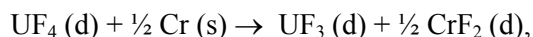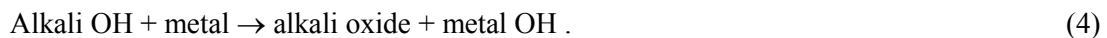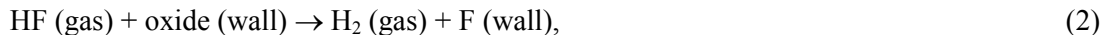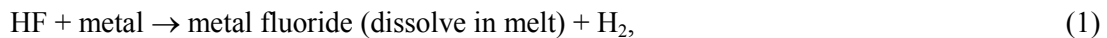
has a favorable free energy of formation at 500 – 800 °C. Since CrF_2 is one of the most stable structural metal fluorides, Cr can selectively react with extraneous (impurity) oxidants (fluorides) in the system. Because of the unusually high stability of alkali metal and beryllium fluorides, the corrosion potential of melts without uranium is likely controlled by redox equilibria involving impurities in the melt or gas phase. Gradients in the chemical activities of constituents caused by temperature differences can result in dissolution of metal in one region of the system with subsequent deposition in other portions of the system. The amount of attack will depend on the driving force and dissolution or deposition kinetics for reactions that result in transporting the corroding species to a different part of the loop circuit where they might deposit. In single material systems (e.g., capsule tests) at constant temperature, there would be no activity gradient and the amount of attack would be a function of the relative solubility of the respective corrosion product in the salt or, if the product is volatile, the partial pressure in the atmosphere

71

immediately above the salt. Thus, equilibrium solubility principles would limit the amount of solute and degree of corrosive attack in this type of system. However, a non-isothermal system could also be subject to corrosion from thermal gradient mass transfer if the chemical potential of the corrosion product fluoride, at a given concentration, is a strong function of temperature, and deposition of the corrosion species occurs in the cooler regions of a loop operating with a relatively high temperature differential. Although equilibrium solubility principles limit the amount of solute in a specific volume of salt in a closed system (capsule test) at constant temperature, continued transport of material can occur to the cold section of a non-isothermal system.

Mass transfer can also occur when dissimilar structural materials are included in the same system. The dissimilar materials do not have to be electrically coupled. Two things are required for dissimilar material mass transfer to be a factor. First, an element contained in one of the materials has to have a strong tendency to form an alloy or compound with the second material. More importantly, an element in one of the materials must be subject to oxidative attack or suffer dissolution within the salt solution. The oxidative attack can be either by reaction with impurities or, if a reactive element, with the salt constituents. In either event, once the element goes into solution, it can then migrate through the solution and form the required product if the chemical driving force (activity gradient) is sufficient. If the product does form, this will allow the mechanisms of corrosive attack or dissolution to continue (i.e., favorable thermodynamics) although kinetics may be limited by solid state diffusion. If the attack is solely by reaction with impurities, the problem may dramatically slow with time. However, the reaction will not stop if there is solubility in the salt for a specific element.

In the case of previous fluoride corrosion studies at ORNL, the containment system was generally monometallic, and dissimilar metal effects were not encountered. However, graphite was a major nonstructural component in the reactor system and there was no evidence of graphite interaction with the structural materials at Molten Salt Reactor (MSR) temperatures ($\leq$816 °C).

Even if redox reactions with major salt constituents are limited, materials can interact with oxidizing impurities present in the salt or in the system (capsule or loop). The presence of HF within the salt, which is used for impurity removal in the purification process, as well as moisture or oxides residing on the container or loop walls, can all lead to adverse corrosive reactions. HF can react either directly with the material forming a fluoride as noted in Equation (1) or indirectly with oxides present on the wall of the container as noted in Equations (2-4). All of these reactions should cease when the impurities have reacted.

$$HF + metal \rightarrow metal\ fluoride\ (dissolve\ in\ melt) + H_2, \tag{1}$$

$$HF\ (gas) + oxide\ (wall) \rightarrow H_2\ (gas) + F\ (wall), \tag{2}$$

$$H_2O\ (gas) + alkali\ F\ (melt) \rightarrow HF\ (gas) + alkali\ OH\ (melt),\ and \tag{3}$$

$$Alkali\ OH + metal \rightarrow alkali\ oxide + metal\ OH\ . \tag{4}$$

As alluded to earlier, oxidation of one of the constituents of the material by the reduction of a less stable impurity metal fluoride initially in the salt such as iron or nickel fluoride can occur.[2,3] Examples of this include:

$$Cr + FeF_2 \rightarrow CrF_2 + Fe , \text{ and} \tag{5}$$

$$Zr + 2FeF_2 \rightarrow ZrF_4 + 2Fe . \tag{6}$$

In order to control the redox potential of the fluoride salt in the MSRE, the melt chemistry was made slightly reducing by the addition of a small amount of beryllium metal that reduced approximately 1% of the UF_4 solute to UF_3:

$$Be + 2UF_4 \rightarrow BeF_2 + 2UF_3. \tag{7}$$

As a result of this addition, the 100/1 ratio of UF_4/UF_3 minimized the corrosion of Hastelloy N by UF_4 (where Cr is the most active metal present and therefore the first to be oxidized) because of the equilibrium between the chromium and uranium components:

$$Cr + 2UF_4 \rightarrow CrF_2 + 2UF_3. \tag{8}$$

The redox potential of systems that do not contain uranium may be controlled in another fashion - by addition of a small amount of solute that can exist in two oxidation states, by addition of a sparge gas that is set at the proper redox potential, or by electrochemically setting an applied potential equivalent to the desired redox potential. A redox solute mix of choice would be cerium (IV/III) fluorides which would function very much the same as the uranium redox equilibrium of above, namely

$$Cr + 2CeF_4 \rightarrow CrF_2 + 2CeF_3. \tag{9}$$

However, an even simpler means of controlling the redox potential is frequently used in the laboratory to prevent corrosion of metal containers during the hydrofluorination purification process, which is intended to remove oxide and sulfur contaminants:

$$Cr + 2HF \rightarrow CrF_2 + H_2. \tag{10}$$

If the ratio of H_2/HF is set at approximately 10/1, the redox potential is suitable in preventing the corrosion of the container, and the reaction,

$$BeO + 2HF \rightarrow BeF_2 + H_2O, \tag{11}$$
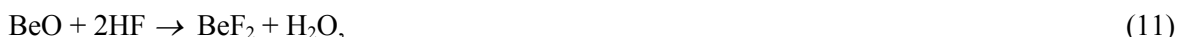
is used to convert dissolved oxides (and similarly hydroxides) to water vapor which is swept from the system in the flowing sparge gas. (When the laboratory container is made of nickel, this less reactive metal allows a lower H_2/HF ratio to be used and thus hasten the oxide purification process.)

The results of ORNL's work for the MSRE showed that Hastelloy N corrosion was manifest as void formation in the base metal due to chromium diffusion to the salt metal interface where it was oxidized by impurities in the salt or by UF_4. The latter effect, oxidation by UF_4, was controlled in the MSRE by the use of beryllium metal, as previously explained using Equations (7) and (8). Essentially, nickel-based alloys with the required mechanical properties are the materials of first choice to be evaluated for use in any molten fluoride salt environment.

A5. CANDIDATE MATERIALS FOR INTERMEDIATE LOOP

Based on past experience, an initial candidate list of materials for evaluation in the chosen heat transfer molten fluoride salt was developed. This list is presented in Table A1.

Table A1. Potential candidate materials for use in molten fluoride salts.

Material	Fluoride salt corrosion resistance	Fabricability	Highest use temperature °C	Comment
Haynes 242	Very good	Good	540	
Hastelloy N	Excellent	Good	730	
Hastelloy X or XR	Needs evaluation	Good	900	May need a protective coat
Haynes 230	Fair	Fair	?	May need a protective coat
Haynes 214	Very good	Poor-fair	1000	
MA 956	Good	Poor-fair	?	May need a protective coat
MA 754	Very good	Poor-fair	?	
Hastelloy B3	Needs evaluation	?	?	May want to use below 750 °C
Cast Ni superalloys	Very good		?	For pumps. May need protective coat
Nb-1Zr	Very good		Above that needed	
SiC (CVD)	Very good	Poor	Above that needed	Need a near net shape and the ability to seal

A6. TESTING

Because of the dearth of data for materials compatibility with molten fluoride salts at the temperatures of interest, an extensive test program is needed. It is recommended that the proposed materials and variants of these be first evaluated in static tests to determine their compatibility with molten fluoride salts. These fluoride salts must be carefully purified to avoid reactions of the structural materials of interest with impurities. Once a subset of these materials has been found, their mechanical properties at temperature, if unknown, must be determined. Those that possess needed compatibility and mechanical properties must be evaluated in flowing thermal-convection loops in order to determine mass transfer effects. Further, the effect of various approaches to redox control on corrosion of these materials must be evaluated. A test matrix for each material (with fluoride salt(s) and redox control approach) of interest is presented in Table A2. Tests are ordered from less costly, easier to execute to more costly, more difficult to execute.

Table A2. Static capsule tests for each material of choice in each salt of choice for down selection of materials; thermal convection loops for down-selected materials.

Test	Temperature (°C)	Time (h)	Comments
Mono-material static capsule	750	100	Screening tests. Allow for evaluation of impurities in molten salt versus thermodynamic stability.
	750	500	
	850	100	
	850	500	
	950	100	
	950	500	
	1000	100	
	1000	500	
Dissimilar materials static capsule Material A for capsule and Material B for specimen (much smaller surface area)	750	500	Determine thermodynamic chemical activity driven corrosion effects. (Assumes that dissimilar materials will be employed in the molten salt environment.) Use materials that pass above screening. Repeat if more combinations of materials will be exposed to the molten salt environment.
	850	500	
	950	500	
	1000	500	
Dissimilar materials static capsule Material B for capsule and Material A for specimen (much smaller surface area)	750	500	
	850	500	
	950	500	
	1000	500	
Down-selected mono-material thermal-convection loop Final down-selected mono-material and bi-materials thermal convection loop	Gradient from 1000 to 725	3000	Determine temperature driven mass transfer. Electrochemical monitoring of salt reservoir during test; periodic chemical analyses of salt content; post-test evaluation of specimens and loop. Repeat for each down-selected material.
Down-selected bi-materials thermal-convection loop Final down-selected bi-materials thermal-convection loop	Gradient from 1000 to 725	10,000	Loop made of one material. Specimens made of a different material. (Assume that different materials will be employed in the molten salt.) Determine additional effects of thermodynamic activity driven mass transfer. Electrochemical monitoring of salt reservoir during test; periodic chemical analyses of salt content; post-test evaluation of specimens and loop. Repeat for each down-selected combination of materials chosen.

A7. SUMMARY

Past experience with materials performance in molten fluoride salts was reviewed so as to provide the context for the known mechanisms of corrosion and the tests used to determine the mechanisms. Based on past results, nickel-based alloys are the materials of choice for containment of molten fluoride salts. However, the existing database is narrow and does not extend to the temperatures of interest for the intermediate heat exchanger. Materials were identified that must be further evaluated at the temperatures of interest. Static (capsule) tests are proposed for screening the initial materials matrix. Thermal-convection loop (flowing) tests are proposed for further evaluation of mass transfer effects of the viable candidates.

A8. REFERENCES

1. ORNL, 2004, *Materials Requirement for Nuclear Hydrogen Generation Systems*, to be issued.

2. Williams, D. F., 2005, *Assessment of Properties of Candidate Liquid Salt Coolants for the Advanced High temperature Reactor*, to be issued.

3. Adamson, G. M, R. S. Crouse, and W. D. Manly, 1959, *Interim Report on Corrosion by Alkali Metal Fluorides: Work to May 1, 1953*, ORNL-2337.

4. Adamson, G. M., R. S. Crouse, and W. D. Manly, 1961, *Interim Report on Corrosion by Zirconium-Base Fluorides*, ORNL-2338.

5. DeVan, J. H., 1960, M. S. Thesis, University of Tennessee.

6. Briggs, R. B., 1962, *MSR Program Semiannual Program Report, August 31, 1961*, pp. 93-94, ORNL-3215.